Influences of Free Thiols on the Product Quality of Therapeutic Antibodies

By

Copyright 2021

Michael Tae-Jong Kim

Submitted to the graduate degree program in Chemistry and the Graduate Faculty of the University of Kansas in partial fulfillment of the requirements for the degree of Doctor of Philosophy

_____

Chairperson – David D. Weis, Ph.D.

_____

Heather Desaire, Ph.D.

_____

Michael J. Hageman, Ph.D.

_____

Michael A. Johnson, Ph.D.

_____

Susan M. Lunte, Ph.D.

Date Defended: May 17th, 2021

The dissertation committee for Michael Tae-Jong Kim certifies that this is the approved

version of the following dissertation:

Influences of Free Thiols on the Product Quality of

Therapeutic Antibodies

_____

Chairperson – David D. Weis, Ph.D.

Date Approved: May 17th, 2021

Abstract

Therapeutic antibodies are an important class of modern medicines. During the biomanufacturing of therapeutic antibodies, many attributes relevant to product quality must be considered to ensure an efficacious and safe end product. One of those attributes is the free thiol, or an unpaired cysteine residue, which is interesting because of its innate and diverse reactivities. In this thesis, we first review topics - including the structure and function of antibodies, antibodies as therapeutics, the biomanufacturing of therapeutic antibodies, free thiols as a post-translational modification, and basic reactions involving free thiols – and then discuss three case studies that explore free thiols as they pertain to the product quality of therapeutic antibodies.

We explored the physiological outcome of free thiols on therapeutic antibodies after administration. We designed non-clinical studies where therapeutic antibodies with elevated free thiols at various sites are administered. Plasma samples were collected at various timepoints and we utilized a bioanalysis workflow involving immunopurification and mass spectrometry techniques to track site-specific free thiol levels at each timepoint. We observed that *in vivo* free thiol reoxidation kinetics are molecule- and disulfide site-dependent. We drew a novel connection positively associating free thiol reoxidation propensity and its solvent accessibility, providing some mechanistic basis explaining the different reoxidation rates observed. In this study, we examined the *in vivo* free thiol reoxidation in a more diverse panel of therapeutic antibodies than any previous study. We also determined *in vivo* free thiol reoxidation with far more site-specificity than any previous study.

Next, we explored the possibility of enhancing a classic optical method with a novel yet simple augmentation step to significantly improve quantitation limits of free thiols. We screened commercially available fluorogenic probes and identified one that successfully transduces the UV absorbance signal of the Ellman's method into a fluorescent signal. The augmented method, which we coin the Fluorescent Ellman's method, exhibited superior quantitation limits for free thiol detection compared with the Ellman's method while preserving the key advantages of the Ellman's method. We demonstrated the usefulness of the Fluorescent Ellman's method by quantifying the free thiol content of different antibody therapeutics, including several that would be challenging or impossible to analyze by alternative chromatography methods for free thiol determination. The Fluorescent Ellman's method is a rapid, sensitive, inexpensive, and substrate-agnostic means of determining free thiol content.

Finally, we explored the co-purification of a host cell protein which harbors a free thiol and a therapeutic antibody. This complex study involved identifying the contaminant host cell protein, expressing the recombinant host cell protein, and designing experiments to replicate the co-purification phenomena. Initial attempts to replicate the co-purification phenomena were confounded by the host cell protein's free thiol. After alkylating the free thiol however, co-purification was successfully replicated using a scaled-down Protein A purification system. Co-purification was also successfully replicated after bioconjugating affinity handles to the host cell protein's free thiol and performing magnetic bead pulldowns. After exhausting the more accessible analytical methods, we performed diazirine photo-crosslinking experiments coupled with mass

spectrometry to confidently implicate the therapeutic antibody's CDR loops in the host

cell protein-antibody interaction.

Acknowledgements

I thank my research advisor, Dr. David Weis, for taking a chance on me as a distance and industrial PhD student. He found creative and virtual ways to include me in group meetings and have regular check-ins on my research progress. I also thank him for his commitment to my growth as a scientist, particularly for providing candid and timely feedback, for mentoring me through the writing process, and for sharing his insights regarding starting and running a lab.

I thank the University of Kansas, the KU Department of Chemistry, and the current and past KU Department of Chemistry leadership for endorsing a distance PhD agreement. I am grateful to the KU Department of Pharmaceutical Chemistry department for being ahead of the curve in terms of online course offerings, which I took full advantage of for several elective courses.

I thank the current and past members of the Weis Lab for the fond memories during my brief residences in Lawrence in 2012 and 2014. Your warm welcome made Lawrence feel like a second home and really helped me to settle in.

I thank the members of my final defense committee, Dr. Heather Desaire, Dr. Susan Lunte, Dr. Michael Johnson, Dr. Michael Hageman, and Dr. David Weis, for their time and service in critically evaluating this thesis. I also thank the members of my oral examination committee, Dr. Mario Rivera, Dr. Michael Johnson, Dr. David Volkin, Dr. Heather Desaire, and Dr. David Weis, for challenging me and for setting a high standard early on in my studies.

I thank my past and current Genentech mentors and managers, Dr. Boyan Zhang, Dr. Yan Chen, Mr. Galahad Deperalta, and Dr. Feng Yang for their

encouragement and support. I thank Dr. Boyan Zhang and Ms. Pat Rancatore in particular for encouraging me to seek opportunities to pursue graduate studies while working at Genentech. I extend a special thanks to Dr. Yan Chen who invested in my scientific training early on and continues to be a strong advocate for my development.

I thank my collaborators, Mr. Aron Lee, Ms. Rashmi Sharma, Mr. Justin Jeong, Dr. Bingchuan Wei, Dr. Martin Lechmann, Ms. Sharmila Rajan, Dr. Vittal Shivva, Dr. Laura Simmons, and Mr. Adrian Nava without whom this work would not have been possible.

I thank my entire family for their encouragement and support. I thank my parents Seok Ho and Gyung Ae Kim for the life lessons, which are too many to enumerate. In the context of this thesis, I thank my parents for teaching me the importance of perseverance because most things worth doing are hard. I thank Gerald and Paula Karpman for being as excited, or even more excited at times, for my thesis progress. I am especially thankful for my wife, Malissa Karpman, whose unfailing support and patience was so essential during the long experiment nights and thesis writing process.

Table of Contents

Chapter 1.   Introduction

1.1. Antibodies

Antibodies, which belong to the family of immunoglobulins, are the workhorse of the human immune defense system. Impairment of antibody production or antibody function in humans are associated with serious disorders such as severe combined immunodeficiency (SCID) and autoimmune diseases. Typically found at high serum concentrations of approximately 11 mg/mL[1] in healthy humans, antibodies perform the critical function of identifying foreign epitopes on antigens (i.e. allergens, bacteria, viruses, etc.) by tightly binding to them. This antibody-antigen binding event can then modulate downstream immune cell interactions which often lead to the destruction or clearance of foreign entities.

Immunoglobulin G (IgG) is the most abundant class of antibodies and will be our focus. There are four naturally-occurring IgG subclasses in humans: IgG1, IgG2, IgG3, and IgG4. The structure and function of IgGs are covered in the subsequent sections.

1.1.1. Structural Components

An IgG is a homodimer consisting of two distinct chains called heavy chain and light chain. The heavy and light chains are approximately 50 and 25 kDa, respectively. An antibody can also be referred to by its regionally specific parts, which are denoted the Fab and Fc regions (short for "fragment antigen binding" and "fragment crystallizable", respectively).

An antibody can be further granularized from regions into immunoglobulin domains, which have a secondary structure characterized by a β sandwich (built from β sheets). There are four such domains on the heavy chain named VH, CH1, CH2, and

CH3, where the "V" and "C" denote variable and constant domains, respectively, and the "H" denotes heavy chain. There are two such domains on the light chain named VL and CL, where the "L" denotes light chain. As their names suggest, the variable and constant domains contain amino acid sequences that are highly differentiated or highly homologous among different IgGs, respectively. The VH, CH1, VL, and CL domains belong to the Fab while the CH2 and CH3 domains belong to the Fc.

Located between the CH1 and CH2 domains is a stretch of amino acids referred to as the hinge region of IgGs. The hinge region gives flexibility to the antibody, allowing the antibody to assume a variety of shapes as well as allowing the Fab and Fc regions to efficiently sample a larger space [2]. The hinge regions of the IgG subclasses differ significantly from each other in terms of length and interchain disulfide connections, which is discussed further in the next section.

Disulfide Bonds. An important structural element and post-translational modification is the disulfide bond, which is a covalent bond formed between two vicinal cysteine amino acids. Each immunoglobulin domain of an IgG antibody contains one intrachain disulfide bond that connects two cysteine residues within the same chain (i.e. heavy chain or light chain) and is responsible for maintaining the β sandwich. There are also interchain disulfide bonds that bridge between either heavy chain/light chain or heavy chain/heavy chain through two cysteine residues. The classical disulfide bond connections for different IgG subclasses are shown in **Figure 1.1**. This is a simplified representation of the disulfide bond connections of IgGs and in reality the IgG2 and IgG4 subclasses have been shown to have disulfide isoforms, [2-5] which deviate from the classical bond

connections. It is worth noting that the classical disulfide bonds and disulfide isoforms will not usually account for all of the cysteines in IgGs. Cysteines can also be disulfide bonded to cysteines other than their natural vicinal partners to form shuffled (or mispaired) disulfides; they can form covalent bonds with other thiol substrates such as free cysteine (cysteinylation) or glutathione (glutathionylation); or they can remain unbonded as free thiols (discussed later in Section 1.4).
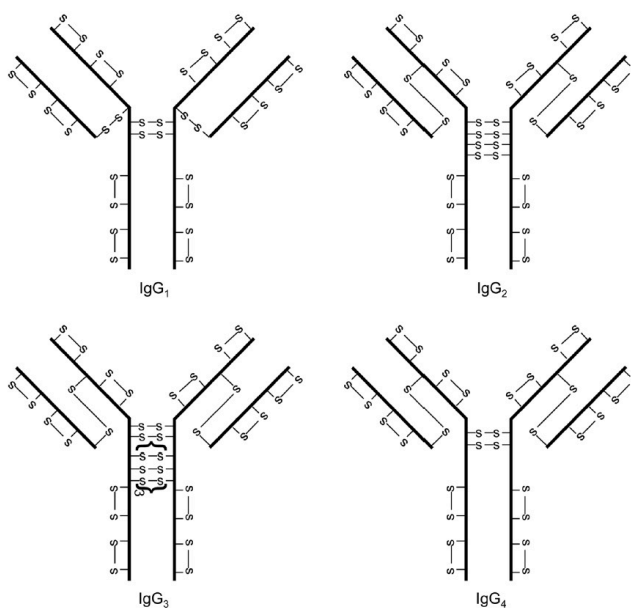
Figure 1.1. Classical disulfide linkages for IgG1, IgG2, IgG3, and IgG4. Used with permission of Taylor & Francis, from ref. [3]; permission conveyed through Copyright Clearance Center, Inc. The subscript on the interchain heavy chain-heavy chain disulfide bonds in IgG3 denote a repeating set of disulfide bonds in this IgG isoform.

Fc Glycosylation. Glycosylation of the Fc region is another important post-translational modification. The Fc region contains two conserved asparagine residues (N297 on each heavy chain) which have the N-X-S/T motif necessary for N-glycosylation. The core

structure – the common denominator among the possible Fc glycans - is comprised of two N-acetylglucosamine (GlcNAc) residues and three mannose residues.[2, 6] The remainder of the Fc glycan is built by appending additional residues to this core structure such as GlcNAc, mannose, N-acetyl neuraminic acid (sialic acid), or core fucose.

1.1.2. Functional Components

<u>Functional Components of the Fab</u>. Antigen recognition and binding occur in the Fab region of antibodies. The antigen-recognizing region within the Fab, or the paratope, is comprised of one or more of six solvent-exposed loops called complementarity-determining regions (CDR). Three of these reside on the heavy chain of the Fab (i.e. CDR-H1, CDR-H2, CDR-H3) while the other three reside on the light chain (i.e. CDR-L1, CDR-L2, CDR-L3). Remarkably, humans (and most mammals) can produce highly specific antibodies to bind to virtually any epitope. The enormous diversity of human variable domain sequences (i.e. VH and VL) which makes this possible is the result of genetic recombination, which is extensively reviewed elsewhere.

The binding strength of an antibody to an antigen can be characterized by the equilibrium dissociation constant, K_d, which can be expressed as:

$$K_d = \frac{k_{off}}{k_{on}} = \frac{[Antibody][Antigen]}{[Antibody\ Antigen\ complex]}$$

where k_{off} is the dissociation kinetic rate constant, k_{on} is the association kinetic rate constant, and [Antibody], [Antigen], and [Antibody Antigen Complex] are the

concentrations of those respective species. It is not unusual for antibody-antigen interactions to have K_d values in the low nM or high pM range.

Functional Components of the Fc. The Fc region of an antibody is multifunctional and is involved in determining the IgG half-life in circulation as well as mediating various immunomodulatory responses. The half-life in circulation of IgG (~20 days for IgG1/2/4 and ~7 days for IgG3 [2]) is long relative to many other serum proteins, and is attributable to Fc interactions with FcRn, the neonatal receptor, which salvages IgGs from degradation / catabolism pathways in acidic lysosomes. The Fc region can also facilitate immunomodulatory responses (effector function) that lead to destruction of the bound target via complement dependent cytotoxicity (CDC), antibody dependent cell cytotoxicity (ADCC), and/or antibody dependent cellular phagocytosis (ADCP). Complement dependent cytotoxicity is mediated by Fc binding to C1q, while antibody dependent cell cytotoxicity and antibody dependent cellular phagocytosis are mediated by Fc binding to FcγRIIIA and to other Fcγ receptors (FcγR), [7, 8] respectively. The IgG subclasses (IgG1/2/3/4) exhibit different potencies with regards to Fc effector functions because of their differences in affinity to FcγRs and C1q.[2] Glycosylation patterns can also influence the potency of these Fc effector functions by altering the affinities to FcγR and C1q; for example, afucosylated IgGs are well-known for increased binding affinity to FcγRIIIA and increased ADCC activity.[9]

1.2. Antibodies as Therapeutics

Therapeutic antibodies are an ever-increasing part of the modern medicine repertoire. Antibodies make attractive therapies because they are well-tolerated, have favorable pharmacokinetics, can engage in specific and high affinity target binding, and facilitate various mechanisms of action as discussed in later sections. The first therapeutic antibody product was approved by the FDA in 1986. By 2017, 57 antibodies as well as 11 biosimilars were available on the market (approved by either FDA or EMA) with the annual revenue from these antibody products numbering 98 billion USD.[10] These therapeutic antibodies can treat a wide range of diseases in oncology, hematology, dermatology, rheumatology, gastroenterology, etc. [10] and the number of approved indications for therapeutic antibodies are expected to grow year over year.

1.2.1. Design Considerations

Specific Target Engagement. The first step to successfully developing a therapeutic antibody for a given disease is ensuring specific target engagement i.e. antibody-antigen binding. Antibodies are versatile as a therapeutic class because they can bind to virtually any target with high specificity and affinity given the right combination of amino acid sequences in its CDRs. Identifying the right combination of CDR amino acid sequences, however, is not a trivial task and several technologies have been developed to facilitate the screening process to find the right antibody given a target antigen. Prevalent screening strategies include hybridoma technology, phage display libraries, transgenic mice, and direct human B-cell isolation.[11]

Mechanism of Action. Once a suitable antibody for the target has been identified, therapeutic antibodies can then be used to intervene in disease pathways through a multitude of mechanisms of action (MOA). Health authorities have a keen interest in the MOA(s) that are responsible for clinical efficacy and generally expect sponsors to prove their understanding of their therapeutic MOA(s). The various therapeutic MOAs include but are not limited to antagonism of soluble targets, agonism or antagonism of cell surface receptors to activate or inhibit signaling cascades, respectively, initiating antibody-dependent cell cytotoxicity / antibody-dependent cell phagocytosis / complement dependent cytotoxicity, etc. Antibody effector function that is appropriate for the intended MOA is an important consideration and requires judicious choice of IgG subclass as well as control over the Fc glycosylation profiles. Depending on the target indication, it may even be desirable to nullify antibody effector function by engineering an Fc without glycosylation (aglycosylated Fc).

Chimeric, Humanized, or Fully Human. Fully human therapeutic antibodies are generally well-tolerated in patients. However, it was not until recent years that it became possible to engineer the necessary CDRs into a fully human antibody framework. During the nascent years of therapeutic antibody development, therapeutic antibodies consisted of fully mouse IgGs and slowly evolved to the necessary CDRs being grafted onto chimeric IgG frameworks, to humanized IgG frameworks, and finally to fully human IgG frameworks. Therapeutic antibody homology to fully human antibodies is an important consideration with regards to minimizing safety and immunogenicity risks to patients.

1.2.2. New Antibody-Based Therapeutic Modalities

The field of antibody therapeutics continues to be an evolving, dynamic landscape. In the past, therapeutic antibodies have largely comprised of standard antibodies, which were highly similar to naturally-occurring antibody frameworks. While these standard antibodies will continue to be an important therapeutic modality moving forward, the new generation of antibody-based therapeutics are ushering in novel formats and modalities such as antibody drug conjugates (ADC), Fc fusion proteins, bispecific antibodies, chimeric antigen receptor T cells (CAR-T), immunocytokines, radioimmunotherapeutics, Fabs, nanobodies, etc.[12, 13] These novel modalities can enable certain mechanisms of action that were either unavailable to or inefficient with standard antibodies.

1.3. Biomanufacturing of Antibody Therapeutics

1.3.1. Cell Culture Production

Current state-of-the-art synthetic methods are still not capable of producing proteins as complex as antibodies at reasonable yields. For this reason, the biotechnology industry leverages the natural protein synthesis machinery of host cells for commercial therapeutic antibody production. Chinese Hamster Ovary (CHO) is a commonly used mammalian host cell that is recombinantly engineered to produce therapeutic proteins such as antibodies (60% of commercially-produced therapeutic antibodies are expressed in CHO while a large part of the remainder is expressed in mouse cell lines such as NS0 or Sp2/0 cells [10]). Mammalian host systems present

advantages to their prokaryotic counterparts such as *E. coli*. Despite being more

sensitive to cell culture conditions and requiring longer inoculation and production runs,

mammalian host cells are capable of expressing and secreting correctly folded

therapeutic proteins with proper post-translational processing i.e. expected disulfide

pairing and Fc glycosylation. Large scale CHO manufacturing generally consists of

either fed-batch bioreactors or perfusion bioreactors (**Figure 1.2**) that are equipped with

impellers, acid/base pumps, oxygen spargers, and sophisticated in-line monitoring

systems (i.e. pH, dissolved oxygen). The cell culture part of the manufacturing

bioprocess is referred to as the "upstream" process.
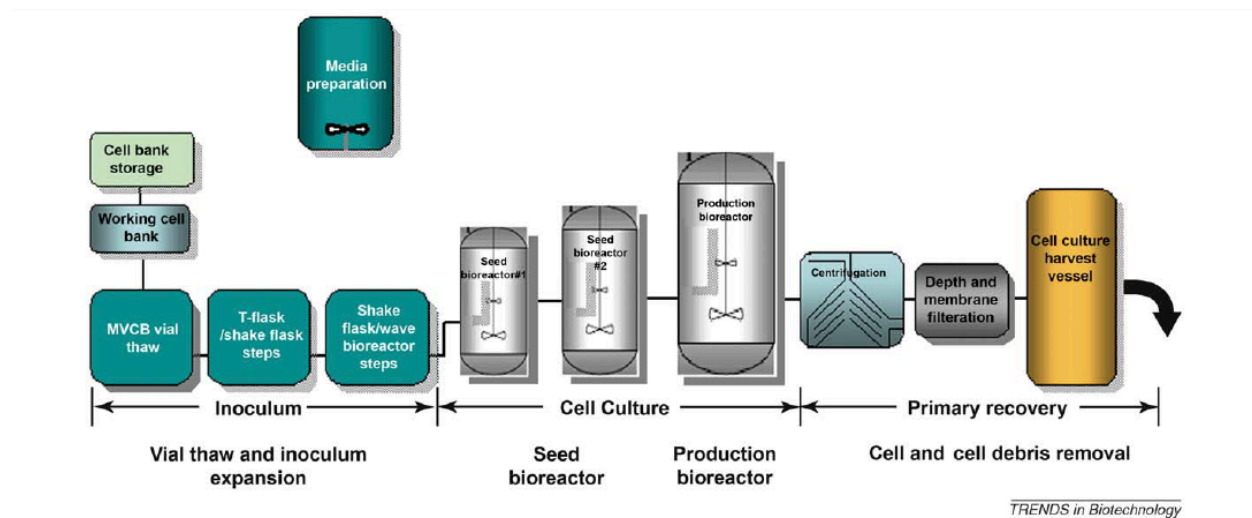
Figure 1.2. Upstream bioprocessing flowchart for recombinant IgG manufacturing

including cell culture production and harvest. Used with permission of Elsevier, from ref.

[14]; permission conveyed through Copyright Clearance Center, Inc.

1.3.2. Harvest and Purification

After CHO cell production, therapeutic antibodies must be harvested from the cell

culture broth and purified to yield a product that is safe to administer to patients. The

harvest and purification part of the manufacturing bioprocess is referred to as the

"downstream" component. Antibodies are conveniently secreted by CHO cells

extracellularly, which precludes the need for cell lysis to obtain the product. Therefore,

harvesting antibodies from the cell culture broth involves a centrifugation unit operation

to separate cells and cellular debris from the supernatant, which contains the secreted

antibodies.[13]

Subsequent purification unit operations (**Figure 1.3**) most commonly include a

combination of affinity chromatography (i.e. Protein A), depth filtration, and multiple

polishing chromatography steps (cation exchange and anion exchange run in either

flow-through or bind-and-elute modes [15]).[13] These purification unit operations are multi-

purpose as they seek to 1) separate and enrich the therapeutic antibody fraction from

other protein and small molecule impurities in the cell culture supernatant and 2)

improve the product quality of the final antibody product (i.e. by removing undesired

host-cell protein impurities, reducing high molecular weight forms, or changing the

charge heterogeneity profile).[13, 15] The last step in a purification train usually consists of

a tangential flow filtration (TFF) unit operation, also known as ultrafiltration/diafiltration

(UFDF) unit operation, where the antibody is concentrated and buffer-exchanged into its

final formulation.
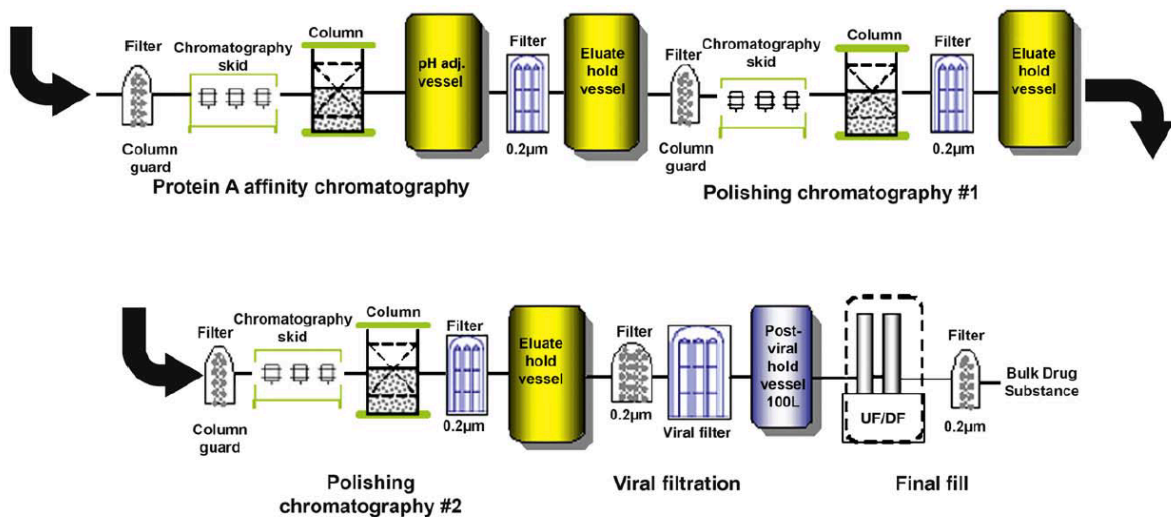
Figure 1.3. Downstream bioprocessing flowchart for recombinant IgG manufacturing including multiple chromatography unit operations and ultrafiltration / diafiltration (UF/DF). Used with permission of Elsevier, from ref. [14]; permission conveyed through Copyright Clearance Center, Inc.

1.3.3. Formulation

Formulation involves determining a suitable matrix of therapeutic antibody and excipients to enable long-term storage of the product and successful dosing of patients. A judicious choice of the target protein concentration (or strength) of the therapeutic antibody in the final formation includes weighing factors such as route of administration, dose, dosing frequency, and target patient population. Also, the excipients and their concentrations in a given formulation (which are often proprietary) help maintain the stability of the product under a variety of storage conditions; the excipients themselves, of course, must be safe to administer to patients. The effectiveness of a particular excipient composition can be assessed by determining the degradation susceptibility of

the formulated product to a variety of stresses that it may encounter during storage (i.e temperature excursions, freeze-thaw, light exposure, vibrational energy). A holistic understanding of the degradation susceptibility and real-time stability informs the appropriate shelf-life and expiry of the product and is a health authority expectation (ICH guideline Q5C).

1.3.4. Product Quality

Finally, ensuring a therapeutics' safety and efficacy through suitable control over product quality is an important commitment of biotechnology industries to patients and a health authority expectation. Product quality of therapeutic antibodies must be demonstrated and verified throughout the manufacturing process (via in-process controls) and in the final product. Demonstrating control of product quality hinges upon two complementary approaches: 1. analytical and bioanalytical characterization which includes in-process sample / lot release testing and extended characterization and 2. establishment of process consistency.

The complexity and heterogeneity of therapeutic antibody products yield a multi-dimensional medley of attributes that potentially impact safety and efficacy. The levels of potentially immunogenic species - such as high-molecular weight forms, exposure of immunogenic epitopes from loss of higher order structure, host cell protein impurities – is a product attribute that can pose a serious safety risk. Safety can also be compromised by attributes such as residual solvent levels, microbial bioburden, or other adventitious agent levels introduced during manufacturing. The efficacy of a therapeutic antibody can be modulated by product attributes that impact a given therapeutic's

particular mechanism of action; these attributes include but are not limited to fragmentation of the antibody, loss of higher order structure, or post-translational modifications such as deamidation, isomerization, oxidation, glycosylation, free thiols, etc. Attributes that impact the pharmacokinetic properties of a therapeutic antibody such as high mannose glycoforms can also modulate efficacy by changing a patient's exposure to a therapeutic.[16, 17]

The attributes that potentially impact safety and efficacy of a therapeutic antibody product are initially classified as potential critical quality attributes (pCQA).[18] As we gain more understanding of pCQAs and their impacts to patients, their status may be downgraded to non-critical quality attributes (non-CQA) or escalated to critical quality attributes (CQA).

1.4. Free Thiols and Antibody Product Quality

Free thiols, in the context of proteins, are unpaired cysteine residues that are neither capped nor disulfide bonded. Free thiols are prevalent in some proteins such as serum albumin and many different enzymes, where the cysteine is unpaired by design, with no natural vicinal cysteine disulfide partner. While pairs of vicinal cysteine residues on antibodies typically form disulfide bonds (**Figure 1.1**), free thiols can still be found in antibodies naturally. In special cases, free thiols may be intentionally introduced to antibodies (see 1.4.2.).

1.4.1. Free thiols: A Potentially Detrimental Modification

Cysteines are highly conserved amino acid residues among homologous proteins – second only to tryptophan residues. This highlights the importance of cysteines to a protein's structure and/or function. It is not surprising then that the presence of free thiols which were intended for disulfide bonding may have deleterious impacts to an antibody's product quality and are generally considered undesired post-translational modifications.

There are several potential deleterious effects of free thiols on antibodies: free thiols can lower thermal melting temperatures, which may have consequences for an antibody's stability profile;[19] free thiols, especially in the CH1 disulfide and to a lesser degree in the CH3 disulfide, have been implicated in agitation-induced aggregation in IgG2s;[20, 21] they can also render an IgG to be subpotent,[22] though this is not always the case [23]. For these reasons, free thiols are considered potential critical quality attributes for therapeutic antibodies.

The exact mechanism of free thiol origination in antibodies is not well-understood. Some plausible root causes of free thiols on antibodies include incomplete disulfide bond formation during antibody folding or the reduction of disulfide bonds after secretion extracellularly. Antibody folding is a complex process that is orchestrated in the endoplasmic reticulum by molecular chaperones, enzymes, rate-limiting proline isomerization reactions, autonomous folding of certain IgG domains, and disulfide bond formation.[24, 25] While disulfide bond formation can play an important role in catalyzing antibody folding by encouraging the hydrophobic cores to interact with one another and discouraging aggregation, it is not always required for proper antibody folding.[24]

Therefore, it is possible for an IgG with an unformed disulfide bond (i.e. free thiols) to pass the endoplasmic reticulum's quality control and get successfully secreted.[26] The speed with which a particular IgG domain folds may also impact the propensity for incomplete disulfide formation. Once secreted, the IgG is subject to the extracellular conditions including the redox environment and redox-active enzymes,[27-29] which may present additional opportunities to form free thiols.

1.4.2. Free Thiols: A Useful Modification

However, not all free thiols have deleterious effects. On the contrary, the presence of free thiols on proteins can be advantageous for bioconjugation purposes. For example, free thiols can be used to conjugate antibodies to a variety of partners such as cytotoxic drugs, radioimaging agents,[30] affinity tags, fluorescent probes, peptides etc. One method for deliberately introducing free thiols into antibodies is selectively reducing antibody interchain disulfide bonds, liberating two free thiols per reduced disulfide bond, using stoichiometric amounts of TCEP; this approach was used in the manufacture of two FDA-approved antibody-drug conjugate therapies, Adcetris and Polivy. Alternatively, unpaired cysteines can also be genetically engineered into antibody sequences[31, 32] and even more exotic methods for incorporating free thiols into antibodies have been reported previously.[33]

1.5. Free Thiol Properties and Reactivity

1.5.1. Properties

pK$_a$. An unpaired cysteine can exist as the protonated thiol (R-SH) or the deprotonated thiolate (R-S⁻). The expected acid-base equilibria of thiol to thiolate at any given pH is dependent on the particular cysteine's pK$_a$ and governed by the Henderson-Hasselbalch equation:

$$pH = pK_a + \log \left(\frac{[R-S^-]}{[R-SH]}\right)$$

where $[R-S^-]$ and $[R-SH]$ represent the concentrations of the thiolate and thiol, respectively. While a cysteine molecule free in solution has a pK$_a$ ~ 8.5,[34] the pK$_a$ of a cysteine in a protein is modulated significantly by the surrounding microenvironment (i.e. position in an alpha helix,[35] hydrogen bonding from spatially adjacent amino acids in the 3D structure, presence of vicinal aromatic groups).

Redox potential. Cysteines are also electrochemically active molecules. A common electrochemical reaction for unpaired cysteines is their oxidation with vicinal cysteines (or free cysteine and glutathione in solution) to form disulfide or mixed disulfide bonds. The redox equilibria for each pair of reduced cysteine and oxidized form can be estimated by the Nernst equation:

$$\mathcal{E} = \mathcal{E}° - \frac{RT}{nF}\ln (Q)$$

where $\mathcal{E}$ is the half-cell reduction potential, $\mathcal{E}°$ is the half-cell standard reduction potential, R is the universal gas constant, T is the temperature, n is the number of electrons involved in the redox reaction, F is the Faraday's constant, and Q is the mass action expression. As a frame of reference, the cysteine / cystine (in solution) redox pair

have a half-cell reduction potential of approximately -220 mV (pH 7, 25 °C),[36] but

reduction potentials of cysteines on proteins will depend on their microenvironment and

the particular cysteine's pKa.[37, 38] A detailed treatment of the determination of standard

reduction potentials for thiol redox pairs can be found elsewhere.[36-38]

1.5.2. Example Reactions

Free thiols can react efficiently with electrophiles, oxidants, and can bind efficiently to

various metals. Below are a few example thiol reactions that were utilized in our studies.

<u>Thiol-Michael Addition with Maleimides</u>. The Michael addition reaction, which can be

broadly characterized as the nucleophilic addition reaction into an α,β-unsaturated

carbonyl in the presence of a catalyst, was first described by Arthur Michael in the

1880's. The thiol-Michael addition is a subcategory of this reaction where the

nucleophile is a thiol, and among the α,β-unsaturated substrates that can participate in

the thiol-Michael addition reactions, substrates that contain maleimides are the most

widely known and utilized. One of the defining features of the thiol-Michael addition with

maleimides is it can achieve high product yields under a wider range of pH (including as

low as pH 5) and with a greater level of specificity than typical thiol nucleophilic

reactions – though these benefits may come at the expense of the stability of the newly

formed bond. The facile reaction conditions and reaction specificity have led some to

refer to thiol-Michael addition with maleimides as the earliest "click" chemistry reaction.

Nucleophilic Attack of Alkyl-Halides. Another reaction that is commonly used is the SN2 nucleophilic attack of alkyl-halides, such as iodoacetic acid or iodoacetamide, by thiols. These reactions lead to the displacement of the halide leaving group by the thiol and the formation of a new sulfur-carbon bond, which is considered irreversible. The major consideration here is that thiol reactivity in the context of SN2 reactions heavily depends on the thiolate/thiol equilibrium as thiolates can react $\sim10^{10}$-fold faster than their corresponding protonated thiols.[39]

Thiol Exchange with Disulfides. Thiols can attack an existing disulfide bond, cleaving it and forming a different disulfide bond in its place. One of the important factors that govern thiol exchange reactions between free thiols and disulfides is the strength of the cleaved disulfide bond relative to that of the formed disulfide bond. The strength of a disulfide bond can be characterized by its bond dissociation energy (BDE). Disulfides between two cysteine molecules and other dialkyl disulfides have fairly constant BDE hovering around 70 kcal/mol. Interestingly, diphenyl disulfides have BDE that are roughly 1/3 that of dialkyl disulfides. One compelling explanation for the dramatically lower bond strength for the former is resonance stabilization of the arenethiyl radical.[40] The dramatically lower BDE for diphenyl disulfides helps explain how DTNB, the Ellman's reagent, undergoes rapid exchange with free thiols. Other factors that can contribute to the propensity and rate of a thiol exchange reaction with a disulfide bond include steric, electrochemical, and pK_a effects.[39]

<u>Oxidation with Other Thiols to Form Disulfides</u>. Thiols can participate in oxidation reactions with small molecule thiol substrates such as free cysteine or glutathione to form mixed disulfides. Thiols on protein cysteines can also oxidize with vicinal protein cysteines to form canonical disulfide bonds, or oxidize with other protein cysteines to form shuffled disulfide bonds.

1.6.   Overview of Thesis

Ensuring product quality during the biomanufacturing of therapeutic antibodies is paramount to delivering safe and efficacious therapeutics to patients. One attribute that could influence a therapeutic antibody's product quality is the free thiol, which is an interesting functional group in the biological context due to its nucleophilic and/or redox character, and its involvement in post-translational modifications. This thesis aggregates three studies that involve free thiols and the product quality of therapeutic antibodies.

In Chapter 2, we probe the reoxidation of free thiols on IgG1 therapeutic antibodies after intravenous administration in a non-clinical rat model. *In vivo* biotransformation of thirty-five free thiol sites in total (7 disulfide pairs in VL, CL, VH, CH1, HH, CH2, CH3 domains across 5 therapeutic antibodies) were monitored after immunoaffinity purification using a denaturing differential isotopic tagging procedure coupled with LC-MS of tryptic digests. Our results show that the kinetics of *in vivo* free thiol reoxidation is a molecule- and site-specific property. We also show that a free thiol's reoxidation propensity *in vivo* is positively associated with its solvent accessibility. The data and discussion presented in Chapter 2 shed valuable insights into the *in vivo*

fate of free thiols in several recombinant IgG1s and its implications for free thiols as a product quality attribute in therapeutic antibody products.

In Chapter 3, we re-examine the Ellman's method, which is the classic optical method for free thiol detection. If not for its high limits of quantitation, the Ellman's method would be well suited for routinely monitoring free thiol content in therapeutic antibodies. We demonstrate that adding an incubation step with the fluorogenic probe methyl maleimidobenzochromenecarboxylate (MMBC) at the end of the Ellman's method effectively transduces the UV absorption signal into a fluorescent signal, and improves the quantitation limits of the Ellman's method by approximately 4-fold, even with a 2-fold dilution due to MMBC addition. We demonstrate the general usefulness of the augmented method, which we coined the Fluorescent Ellman's method, by using it to determine free thiol content in a variety of antibody therapeutics.

In Chapter 4, we pivot to discuss a host cell protein which co-purified with a Genentech therapeutic antibody. We interrogate the host cell protein-antibody interaction that mediates co-purification. One of the interesting aspects of this study is that the host cell protein contains a free thiol. Initially, the free thiol on the host cell protein leads to confounding experimental results by forming a non-representative disulfide-mediated complex with the therapeutic antibody. However, we leverage the free thiol in later experiments to site-specifically conjugate an affinity handle to the host cell protein, enabling specific pulldown experiments where we interrogated the host cell protein-antibody interaction.

1.7. References

1. Gonzalez-Quintela, A.; Alende, R.; Gude, F.; Campos, J.; Rey, J.; Meijide, L. M.; Fernandez-Merino, C.; Vidal, C., Serum levels of immunoglobulins (IgG, IgA, IgM) in a general adult population and their relationship with alcohol consumption, smoking and common metabolic abnormalities. *Clin Exp Immunol* **2008,** *151* (1), 42-50.
2. Vidarsson, G.; Dekkers, G.; Rispens, T., IgG subclasses and allotypes: from structure to effector functions. *Front Immunol* **2014,** *5*, 520.
3. Liu, H.; May, K., Disulfide bond structures of IgG molecules: structural variations, chemical modifications and possible impacts to stability and biological function. *MAbs* **2012,** *4* (1), 17-23.
4. Wypych, J.; Li, M.; Guo, A.; Zhang, Z.; Martinez, T.; Allen, M. J.; Fodor, S.; Kelner, D. N.; Flynn, G. C.; Liu, Y. D.; Bondarenko, P. V.; Ricci, M. S.; Dillon, T. M.; Balland, A., Human IgG2 antibodies display disulfide-mediated structural isoforms. *J Biol Chem* **2008,** *283* (23), 16194-205.
5. Liu, Y. D.; Chen, X.; Enk, J. Z.; Plant, M.; Dillon, T. M.; Flynn, G. C., Human IgG2 antibody disulfide rearrangement in vivo. *J Biol Chem* **2008,** *283* (43), 29266-72.
6. Cymer, F.; Beck, H.; Rohde, A.; Reusch, D., Therapeutic monoclonal antibody N-glycosylation - Structure, function and therapeutic potential. *Biologicals* **2018,** *52*, 1-11.
7. Shields, R. L.; Namenuk, A. K.; Hong, K.; Meng, Y. G.; Rae, J.; Briggs, J.; Xie, D.; Lai, J.; Stadlen, A.; Li, B.; Fox, J. A.; Presta, L. G., High resolution mapping of the binding site on human IgG1 for Fc gamma RI, Fc gamma RII, Fc gamma RIII, and FcRn and design of IgG1 variants with improved binding to the Fc gamma R. *J Biol Chem* **2001,** *276* (9), 6591-604.
8. Jefferis, R.; Lund, J., Interaction sites on human IgG-Fc for FcgammaR: current models. *Immunol Lett* **2002,** *82* (1-2), 57-65.
9. Shields, R. L.; Lai, J.; Keck, R.; O'Connell, L. Y.; Hong, K.; Meng, Y. G.; Weikert, S. H.; Presta, L. G., Lack of fucose on human IgG1 N-linked oligosaccharide improves binding to human Fcgamma RIII and antibody-dependent cellular toxicity. *J Biol Chem* **2002,** *277* (30), 26733-40.
10. Grilo, A. L.; Mantalaris, A., The Increasingly Human and Profitable Monoclonal Antibody Market. *Trends Biotechnol* **2019,** *37* (1), 9-16.
11. Lu, R. M.; Hwang, Y. C.; Liu, I. J.; Lee, C. C.; Tsai, H. Z.; Li, H. J.; Wu, H. C., Development of therapeutic antibodies for the treatment of diseases. *J Biomed Sci* **2020,** *27* (1), 1.
12. Strohl, W. R., Current progress in innovative engineered antibodies. *Protein Cell* **2018,** *9* (1), 86-120.
13. Shukla, A. A.; Wolfe, L. S.; Mostafa, S. S.; Norman, C., Evolving trends in mAb production processes. *Bioeng Transl Med* **2017,** *2* (1), 58-69.
14. Shukla, A. A.; Thommes, J., Recent advances in large-scale production of monoclonal antibodies and related proteins. *Trends Biotechnol* **2010,** *28* (5), 253-61.

15.   Gagnon, P., Technology trends in antibody purification. *J Chromatogr A* **2012,** *1221*, 57-70.

16.   Goetze, A. M.; Liu, Y. D.; Zhang, Z.; Shah, B.; Lee, E.; Bondarenko, P. V.; Flynn, G. C., High-mannose glycans on the Fc region of therapeutic IgG antibodies increase serum clearance in humans. *Glycobiology* **2011,** *21* (7), 949-59.

17.   Alessandri, L.; Ouellette, D.; Acquah, A.; Rieser, M.; Leblond, D.; Saltarelli, M.; Radziejewski, C.; Fujimori, T.; Correia, I., Increased serum clearance of oligomannose species present on a human IgG1 molecule. *MAbs* **2012,** *4* (4), 509-20.

18.   Alt, N.; Zhang, T. Y.; Motchnik, P.; Taticek, R.; Quarmby, V.; Schlothauer, T.; Beck, H.; Emrich, T.; Harris, R. J., Determination of critical quality attributes for monoclonal antibodies using quality by design principles. *Biologicals* **2016,** *44* (5), 291-305.

19.   Mahler, H. C.; Friess, W.; Grauschopf, U.; Kiese, S., Protein aggregation: pathways, induction factors and analysis. *J Pharm Sci* **2009,** *98* (9), 2909-34.

20.   Brych, S. R.; Gokarn, Y. R.; Hultgen, H.; Stevenson, R. J.; Rajan, R.; Matsumura, M., Characterization of antibody aggregation: role of buried, unpaired cysteines in particle formation. *J Pharm Sci* **2010,** *99* (2), 764-81.

21.   Huh, J. H.; White, A. J.; Brych, S. R.; Franey, H.; Matsumura, M., The identification of free cysteine residues within antibodies and a potential role for free cysteine residues in covalent aggregation because of agitation stress. *J Pharm Sci* **2013,** *102* (6), 1701-1711.

22.   Harris, R. J., Heterogeneity of recombinant antibodies: linking structure to function. *Dev Biol (Basel)* **2005,** *122*, 117-27.

23.   Zhang, T.; Zhang, J.; Hewitt, D.; Tran, B.; Gao, X.; Qiu, Z. J.; Tejada, M.; Gazzano-Santoro, H.; Kao, Y. H., Identification and characterization of buried unpaired cysteines in a recombinant monoclonal IgG1 antibody. *Anal Chem* **2012,** *84* (16), 7112-23.

24.   Feige, M. J.; Hendershot, L. M.; Buchner, J., How antibodies fold. *Trends Biochem Sci* **2010,** *35* (4), 189-98.

25.   Vinci, F.; Catharino, S.; Frey, S.; Buchner, J.; Marino, G.; Pucci, P.; Ruoppolo, M., Hierarchical formation of disulfide bonds in the immunoglobulin Fc fragment is assisted by protein-disulfide isomerase. *J Biol Chem* **2004,** *279* (15), 15059-66.

26.   Zhang, W.; Czupryn, M. J., Free sulfhydryl in recombinant monoclonal antibodies. *Biotechnol Prog* **2002,** *18* (3), 509-13.

27.   Trexler-Schmidt, M.; Sargis, S.; Chiu, J.; Sze-Khoo, S.; Mun, M.; Kao, Y. H.; Laird, M. W., Identification and prevention of antibody disulfide bond reduction during cell culture manufacturing. *Biotechnol Bioeng* **2010,** *106* (3), 452-61.

28.   Kao, Y. H.; Hewitt, D. P.; Trexler-Schmidt, M.; Laird, M. W., Mechanism of antibody reduction in cell culture production processes. *Biotechnol Bioeng* **2010,** *107* (4), 622-32.

29. Gurjar, S. A.; Wheeler, J. X.; Wadhwa, M.; Thorpe, R.; Kimber, I.; Derrick, J. P.; Dearman, R. J.; Metcalfe, C., The impact of thioredoxin reduction of allosteric disulfide bonds on the therapeutic potential of monoclonal antibodies. *J Biol Chem* **2019,** *294* (51), 19616-19634.

30. Tinianow, J. N.; Gill, H. S.; Ogasawara, A.; Flores, J. E.; Vanderbilt, A. N.; Luis, E.; Vandlen, R.; Darwish, M.; Junutula, J. R.; Williams, S. P.; Marik, J., Site-specifically 89Zr-labeled monoclonal antibodies for ImmunoPET. *Nucl Med Biol* **2010,** *37* (3), 289-97.

31. Shen, B. Q.; Xu, K.; Liu, L.; Raab, H.; Bhakta, S.; Kenrick, M.; Parsons-Reponte, K. L.; Tien, J.; Yu, S. F.; Mai, E.; Li, D.; Tibbitts, J.; Baudys, J.; Saad, O. M.; Scales, S. J.; McDonald, P. J.; Hass, P. E.; Eigenbrot, C.; Nguyen, T.; Solis, W. A.; Fuji, R. N.; Flagella, K. M.; Patel, D.; Spencer, S. D.; Khawli, L. A.; Ebens, A.; Wong, W. L.; Vandlen, R.; Kaur, S.; Sliwkowski, M. X.; Scheller, R. H.; Polakis, P.; Junutula, J. R., Conjugation site modulates the in vivo stability and therapeutic activity of antibody-drug conjugates. *Nat Biotechnol* **2012,** *30* (2), 184-9.

32. Junutula, J. R.; Raab, H.; Clark, S.; Bhakta, S.; Leipold, D. D.; Weir, S.; Chen, Y.; Simpson, M.; Tsai, S. P.; Dennis, M. S.; Lu, Y.; Meng, Y. G.; Ng, C.; Yang, J.; Lee, C. C.; Duenas, E.; Gorrell, J.; Katta, V.; Kim, A.; McDorman, K.; Flagella, K.; Venook, R.; Ross, S.; Spencer, S. D.; Lee Wong, W.; Lowman, H. B.; Vandlen, R.; Sliwkowski, M. X.; Scheller, R. H.; Polakis, P.; Mallet, W., Site-specific conjugation of a cytotoxic drug to an antibody improves the therapeutic index. *Nat Biotechnol* **2008,** *26* (8), 925-32.

33. Alves, N. J.; Mustafaoglu, N.; Bilgicer, B., Conjugation of a reactive thiol at the nucleotide binding site for site-specific antibody functionalization. *Bioconjug Chem* **2014,** *25* (7), 1198-202.

34. Poole, L. B., The basics of thiols and cysteines in redox biology and chemistry. *Free Radic Biol Med* **2015,** *80*, 148-57.

35. Kortemme, T.; Creighton, T. E., Ionisation of cysteine residues at the termini of model alpha-helical peptides. Relevance to unusual thiol pKa values in proteins of the thioredoxin family. *J Mol Biol* **1995,** *253* (5), 799-812.

36. Jocelyn, P. C., The standard redox potential of cysteine-cystine from the thiol-disulphide exchange reaction with glutathione and lipoic acid. *Eur J Biochem* **1967,** *2* (3), 327-31.

37. Schafer, F. Q.; Buettner, G. R., Redox environment of the cell as viewed through the redox state of the glutathione disulfide/glutathione couple. *Free Radic Biol Med* **2001,** *30* (11), 1191-212.

38. Mirzahosseini, A.; Noszal, B., Species-Specific Standard Redox Potential of Thiol-Disulfide Systems: A Key Parameter to Develop Agents against Oxidative Stress. *Sci Rep* **2016,** *6*, 37596.

39. Winther, J. R.; Thorpe, C., Quantification of thiols and disulfides. *Biochim Biophys Acta* **2014,** *1840* (2), 838-46.

40. Oae, S., *Organic Sulfur Chemistry: Structure and Mechanism*. 1st ed.; CRC press: Boca Raton, FL, 1992.

Chapter 2.   In Vivo Transformation Kinetics of Free Thiols in Multiple Domains of IgG1 Antibodies in Rats

2.1. Introduction

Free thiols in therapeutic mAbs are generally undesired post-translational modifications. Certain cell culture parameters, such as copper sulfate concentration, have been shown to modulate the extent of free thiol formation.[1] However, the governing mechanism driving free thiol formation is not fully understood and, to date, a full-length monoclonal antibody (mAb) absent of any free thiols has not been successfully expressed. In fact, recombinant IgG1s, which contain 12 intrachain and 4 interchain disulfide bonds (**Figure 2.1**), usually have low (<5% site occupancy) yet detectable free thiols in each of its disulfide bonds.[2-4] In rare cases, considerably elevated levels of free thiols (between 5-30% site occupancy) have been reported in recombinant IgGs.[5-9]

Free thiols in constant domains of mAbs do not pose a likely risk from a safety and immunogenicity standpoint because healthy human subjects have circulating endogenous IgGs with free thiols ranging from 0.57 to 3.78% per site.[4, 10] However, free thiols in variable domains of mAbs could create a neoepitope or otherwise cause immunogenicity, for example by affecting antigen presentation.[11] Additionally, free thiols can lower thermal melting temperatures of mAbs and may affect mAb's stability.[12] Free thiols, especially in the CH1 disulfide and to a lesser degree in the CH3 disulfide, have been implicated in agitation-induced aggregation in IgG2s.[4, 13] They can also render a mAb to be subpotent,[6] although in other cases free thiol-containing mAbs were found to be equally potent,[7] and their impacts to mAb pharmacokinetics are unclear. For these reasons, free thiols are considered potential critical quality attributes.
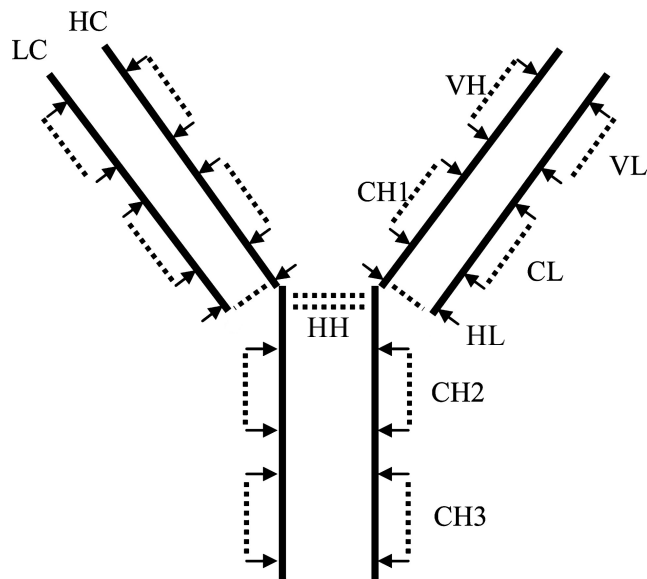
Figure 2.1. Intrachain and interchain disulfide bonds in an IgG1. There are two distinct interchain disulfide bonds between the heavy chains but they are both annotated "HH" for simplicity. Adapted with permission from ref. [14]. Copyright 2010 American Chemical Society.

To determine the criticality of free thiols to product quality, a risk-based assessment is performed. The risk assessment of a quality attribute usually entails generating a sample sufficiently enriched in the attribute of interest (typically >50%), either by inducing it via stress conditions, inducing it via manufacturing process perturbations, or fraction collecting it using a suitable separation technique. The sample can then be dosed in a pharmacokinetic study and/or subjected to various *in vitro* tests to assay for antigen binding competency, effector functions, FcRn affinity, etc., in order to establish the criticality of the quality attribute. However, enrichment of free thiol-containing mAbs (in a biologically active form) – especially when the free thiols occur at intrachain disulfides - is notoriously difficult and sometimes impossible using either

conventional stress conditions or separation techniques. Therefore, a detailed

understanding of the physiological outcomes of mAb free thiols *in vivo* post-

administration is valuable to determine the criticality of free thiol.

Ouellette et al previously reported the rapid transformation (~1 hour) of a VH free

thiol of a mAb administered to rats.[5] However, their study was limited to monitoring the

transformation of one site of elevated free thiol content in one mAb, and it was unclear

how translatable and broadly applicable their findings would be for other mAb molecules

and other free thiol sites. Liu et al more recently demonstrated that elevated VH free

thiols but not VL free thiols on mAbs reoxidized in an *in vitro* redox continuous flow

system, which was designed to mimic redox conditions in human circulation,[15] but these

findings needed to be verified *in vivo*. In our study, we expanded the available *in vivo*

dataset with an additional five mAbs and elevated free thiols (> 5% SH) in not only VH

but also VL and CH2 domains. We intravenously dosed a diverse panel of IgG1 mAbs

with various levels of free thiols in rats, recovered the mAbs at several time points post-

administration, and interrogated their site-specific free thiol levels using a mass

spectrometry method similar to that published by Robotham et al.[3] The data was used

to further illuminate the issue of mAb free thiol criticality. To our knowledge, this is the

first report of *in vivo* kinetics of site-specific free thiol transformation from such a diverse

panel of mAbs.

2.2. Materials and Methods

2.2.1. Materials

The five recombinant IgGs (mAb1-5) used in this study were expressed and purified in-house (Genentech, Inc., South San Francisco, CA and Hoffman-La Roche, Inc., Basel, Switzerland), and are listed in **Table 2.1** (mAb4 and mAb5 used in our study, respectively, are the same as mAb5 and mAb2 used the Liu et al study [15]). Healthy rat plasma for the in vitro spiking study was purchased from BioIVT (Westbury, NY). Goat anti-hu IgG (H+L) antibodies used to affinity purify the recombinant IgGs from the rat plasma were obtained from Jackson Immunoresearch (West Grove, PA). Tosylactivated MyOne Dynabeads, Dynamag-2/Dynamag-96 magnets for the magnetic pulldowns, BOLT ™ 4-12% BisTris mini gels, NuPAGE® MES SDS running buffer (20×) were purchased from Life Technologies (Waltham, MA). Precision Plus Protein™ unstained protein standard was purchased from Bio-Rad (Hercules, CA). N-d5-ethyl maleimide (d5-NEM) was purchased from Cambridge Isotope Laboratories (Tewksbury, MA). Bondbreaker tris(2-carboxyethyl)phosphine (TCEP) and N-ethyl maleimide (NEM) were purchased from Thermo Scientific (Waltham, MA). Guanidine-HCl and YM-30 centrifugal filter units were purchased from EMD Millipore (Burlington, MA). Sodium chloride, sodium phosphate, HEPES, and L-cysteine were purchased from Sigma (St. Louis, MO). Mass spectrometry-grade trypsin was acquired from Promega (Madison, WI).

Table 2.1. Select properties of the recombinant IgGs (mAb1-5) used in this study. mAb3 is a one-armed antibody, which has one less Fab relative to a typical full-length antibody. mAb4 and mAb5, respectively, are the same as mAb5 and mAb2 used the Liu et al study.[15]

Molecule	Format	Molecular Weight	Expression System	Fc Glycosylation	Domain w/ Elevated Free Thiol
mAb1	Full length IgG1	~148 kDa	CHO	yes	VH
mAb2	Full length IgG1	~148 kDa	CHO	yes	None
mAb3	One-armed IgG1	~99 kDa	E.coli	no	CH2
mAb4	Full length IgG1	~148 kDa	CHO	yes	VL
mAb5	Full length IgG1	~149 kDa	CHO	yes	VH

2.2.2. Preparation of rat plasma samples

Five recombinant IgGs (mAb1-5) were administered to different female Wistar rats (Covance Laboratories, Harrogate North Yorkshire, England) as a single intravenous bolus of 50 mg/kg. Each molecule was administered in biological triplicate for a total of 15 rats. Three hundred microliters of blood were collected from each rat at various timepoints ranging from 5 minutes to 168 hours post-dose. Blood samples were collected in K_2EDTA tubes, gently mixed on ice, and centrifuged at 1800 g for 10 minutes at 4 °C to yield 150 μL of plasma. Plasma samples were shipped at -20 °C and stored at -70 °C upon receiving. The recombinant IgGs were recovered from the plasma samples via immunoaffinity magnetic bead pulldowns as described below and analyzed by (denaturing) differential alkylation followed by peptide mapping LC-MS as described

below. The recombinant IgGs recovered from select timepoints (5 min, 48 hour, and 168 hour) were also analyzed by intact mass LC-MS.

2.2.3. Preparation of spiked rat plasma samples

In order to examine the suitability of the pulldown method used in this study and to establish t_0 free thiol values, in vitro samples were prepared by spiking 170 μg/mL IgG (mAb1-5) into healthy rat plasma (an unspiked healthy rat plasma sample was included as a negative control). The recombinant IgGs were recovered from the spiked plasma samples using immunoaffinity magnetic bead pulldowns as described below and the purity of the pulldowns was assessed using SDS-PAGE. The recovered IgGs were also analyzed by (denaturing) differential alkylation followed by peptide mapping LC-MS as described below to establish t_0 free thiol values.

In brief, SDS-PAGE was performed by first neutralizing 10 μL of elution samples with 1M HEPES base. Neutralized samples – as well as an unspiked healthy rat plasma sample that had not been subjected to immunoaffinity purification (positive control) – were incubated 1:1 with 2x Laemelli buffer at 70 °C for 10 minutes. Proteins were separated on a 4-12% BisTris gel in a XCell SureLock® Mini-Cell electrophoresis chamber (Life Technologies, Waltham, MA) according to manufacturer's instructions using NuPAGE® MES SDS running buffer. 10 μL of Precision Plus Protein™ unstained protein standard was included as the ladder.

2.2.4. Anti-human antibody coupling and immunoaffinity magnetic bead pulldowns from rat plasma

Anti-hu IgG (H+L) antibodies were conjugated to Tosylactivated MyOne Dynabeads per manufacturer's protocol. The anti-hu IgG beads were then stored in 0.1% BSA, 0.1 M Na_2HPO_4, 0.15 M NaCl, 0.05% polysorbate 20, pH 7.4 and kept at 2 – 8 °C for up to 4 months. To perform immunoaffinity magnetic bead pulldowns, 75 μL of rat plasma samples were gently mixed with 9 mg of anti-hu IgG beads (pre-equilibrated with wash buffer: 0.1 M Na_2HPO_4, 0.15 M NaCl, 0.05% polysorbate 20, pH 7.4) along with 300 μL of wash buffer for 1.5 hours at RT. After settling the beads by applying a magnet, the supernatant was exchanged with wash buffer. This step of settling the beads and exchanging the supernatant was repeated again with wash buffer and once with MilliQ water. In order to minimize carryover from proteins adsorbed onto the walls of the sample vessel, the beads were transferred to a new sample vessel prior to elution. The recombinant IgGs were eluted by vortexing the beads for 10 minutes at RT in 50 μL of 1% formic acid in water.

2.2.5. (Denaturing) differential NEM and d5-NEM alkylation

To determine site-specific free thiol content, a denaturing differential NEM and d5-NEM alkylation procedure was used. While this procedure was conceptually similar to the method published by Robotham and Kelly,[3] the implementation was different and is graphically represented in **Figure 2.2**. In brief, the affinity purified IgG (50 μL) was denatured by dissolving 48 mg of solid guanidine-HCl. After adding 100 mM

CH$_3$COONa and titrating the pH to ~6 with 1 N NaOH (100 μL total reaction volume),

the samples were incubated with 5 mM NEM at 37 °C for 2 hours to alkylate any free

thiols. Excess NEM was quenched by incubating 6.4 mM cysteine at 37 °C for 15

minutes. Then, samples were reduced by treating with 8.7 mM TCEP for 30 minutes at

37 °C, and the thiols liberated from reduced disulfide bonds were differentially alkylated

with 16.2 mM d5-NEM at 37 °C for 2 hours. Excess d5-NEM was quenched with 16.9

mM cysteine at 37 °C for 15 minutes.
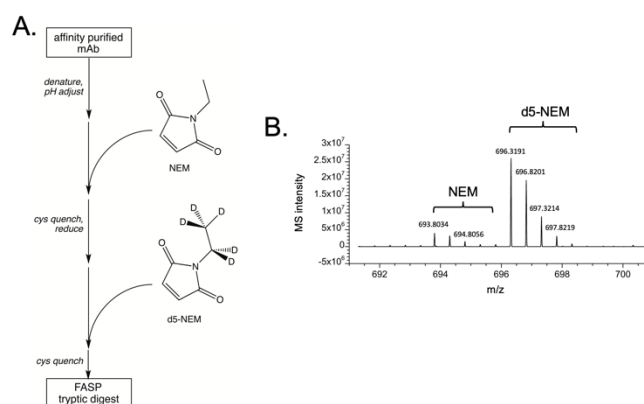
Figure 2.2. A) Differential NEM and d5-NEM alkylation workflow under denaturing

conditions that enables site-specific free thiol quantitation. B) Mass spectrum depicting

the distinct mass features of an example peptide containing a free thiol (NEM) versus

the same peptide but liberated from a disulfide bond (d5-NEM).

2.2.6. (Native) differential NEM and d5-NEM alkylation of starting materials

To determine site-specific and solvent-accessible free thiol content, a native differential

NEM and d5-NEM alkylation procedure was used. Twenty-five micrograms of

recombinant IgG starting materials were diluted in 50 μL of 200 mM CH$_3$COONa buffer,

pH 5.5. Alkylation of free thiols under native conditions was performed by incubating

samples with 5 mM NEM for 2 hours at 37 °C. Excess NEM was quenched with 6.4 mM

cysteine for 15 minutes at 37 °C. After alkylating free thiols under native conditions,

samples were denatured by dissolving 48 mg of solid guanidine-HCl (100 μL total

reaction volume). The remaining steps (reduction, d5-NEM alkylation, cysteine

quenching excess d5-NEM) were identical to those described in the (denaturing)

differential alkylation procedure above.

2.2.7. Filter-assisted sample preparation (FASP)

The differentially alkylated samples were proteolytically digested with trypsin using an

adapted FASP procedure originally described by Wisniewski et al.[16] One hundred

microliters of differentially alkylated sample was loaded onto a YM-30 centrifugal filter

cartridge, centrifuged (14,000 g for 20 minutes), and the filtrate was discarded. The

cartridges were washed two times with 100 μL of digest buffer (100 μL of 100 mM

MOPS, 1 mM CaCl$_2$, pH 7.5) with a spin cycle (14,000 g for 10 minutes) after each

subsequent wash. With the retentate still in the filter unit, 100 μL of digest buffer was

added to the retentate and the sample was digested with 2 μg trypsin for 4 hours at 37

°C. After the digestion, the cartridges were transferred to new tubes and subjected to a

final spin cycle (14,000 g for 20 minutes) and the filtrate was collected for downstream

LC-MS peptide mapping analysis.

2.2.8. Peptide mapping LC-MS analysis

Five hundred nanograms of digested material was injected onto a Waters nanoAcquity

UHPLC system equipped with a trapping column (Waters CSH C18, 300 μm x 50 mm,

1.8 μm, Milford, MA), which was maintained at 61 °C and pre-equilibrated with 0.5%

solvent B (mobile phase A: 0.1% formic acid in water, mobile phase B: 0.1% formic acid

in acetonitrile). The samples were washed with 0.5% solvent B on the trapping column

at a flowrate of 5 μL/min for 6 minutes before diverting the flow to the analytical column

(Waters CSH C18, 300 μm x 100 mm, 1.8 μm, Milford, MA), which was maintained at 50

°C. The peptides were separated on the analytical column using a 5 minute linear

gradient from 1 to 13% solvent B followed by a 18 minute linear gradient from 13-35%

solvent B. The analytical column eluent was coupled to a Thermo Fusion Orbitrap

hybrid mass spectrometer (Waltham, MA) equipped with an ESI source. Mass spectra

from 200 to 2000 m/z were collected at 60,000 resolution using an electrospray voltage

of 3500 V and a source temperature of 275 °C. Extracted ion chromatograms (XIC)

using a 10 ppm window were generated using Skyline and exported results were

curated (reshape2 library) and graphed (ggplot2 library) using custom R scripts.

2.2.9. Quantitative analysis of site-specific free thiol levels

Denaturing differential NEM and d5-NEM tagging followed by peptide mapping analysis

yielded mass spectral features of free thiol cysteines distinct from originally disulfided

cysteines (**Figure 2.2B**).The free thiol site occupancy (%SH) was calculated for each

cysteine using the following relationship:

$$\%SH = \frac{A_{NEM}}{(A_{d5NEM} + A_{NEM})} \times 100$$

35

where A_{NEM} and A_{d5NEM} respectively depict the extracted ion chromatogram peak areas of peptides containing free thiol cysteines and the corresponding peptides containing liberated disulfided cysteines. The %SH values from cysteine pairs belonging to the same disulfide were averaged to yield a %SH value for each disulfide site (VL, CL, VH, CH1, HH, CH2, CH3). The %SH for HH represented the aggregate free thiol content on both HH interchain disulfide bonds; the two HH disulfide bonds reside on the same tryptic peptide, and as a result, free thiols on either disulfide bond yield indistinguishable species using the differential isotopically labeled workflow. %SH at the HL site was not quantified because the tryptic peptides corresponding to HL site were not observed, possibly eluting in the void volume.

2.2.10.   Intact LC-MS analysis

In order to examine the intact mass heterogeneity of the recovered therapeutics, 4 µL of select affinity purified timepoints (5 min, 48 hour, and 168 hour) were diluted with 40 µL of MilliQ water. One µg was then injected onto a Waters H-Class UHPLC system (Milford, MA) equipped with a reversed-phase PLRP-S column (Agilent, 2.1 x 150 mm, 8 µm, Santa Clara, CA), maintained at 70 °C and pre-equilibrated with 20% solvent B (mobile phase A: 0.1% formic acid in water, mobile phase B: 0.1% formic acid in acetonitrile). Proteins were eluted at a flowrate of 0.3 mL/min using a 1 minute linear gradient to 30% solvent B, followed by a 7 minute gradient to 42 % solvent B. The column was regenerated by washing for 1 minute with 95 % solvent B and by re-equilibrating for 5 minutes with 20 % solvent B. A switching valve was programmed to divert the LC eluent to waste for the first 4 minutes of the method and afterwards divert

to an ABSciex TTOF 5600 mass spectrometer (Toronto, Canada) equipped with an ESI

source for the remainder of the method. Mass spectra from 500 to 4000 m/z were

collected using an electrospray voltage of 5000 V, source temperature of 350 °C,

declustering potential of 70 V, and collisional energy of 10 V. Raw mass spectral data

were deconvoluted using the BioAnalyst suite in the PeakView software.

2.3.   Results

2.3.1. Immunoaffinity purification specificity from rat plasma

A specific, immunoaffinity purification procedure was successfully used to enrich

the therapeutic mAbs from a time course study of rat plasma samples. To establish the

efficiency of enrichment, mAbs 1-5 were spiked to a final concentration of 170 μg/mL

into rat plasma and subsequently recovered using immunoaffinity purification. **Figure**

2.3 shows the general size distribution by SDS-PAGE of the rat plasma (loaded neat)

compared to the immunoaffinity purified mAb-spiked rat plasma samples. While the lane

with neat rat plasma contains multiple bands corresponding to endogenous rat IgGs

(~150 kDa) and rat serum albumin (~ 60 kDa) among others, the lanes with

immunoaffinity purified samples each contain one prominent band of similar intensity

that corresponds to the molecular weights of the spiked mAb; mAb3 is an aglycosylated

antibody with a missing Fab fragment with a molecular weight ~99 kDa.
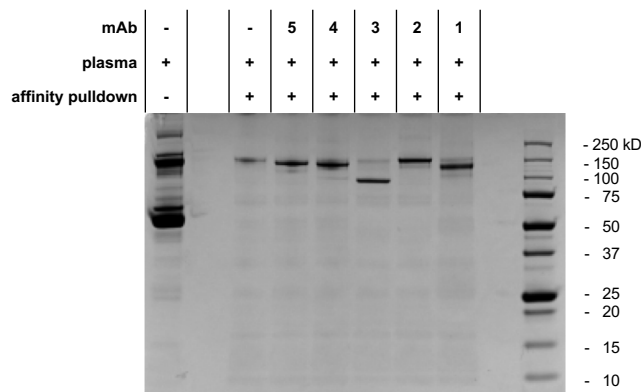
Figure 2.3. Specificity of immunoaffinity pulldowns by Coomassie-stained SDS-PAGE. mAb3 is a one-armed antibody (missing one Fab fragment) with a molecular weight ~99 kDa. Ladder (Precision Plus Protein™ unstained protein standard) is in the right-most lane.

2.3.2. In vivo changes in free thiol content across molecule and disulfide sites

The site-specific free thiol content of the immunopurified mAbs – either from the spiked rat plasma samples (t_0) or from the rat study – was subsequently interrogated using a denaturing differential isotope tagging strategy. We were able to track the site-specific %SH over time of all five mAbs in rats *in vivo* (**Figure 2.4**). For the free thiol sites that changed over time *in vivo* (in mAb1, mAb3, and mAb5), their transformation kinetics fit well to exponential decay models and the first order rate constants are listed in **Table 2.S1**. While all the monitored disulfide sites (in the 5 mAbs tested for this study) had a quantifiable %SH, the free thiols at a majority of these sites were remarkably stable *in vivo* (**Figure 2.4**). Among the minority of sites exhibiting >5% SH in the starting materials: a VL domain free thiol (mAb4) was also stable *in vivo*; two VH domain free thiols (mAb1/5) both decreased over time *in vivo*, albeit at different rates; a

CH2 domain free thiol (mAb3, aglycosylated) decreased over time *in vivo*. There was no obvious correlation between either initial %SH under denaturing conditions or free thiol location and the likelihood that free thiols would transform *in vivo*, highlighting that a free thiol's *in vivo* transformation might be molecule-specific.
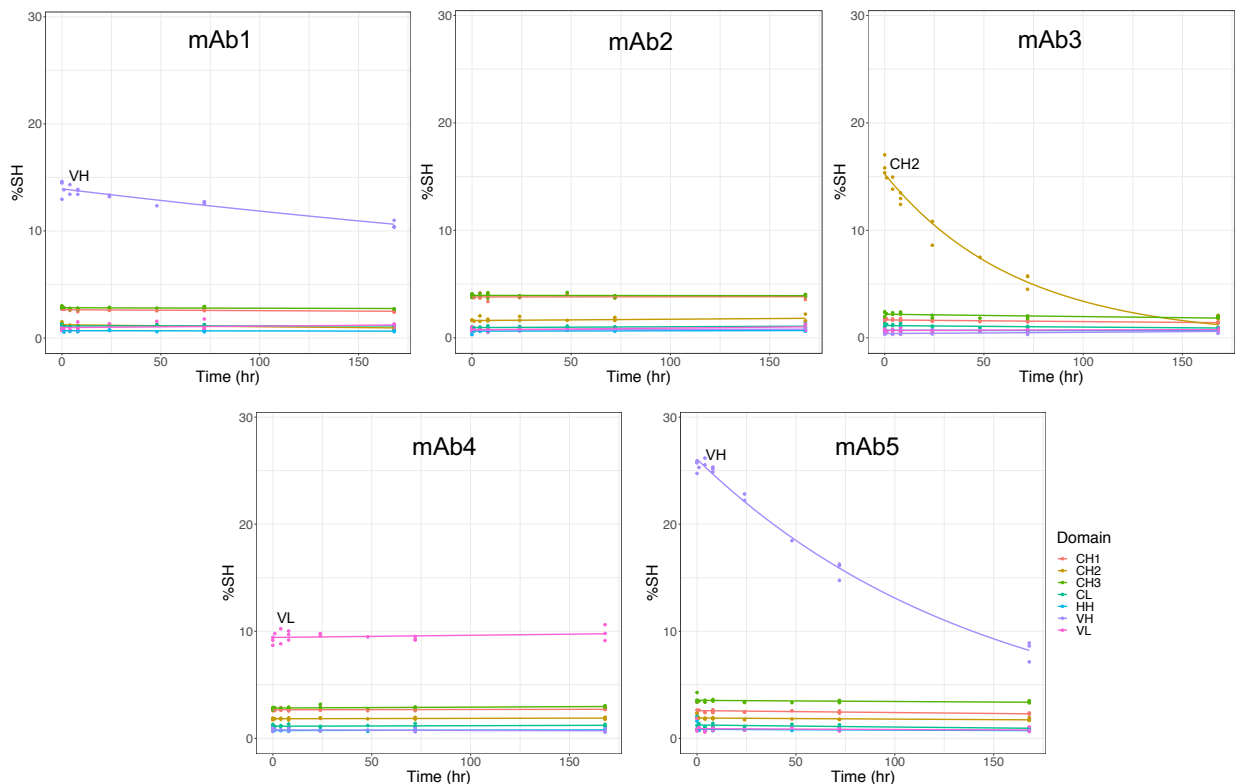
Figure 2.4. *In vivo* free thiol reoxidation kinetics in rats. Each plot represents one of the administered mAbs and shows the free thiol content (%SH under denaturing conditions) as a function of *in vivo* residence time. The colors within each plot correspond to different free thiol sites. Administered mAbs included molecules with elevated free thiols (>5%) in VH domain (mAb1 and mAb5), CH2 domain (mAb3), and VL domain (mAb4).

2.3.3. Intact mass heterogeneity at select timepoints

Select immunopurified timepoints were further analyzed via intact mass LC/MS to examine the mAb's overall mass heterogeneity and the possibility of mixed disulfide (i.e. cysteinylation, glutathionylation, albumin conjugation, etc.) formation as a predominant *in vivo* transformation pathway. Aside from reoxidation of free thiols to form canonical disulfide bonds, *in vivo* formation of mixed disulfides would also lower observed %SH values. The observed deconvoluted masses of immunopurified *in vivo* samples were
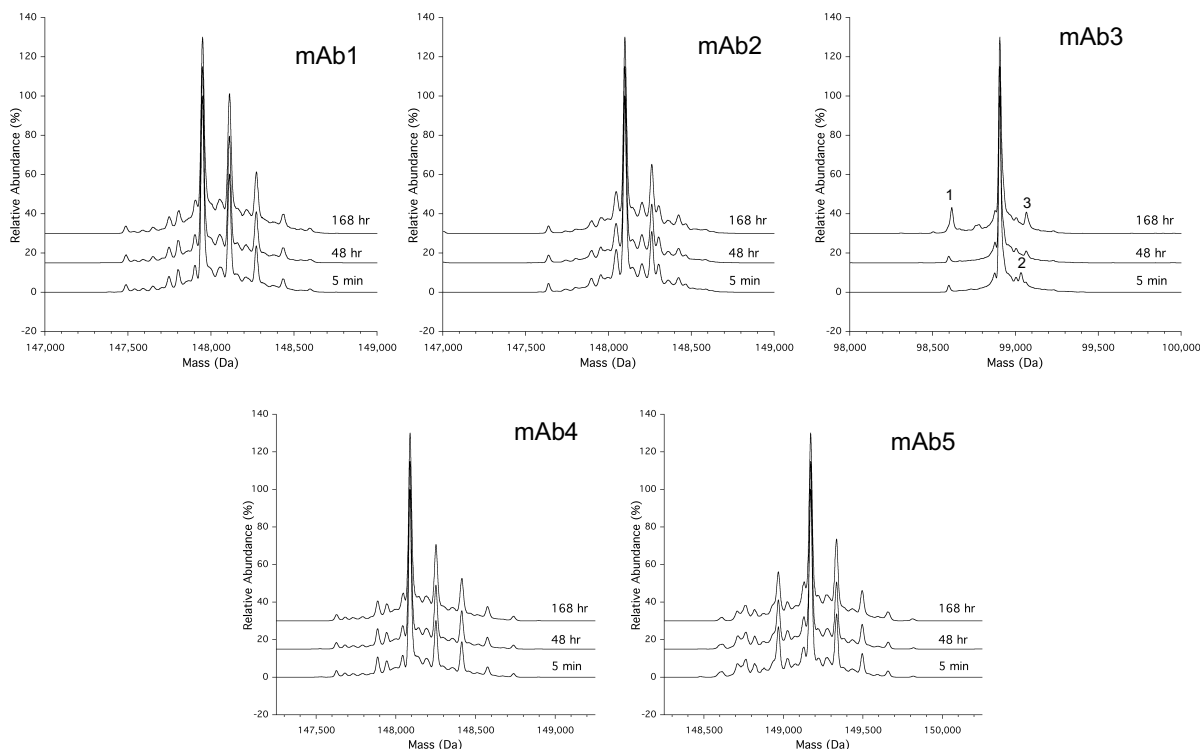
Figure 2.5. Deconvoluted mass profiles of mAb1-5 immunopurified from *in vivo* rat plasma samples at select timepoints (5 min, 48 hr, 168 hr). Peak labels "1", "2", and "3" on mAb3's mass profiles highlight masses that change intensities between the timepoints and correspond to -438, +191, and +234 Da modifications, respectively.

accurate to within 20 ppm of the theoretical masses for mAb1-5 and their associated Fc

glycoforms. The deconvoluted mass profiles of the 5 min, 48 hour, and 168 hour

timepoints appear superimposable for mAbs 1, 2, 4, and 5 (**Figure 2.5**). Subtle

differences in the deconvoluted mass profiles were observed between the mAb3

timepoints, with one mass peak (+191 Da modification) decreasing and two mass peaks

(-438 Da and +234 Da modifications) increasing with time; the identity of these

additional mass peaks have not been determined. Notably, no mass modifications

consistent with common mixed thiol disulfides were observed in any of the deconvoluted

mass profiles. Non-reduced Lys-C peptide mapping of these timepoints did not yield any

hits corresponding to mixed disulfide modifications either, and confirmed that non-

canonical disulfided peptides did not increase with time (data not shown). Having

eliminated the possibility that free thiols were involved in mixed disulfides or disulfide

shuffling *in vivo*, it is reasonable to conclude that the *in vivo* free thiol transformations

observed for mAb1/3/5 were reoxidations yielding their respective and expected

canonical disulfide bonds.

2.3.4. Solvent accessibility positively correlates with in vivo reoxidation rates

To determine if solvent-accessibility plays a role in free thiol reoxidation *in vivo*,

the free thiol content of the starting mAb materials was determined using a native

differential isotope tagging procedure to detect free thiols that were solvent-accessible

by NEM in their natively-folded parental molecule. **Figure 2.6** compares the free thiol

content under either native (**Figure 2.6A**) or denaturing conditions (**Figure 2.6B**) to the

extent of free thiol transformation at a given site *in vivo* after 168 hours, %SH$_{\Delta168}$, which

was calculated as:

$$\%SH_{\Delta168} = \%SH_{168} - \%SH_0$$

where %SH$_0$ and %SH$_{168}$ represent the free thiol site occupancy at 0 hr and 168 hr,

respectively. There is a relationship between the %SH determined under native

conditions and the extent of free thiol transformation *in vivo* over the 168 hour time

period (**Figure 2.6A**). In contrast, we did not observe a relationship between the %SH

determined under denaturing conditions and the extent of free thiol transformation *in

vivo* over the 168 hour time period (**Figure 2.6B**).
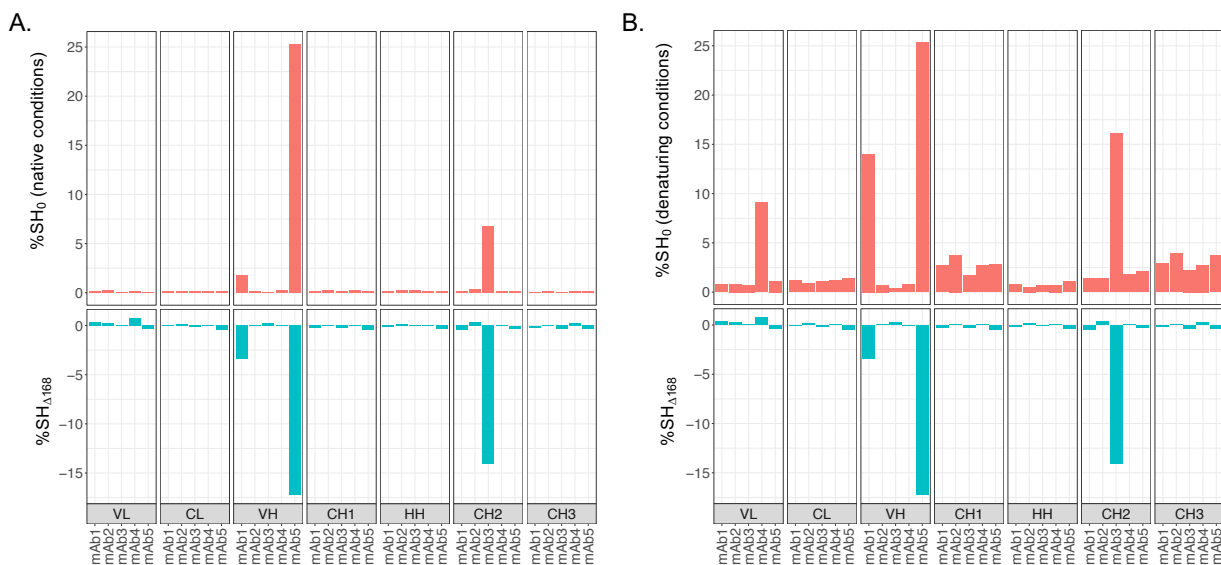
Figure 2.6. Relationship between the extent of free thiol transformation over a 168 hour

period (%SH$_{\Delta168}$) and site-specific free thiol content of starting materials (%SH$_0$)

determined under (A) native and (B) denaturing conditions.

2.4.   Discussion

Broadly speaking, mAb free thiols appear to have two physiological outcomes in

rats: either they remain unchanged or they can transform. A majority of the free thiol

sites in this study (32 out of 35) were unchanged while only three free thiol sites actually transformed *in vivo* (i.e., VH free thiols in mAb1/5, CH2 free thiol in mAb3). VH free thiols transforming in rats was also reported in a previous study conducted by Ouellette et al;[5] however, the authors did not comment on the *in vivo* transformation of any free thiols other than the VH free thiol on their mAb, likely due to the limited specificity and/or resolving power of their approach in using ion-exchange chromatography. CH2 free thiols on an aglycosylated antibody transforming *in vivo*, to our best knowledge, was not reported before.

Hinging on their physiological outcomes *in vivo*, free thiols can have different implications for the quality of a mAb therapeutic product. For the free thiols that were unchanged in this study, it is likely that these free thiol sites are stable or unreactive *in vivo*. Admittedly, a case could be made that these free thiols were unchanged *in vivo* because they were in equilibrium with the surrounding plasma redox environment. The basis for this claim would be that similar %SH levels have been observed in constant domain disulfide bonds of circulating endogenous IgG1s (CH1, 1.76%; CH2, 2.74%; CH3, 2.03%; CL, 1.11%) and endogenous IgG2s (CH1, 3.78%; CH2, 2.01%; CH3, 2.15%; CL, 0.72%).[4] However, in our study, the VL free thiol on mAb4 (~10% SH) well exceeded the %SH levels found in constant domains of endogenous IgGs[4] and yet remained unchanged *in vivo*. Furthermore, we observed that the 32 unchanged sites are the same 32 sites that did not alkylate efficiently in the natively-folded mAb (**Figure 2.6A**). Therefore, it is more likely that these free thiols were unchanged *in vivo* because they are buried and sterically protected, and not because they are in equilibrium with the

surrounding redox environment. The inaccessibility of these unchanged free thiols suggest that they were present in the nascent IgG and were subsequently trapped and preserved in their unoxidized forms as protein folding ensued in the endoplasmic reticulum. While disulfide bond formation can catalyze antibody folding by encouraging the hydrophobic immunoglobulin cores to interact with one another and discouraging aggregation, it is not necessarily a prerequisite of antibody folding.[17] An important corollary to the buried nature of unchanged free thiols is that these particular free thiols have no impact to mAb pharmacokinetics; otherwise, we would have observed an enrichment or depletion of these free thiol levels over time *in vivo*.

The %SH levels of transforming free thiols in our study decreased *in vivo*, likely through reoxidation to form a canonical disulfide under the oxidizing vascular environment in rats. Faster clearance of free thiol-containing mAbs relative to mAbs with fully paired disulfides could also explain the *in vivo* free thiol transformation, but this is unlikely since VH free thiols in mAb1/5 is not expected to affect FcRN salvaging given their distal proximity to the neonatal FcRN binding epitope; a mAb3 sample with over 80% CH2 free thiols showed comparable binding to FcRN compared to a mAb3 sample with fully paired disulfides (data not shown). Ouellette et al also concluded that *in vivo* transformation of VH free thiols yields reoxidized and canonical disulfides based on *in vitro* incubation experiments with their mAb and DTNB.[5] Reformation of the canonical disulfide, which was the intended product during biomanufacturing in the first place, minimizes risk of free thiols to the patient.

Depending on the *in vivo* reoxidation kinetics, a patient's exposure to a transforming free thiol variant may be short-lived, mitigating its risk. Similar arguments based on *in vivo* transformation rates have been made to de-risk other post-translation modifications such as trisulfides,[18] disulfide isoforms,[19, 20] and C-terminal lysines.[21] Ouellette et al demonstrated that their mAb's VH free thiols oxidized rapidly *in vivo* (~1 hour) to reform the correct disulfide linkages, quickly restoring any potential losses in potency due to the free thiol. The free thiols included in this study did not reoxidize as rapidly as the Ouellette et al mAb, although a robust interstudy comparison is confounded by factors including differences in dosing and analytical methodology. Nevertheless, taking the reoxidation kinetics at face value, we can rank order the risk of these free thiols based on *in vivo* reoxidation rates: VH (Ouellette et al mAb) $\ll$ VH (mAb5) $\approx$ CH2 (mAb3) $\ll$ VH (mAb1).

Prediction of a mAb free thiol's physiological outcome without resorting to animal studies would be valuable and made possible by establishing a robust *in vitro in vivo* relationship. Two of the mAbs used in our study (mAb4 and mAb5) were the same mAbs used in the Liu et al study,[15] where the authors investigated free thiol reoxidation using an *in vitro* redox continuous flow system. While the *in vitro* results in the Liu et al study predicted substantially faster reoxidation kinetics for mAb5's VH free thiol relative to our observed *in vivo* results (which cannot be explained at this time), the *in vitro* results accurately predicted that mAb4's VL free thiol would not reoxidize *in vivo* while mAb5's VH free thiol would reoxidize *in vivo*.[15] In our study, we also illuminated a relationship between a free thiol's reactivity to alkylation in a natively-folded mAb *in vitro*

and its likelihood to reoxidize *in vivo*. We observed a stark contrast in the extent of alkylation under native conditions between free thiols that reoxidized versus free thiols that were stable *in vivo*; all of the free thiols that reoxidized *in vivo* (3 out of 3) had >0.5% SH under native conditions and all of the free thiols that were stable *in vivo* (32 out of 32) had <0.5% SH under native conditions (**Figure 2.6A**). This result suggests that free thiols must be accessible in the natively-folded mAb in order to be reoxidized *in vivo*, which implies a mechanism that requires reaction with some species in solution, at least to form a reactive intermediate. These *in vitro in vivo* relationships are promising, and additional studies will confirm whether these *in vitro in vivo* relationships are predictive for other mAbs.

A curious finding worth mentioning was that %SH was partially recovered under native conditions relative to denatured conditions for mAb1 VH and mAb3 CH2, while %SH was fully recovered for mAb5 VH. A plausible hypothesis is that IgGs "breathe" between two states – open and buried – and that free thiols are only able to reoxidize from the open state (**Schematic 2.1**). The rates of "breathing" between the open and buried states may be a molecule-specific property that depends on, for example, hydrophobic interactions that drive spontaneous folding in the absence of disulfide bonds.[17] While a mechanistic understanding of its results was beyond the scope of the current study, free thiol alkylation under native conditions nevertheless is an insightful analytical approach that offers clues into the behavior of natively-folded IgGs and the *in vivo* fates of free thiols.
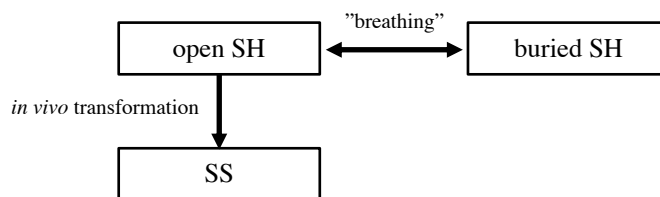
Schematic 2.1. Two-state model of free thiols in mAbs. Free thiols can only be subject to *in vivo* transformation from the open state.

In the previous discussion, we have assumed that the *in vivo* fate of mAb free thiols in a rat model can shed insight on their fate in humans. It is important to address the translatability of *in vivo* transformation rat data to the human context. Redox species and their plasma concentrations in rat and in human have been reported elsewhere.[22-26] The predominant difference is elevated glutathione levels in rats and elevated cysteinyl-glycine levels in humans. This difference can be explained by the lack of basal γ-glutamyl transferase activity in rat plasma, which converts most of the circulating glutathione to cysteinyl-glycine in humans.[27] While the other redox species concentrations between rat and human plasma may be statistically significant, the magnitude of these differences were modest in comparison to the glutathione/cysteinyl-glycine difference and, importantly, both rat and human plasma exhibit oxidizing redox environments. As such, the *in vivo* fate of mAb free thiols in rats might be a useful model for shedding insight on their respective fate in humans.

2.5.   Conclusions

The analytical workflow described herein enabled the recovery of mAbs of interest from rat plasma and the subsequent interrogation of site-specific free thiol

content. By opting for a mass spectrometry-based method, we were able to profile the site-specific free thiol composition of immunopurified timepoints with near full coverage (i.e., %SH at all intra- and inter-chain disulfide bonds save one, the HL interchain disulfide bond). We also dosed rats with a diverse panel of mAbs with elevated free thiols in VH, VL, and CH2. The near full coverage of our analytical method in combination with the diversity of tested molecules afforded new insights regarding *in vivo* free thiol transformation. We show that a wide range of *in vivo* transformation kinetic rates are possible for free thiols, depending on its site and the mAb molecule, with a majority of free thiols being remarkably stable *in vivo*. We recapitulate that the major free thiol transformation *in vivo*, if transformation does occur, is the free thiol's reoxidation back to a canonical disulfide bond. The implications of these *in vivo* observations to the ongoing dialogue of free thiols and their criticality as a quality attribute were discussed. Finally, we highlighted an intriguing relationship between a free thiol's reactivity towards alkylation in a natively-folded mAb and its propensity to transform *in vivo*.

2.6.   References

1.   Chaderjian, W. B.; Chin, E. T.; Harris, R. J.; Etcheverry, T. M., Effect of copper sulfate on performance of a serum-free CHO cell culture process and the level of free thiol in the recombinant antibody expressed. *Biotechnol Prog* **2005,** *21* (2), 550-3.
2.   Xiang, T.; Chumsae, C.; Liu, H., Localization and quantitation of free sulfhydryl in recombinant monoclonal antibodies by differential labeling with 12C and 13C iodoacetic acid and LC-MS analysis. *Anal Chem* **2009,** *81* (19), 8101-8.
3.   Robotham, A. C.; Kelly, J. F., Detection and quantification of free sulfhydryls in monoclonal antibodies using maleimide labeling and mass spectrometry. *MAbs* **2019,** *11* (4), 757-766.

4. Huh, J. H.; White, A. J.; Brych, S. R.; Franey, H.; Matsumura, M., The identification of free cysteine residues within antibodies and a potential role for free cysteine residues in covalent aggregation because of agitation stress. *J Pharm Sci* **2013,** *102* (6), 1701-1711.

5. Ouellette, D.; Alessandri, L.; Chin, A.; Grinnell, C.; Tarcsa, E.; Radziejewski, C.; Correia, I., Studies in serum support rapid formation of disulfide bond between unpaired cysteine residues in the VH domain of an immunoglobulin G1 molecule. *Anal Biochem* **2010,** *397* (1), 37-47.

6. Harris, R. J., Heterogeneity of recombinant antibodies: linking structure to function. *Dev Biol (Basel)* **2005,** *122*, 117-27.

7. Zhang, T.; Zhang, J.; Hewitt, D.; Tran, B.; Gao, X.; Qiu, Z. J.; Tejada, M.; Gazzano-Santoro, H.; Kao, Y. H., Identification and characterization of buried unpaired cysteines in a recombinant monoclonal IgG1 antibody. *Anal Chem* **2012,** *84* (16), 7112-23.

8. Zhang, W.; Czupryn, M. J., Free sulfhydryl in recombinant monoclonal antibodies. *Biotechnol Prog* **2002,** *18* (3), 509-13.

9. Liu, H.; Jeong, J.; Kao, Y. H.; Zhang, Y. T., Characterization of free thiol variants of an IgG1 by reversed phase ultra high pressure liquid chromatography coupled with mass spectrometry. *J Pharm Biomed Anal* **2015,** *109*, 142-9.

10. Buchwald, B. M.; Connell, G. E., Thiol groups of normal human immunoglobulin G. *Biochem J* **1974,** *137* (2), 281-9.

11. Li, P.; Haque, M. A.; Blum, J. S., Role of disulfide bonds in regulating antigen processing and epitope selection. *J Immunol* **2002,** *169* (5), 2444-50.

12. Mahler, H. C.; Friess, W.; Grauschopf, U.; Kiese, S., Protein aggregation: pathways, induction factors and analysis. *J Pharm Sci* **2009,** *98* (9), 2909-34.

13. Brych, S. R.; Gokarn, Y. R.; Hultgen, H.; Stevenson, R. J.; Rajan, R.; Matsumura, M., Characterization of antibody aggregation: role of buried, unpaired cysteines in particle formation. *J Pharm Sci* **2010,** *99* (2), 764-81.

14. Liu, H.; Chumsae, C.; Gaza-Bulseco, G.; Hurkmans, K.; Radziejewski, C. H., Ranking the susceptibility of disulfide bonds in human IgG1 antibodies by reduction, differential alkylation, and LC-MS analysis. *Anal Chem* **2010,** *82* (12), 5219-26.

15. Liu, Y. D.; Chen, Y.; Tsui, G.; Wei, B.; Yang, F.; Yu, C.; Cornell, C., Predictive In Vitro Vitreous and Serum Models and Methods to Assess Thiol-Related Quality Attributes in Protein Therapeutics. *Anal Chem* **2020,** *92* (10), 6869-6876.

16. Wisniewski, J. R.; Zougman, A.; Nagaraj, N.; Mann, M., Universal sample preparation method for proteome analysis. *Nat Methods* **2009,** *6* (5), 359-62.

17. Feige, M. J.; Hendershot, L. M.; Buchner, J., How antibodies fold. *Trends Biochem Sci* **2010,** *35* (4), 189-98.

18. Gu, S.; Wen, D.; Weinreb, P. H.; Sun, Y.; Zhang, L.; Foley, S. F.; Kshirsagar, R.; Evans, D.; Mi, S.; Meier, W.; Pepinsky, R. B., Characterization of trisulfide modification in antibodies. *Anal Biochem* **2010,** *400* (1), 89-98.

19. Liu, Y. D.; Wang, T.; Chou, R.; Chen, L.; Kannan, G.; Stevenson, R.; Goetze, A. M.; Jiang, X. G.; Huang, G.; Dillon, T. M.; Flynn, G. C., IgG2 disulfide isoform conversion kinetics. *Mol Immunol* **2013,** *54* (2), 217-26.
20. Liu, Y. D.; Chen, X.; Enk, J. Z.; Plant, M.; Dillon, T. M.; Flynn, G. C., Human IgG2 antibody disulfide rearrangement in vivo. *J Biol Chem* **2008,** *283* (43), 29266-72.
21. Cai, B.; Pan, H.; Flynn, G. C., C-terminal lysine processing of human immunoglobulin G2 heavy chain in vivo. *Biotechnol Bioeng* **2011,** *108* (2), 404-12.
22. Iciek, M.; Chwatko, G.; Lorenc-Koci, E.; Bald, E.; Wlodek, L., Plasma levels of total, free and protein bound thiols as well as sulfane sulfur in different age groups of rats. *Acta Biochim Pol* **2004,** *51* (3), 815-24.
23. Mansoor, M. A.; Svardal, A. M.; Ueland, P. M., Determination of the in vivo redox status of cysteine, cysteinylglycine, homocysteine, and glutathione in human plasma. *Anal Biochem* **1992,** *200* (2), 218-29.
24. Likogianni, V.; Janel, N.; Ledru, A.; Beaune, P.; Paul, J. L.; Demuth, K., Thiol compounds metabolism in mice, rats and humans: comparative study and potential explanation of rodents protection against vascular diseases. *Clin Chim Acta* **2006,** *372* (1-2), 140-6.
25. Lash, L. H.; Jones, D. P., Distribution of oxidized and reduced forms of glutathione and cysteine in rat plasma. *Arch Biochem Biophys* **1985,** *240* (2), 583-92.
26. Di Giuseppe, D.; Frosali, S.; Priora, R.; Di Simplicio, F. C.; Buonocore, G.; Cellesi, C.; Capecchi, P. L.; Pasini, F. L.; Lazzerini, P. E.; Jakubowski, H.; Di Simplicio, P., The effects of age and hyperhomocysteinemia on the redox forms of plasma thiols. *J Lab Clin Med* **2004,** *144* (5), 235-45.
27. Leonard, T. B.; Neptun, D. A.; Popp, J. A., Serum gamma glutamyl transferase as a specific indicator of bile duct lesions in the rat liver. *Am J Pathol* **1984,** *116* (2), 262-9.

2.7. Supplemental information

Table 2.S1. First order rate constants and initial rates of free thiols that transform *in vivo*.

Molecule	Domain	First order rate constant (hr^{-1})	Initial rate (hr^{-1} %)
mAb1	VH	-1.61E-03	-2.26E-02
mAb3	CH2	-1.23E-02	-1.97E-01
mAb5	VH	-6.91E-03	-1.76E-01

Chapter 3. Augmenting Traditional Ellman's to Fluorescent Ellman's for Enhanced Sensitivity of Free Thiol Detection

3.1. Introduction

Among the available quantitation methods for free thiols (including the mass spectrometry-based method used in **Chapter 2**), optical sensing methods are desirable because they are convenient, rapid, sensitive, and selective.[1] A large family of optical probes for thiol sensing have been developed, which continues to grow as a result of active research. A majority of these are fluorogenic probes that switch "on" upon reacting with thiols and can be broadly classified by their reaction type: Michael addition of a maleimide,[2] release of a sulfonamide[3-5] or sulfonate ester,[6] etc. The quantitation limits for modern fluorogenic probes are typically in the nM or pM range for free thiols.[7] However, a common drawback to fluorogenic probes for thiol sensing is that their sensitivities can depend on the thiol substrate.[3, 8, 9] As a result, fluorogenic probes for thiol sensing usually require either calibration using standards that are identical to the substrates in the test articles or determination of appropriate response factors. Neither of these requirements scales well as the heterogeneity of substrates in the sample increases or when the substrate has multiple potential free thiol sites (e.g., an IgG1 antibody may have up to 16 distinct free thiol sites[10]). Additional drawbacks to fluorogenic probes are that they can be sterically bulky and often have limited solubility in water.

On the other hand, Ellman's reagent, or 5,5'-dithiobis-(2-nitrobenzoic acid) (DTNB), the classic optical probe for free thiol sensing, happens to be highly water soluble, is not bulky, and its sensitivity is agnostic to the thiol substrate. The reason for the latter property is two-fold: first, the low bond dissociation energy of DTNB[11] facilitates the stoichiometric liberation of a TNB^{2-} molecule per thiol substrate (assuming

that DTNB and the thiol substrate are given sufficient time to react) and second, the liberated TNB^{2-} molecule in solution, has the same molar absorptivity at 412 nm irrespective of the thiol substrate that liberated it. The main disadvantage of the Ellman's method is that the quantitation limits are significantly higher (3-4 orders of magnitude) than most fluorogenic methods for free thiol quantitation. This can mean that large quantities of sample are required (e.g. milligrams of a therapeutic antibody) in order to obtain a quantitative free thiol measurement, which is impractical and sometimes prohibitively expensive.

In this study, we explored a simple augmentation to the Ellman's assay for improving method sensitivity. The 2-step reaction schematic of the new assay, coined Fluorescent Ellman's (or F.Ellman), is shown in **Figure 3.1**. In the first step (**Figure 3.1**, step I), free thiols in a sample are exchanged with DTNB to stoichiometrically yield TNB^{2-}, as in Traditional Ellman's. In the second step (**Figure 3.1**, step II), a thiol-specific fluorogenic probe is introduced that reacts with TNB^{2-} to yield a fluorescent signal - either by forming a fluorescent TNB-probe adduct (**Figure 3.1**, step IIA) or by releasing a deprotected fluorescent probe (**Figure 3.1**, step IIB). To develop a viable F.Ellman assay, we screened commercially available thiol-specific fluorogenic probes and optimized the assay conditions for the most sensitive probe. We demonstrated the feasibility of the F.Ellman approach, assessed the boost in sensitivity obtained by transducing a UV absorption signal into a fluorescent signal, and evaluated the method's usefulness by determining free thiol content in complex therapeutic antibody samples.
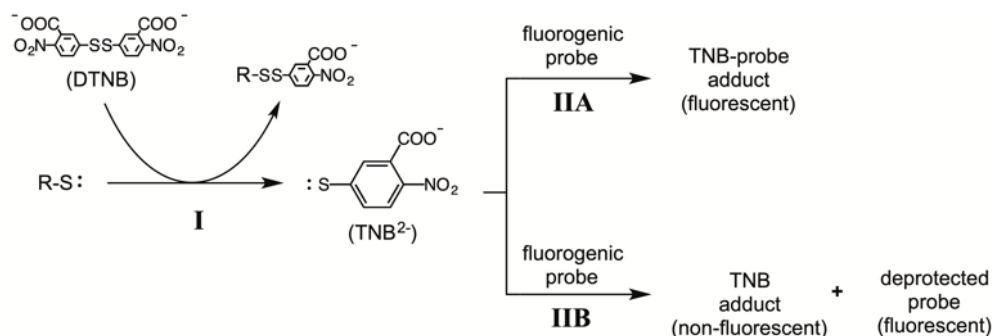
Figure 3.1. Reaction scheme for the Fluorescent Ellmans assay. Incubation of thiol substrates with DTNB (step I) stoichiometrically liberates TNB2- molecules, which are subsequently reacted with thiol-specific fluorogenic probes (step II) to yield a fluorescent signal. These fluorogenic reactions proceed either by forming a fluorescent TNB-probe adduct (IIA) or by yielding a deprotected fluorescent probe (IIB).

3.2.   Materials and Methods

3.2.1. Materials

All antibodies and antibody-drug-conjugates (ADC) tested in this study were produced by Genentech (South San Francisco, CA). The two ADCs tested included one with drugs conjugated to reduced interchain disulfides (ADC-A) and another with drugs conjugated to engineered unpaired cysteines (ADC-B). DTNB, cysteine, glutathione, N-acetyl cysteine, dimethyl sulfoxide (DMSO), sodium phosphate, hemisodium 3-(N-morpholino)propanesulfonic acid (MOPS), and ethylenediaminetetraacetic acid (EDTA) were purchased from Sigma-Aldrich (St. Louis, MO). Guanidine hydrochloride was purchased from EMD Millipore (Burlington, MA). TNB^{2-} was purchased from Biovision (Milpitas, CA). MMBC (methyl maleimidobenzochromenecarboxylate) was purchased from Combi-Blocks (San Diego, CA); 1 mM stocks of MMBC were prepared in DMSO

and kept frozen at -20 ºC until used. Working solutions of MMBC (20 µM) were

prepared by diluting the 1 mM stocks with 100 mM sodium phosphate, pH 7.4. Other

probes tested were purchased from vendors listed in **Table 3.S1**. Other consumables

and equipment used in this study include NBS 96-well half-volume black plates and 96-

well half-volume clear bottom plates from Corning (Corning, NY), a Poroshell 120-C18

reversed phase column (2.7 µm particle diameter, 3.0 x 100mm) and 1290 UHPLC from

Agilent (Santa Clara, CA), a Nanodrop 2000 and a Fusion hybrid mass spectrometer

from Thermo Scientific (Waltham, MA), a SpectraMax i3 plate reader (San Jose, CA),

and a Mettler-Toledo InLab ultra-micro pH meter (Columbus, OH).

3.2.2. Screening Fluorescent and Fluorogenic Probes

Seven fluorescent or fluorogenic probes (**Table S1**) including MMBC were evaluated for

their ability to transduce TNB^{2-} into a fluorescent signal (**Figure 3.1**, step II). In brief, the

probes were reacted according to their manufacturer's recommendations with various

concentrations of TNB^{2-} (ranging from 0 – 2 µM), which was prepared directly from

TNB^{2-} powder dissolved in water. Fluorescence was monitored over a period of 45

minutes, using the manufacturer's recommended excitation/emission wavelength pairs

(**Table 3.S1**).

3.2.3. Characterization of TNB-MMBC adduct

To verify the nature of the resulting TNB-MMBC adduct, the emission and excitation

spectra for the TNB-MMBC adduct were determined. A 10 µM TNB^{2-} standard was

diluted 1:1 with a 20 µM MMBC solution and incubated in the dark at room temperature

(r.t.) for 30 minutes before performing readings using a plate reader. A series of emission wavelengths from 425 to 600 nm were tested while fixing the excitation at the fluorescence probe manufacturer's recommended value of 385 nm (**Figure 3.3**). Maximal fluorescence intensity was achieved by monitoring emission at 510 nm, so then a series of excitation wavelengths from 325 to 475 nm were tested, this time fixing the emission at 510 nm. Maximal fluorescence intensity was achieved by exciting at 375 nm.

The structure of the TNB-MMBC adduct was further interrogated using LC-MS. An equivolume mixture of 10 µM TNB^{2-} standard and 20 µM MMBC solution, both prepared in 20 mM sodium phosphate, pH 7.4 was incubated in the dark at r.t. for 30 minutes. The reaction was quenched via acidification with 10% formic acid to a final concentration of 1% formic acid prior to injection onto a Poroshell 120 EC-C18 reversed phase column that was pre-equilibrated with 10% solvent B (mobile phase A: 0.1% formic acid in water; mobile phase B: 0.1% formic acid in acetonitrile). After holding initial conditions for 2 minutes, the starting reagents and reaction products were separated using a gradient from 10 to 60% solvent B over 5 minutes. The LC eluent was coupled to a fluorescence detector as well as to a Thermo mass spectrometer equipped with an electrospray source (Orbitrap Fusion). Notable mass spectrometer parameters included a spray voltage of 3700 V, ion transfer temperature of 325°C, Orbitrap resolution of 60 K, and a AGC target of 1e5 counts.

3.2.4. Fluorescent Ellman's Method

Cysteine standards (ranging from 0 to 10 µM) and protein samples (targeting a free thiol concentration of 5 µM) were prepared in either native conditions (111 mM MOPS, 1 mM EDTA, pH 7.25) or denaturing conditions (native conditions + 4 M guanidine hydrochloride). Protein concentrations were measured using a Nanodrop - blanking the spectrophotometer with a matched matrix - along with the corresponding protein's extinction coefficient. Samples and standards were then incubated with 0.58 mM DTNB in the dark at r.t. for 60 minutes. Fifty microliters of each sample and standard were transferred in triplicates to a Corning NBS 96-well half-volume black plate, where the destination wells contained 50 µL of 20 µM MMBC solution. Mixing was achieved via plunging of the pipette. Fluorescence readings (ex: 375 nm, em: 510 nm) were taken on a Spectramax i3 plate reader. The thiol concentrations in each protein sample was determined by referencing its fluorescence readings against the calibration curve (linear) derived using the cysteine standards. The free thiol content, on a mole per mole basis, could be calculated by dividing the sample thiol concentrations by the sample protein concentrations determined via Nanodrop 2000. During this procedure, multi-channel pipetting was used wherever possible.

3.2.5. Assessment of method properties

Quantitation and detection limits were determined by using the F.Ellman method to generate a calibration curve (0 – 10 µM cysteine) and to measure 8 replicates (individual sample preparations) of the 0 µM cysteine standards i.e. blanks. For comparison, the Traditional Ellman method (see Supplemental Information for

Traditional Ellman's method details) was used to generate a calibration curve (0 – 40

µM cysteine) and to measure 8 replicates of the 0 µM cysteine standards. The limits of

detection (LOD) and quantitation (LOQ) were calculated for either F.Ellman or

Traditional Ellman methods using the following mathematical relationship:

$$LOD = 3.3 \times \frac{\sigma_b}{m}$$

$$LOQ = 10 \times \frac{\sigma_b}{m}$$

Where σ_b is the standard deviation of the 8 blank measurements and m is the slope of

the cysteine calibration curve.

The F.Ellman method sensitivity to different thiol substrates was evaluated next.

Using either cysteine, N-acetyl cysteine, or glutathione as the thiol substrate, calibration

curves ranging from 0 – 10 µM were generated using the F.Ellman method. This

experiment was performed both under native and denaturing conditions.

In order to assess method accuracy, free thiol content on 11 molecules - including 7

IgG1 antibodies, 2 IgG4 antibodies, 1 bispecific antibody, and 1 antibody Fab fragment -

was determined using the F.Ellman method under denaturing conditions. The F.Ellman

results were compared to free thiol values for the same 11 molecules determined using

a NcHM-tagged reversed phase liquid chromatography assay, which was previously

described.[12] The latter assay was chosen as an appropriate comparator because it

relies on a free thiol detection mechanism that is orthogonal to the F.Ellman method (i.e.

derivatization of free thiols using NcHM, followed by reversed-phase separation with

enhanced selectivity due to NcHM hydrophobicity, and UV absorption peak detection).

Intermediate precision of F.Ellman on an abbreviated sample panel (7 out of 11

molecules) was determined by two different analysts, on different days, using different reagents.

3.2.6. Buffering capacity of phosphate buffer compared with MOPS buffer in the presence of 4 M guanidine hydrochloride

One mL aliquots of denaturing MOPS buffer (100 mM MOPS, 4M guanidine hydrochloride, 1 mM EDTA, pH 7.4) and denaturing phosphate buffer (100 mM sodium phosphate, 4M guanidine hydrochloride, 1 mM EDTA, pH 7.4) were each acid titrated with 1 N hydrochloric acid (10 μL at a time, up to 40 μL). Separate 1 mL aliquots of the same MOPS buffer and phosphate buffer were each base titrated with 1 N sodium hydroxide (10 μL at a time, up to 40 μL). pH measurements were taken after each acid/base titrant addition using a micro pH meter.

3.3.   Results

3.3.1. MMBC as a promising fluorogenic probe

Seven commercially-available thiol-specific fluorescent / fluorogenic probes were tested with TNB^{2-} to establish the feasibility of the F.Ellman approach. Five of the probes failed to produce any dose-dependent fluorescence. Two fluorogenic probes (ThioFluor 623 and MMBC) successfully produced dose-dependent fluorescence to TNB^{2-}, demonstrating proof of concept (**Figure 3.S2**). Out of the two, MMBC (also known as ThioGlo-1) produced ~40x more signal and was the probe chosen for further development.
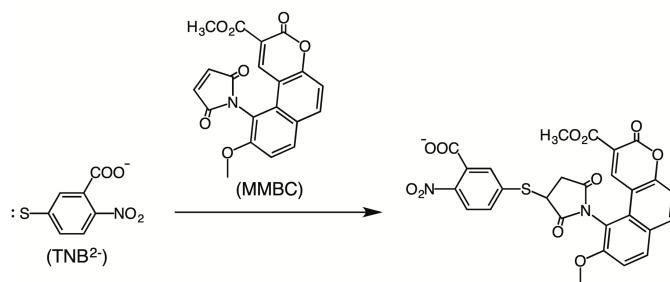
**Figure 3.2.** Reaction schematic of TNB^{2-} and MMBC to yield a fluorescent TNB-MMBC adduct (exact mass: 578.0637 Da, expected structure on far right), following the pathway shown in **Figure 3.1** (IIA).

The reaction between TNB^{2-} and MMBC yields a product that fluoresces at the excitation and emission pair of 375 nm / 510 nm (**Figure 3.3**). **Figure 3.2** shows the likely reaction product based on nucleophilic attack by a thiol (TNB^{2-}) on a maleimide (MMBC). Reversed-phase liquid chromatography coupled with fluorescence detection and mass spectrometry was used to monitor the reaction and confirm this reaction product. Neither the TNB^{2-} nor the MMBC starting materials have appreciable fluorescence but combining TNB^{2-} and MMBC yields two strong fluorescent chromatographic peaks via reversed-phase separation (**Figure 3.4B**). The mass corresponding to both fluorescence peaks is the same, linking the two peaks as isomers, and that mass (579.0706 m/z, MH$^+$, **Figure 3.4C**) is consistent with the proposed TNB-MMBC adduct to within 1 ppm of the theoretical mass (579.0710 m/z, MH$^+$). The later retention times of the fluorescence peaks are also consistent with a TNB-MMBC adduct, which is likely more hydrophobic than either TNB^{2-} or MMBC starting materials.
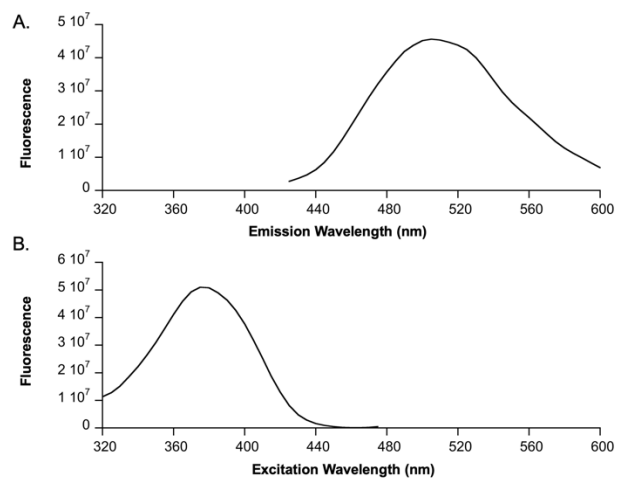
Figure 3.3. Emission and excitation spectrum of the fluorescent TNB-MMBC adduct. (A)

Emission spectrum with excitation wavelength fixed to 385 nm and (B) excitation

spectrum with emission wavelength fixed to 510 nm.
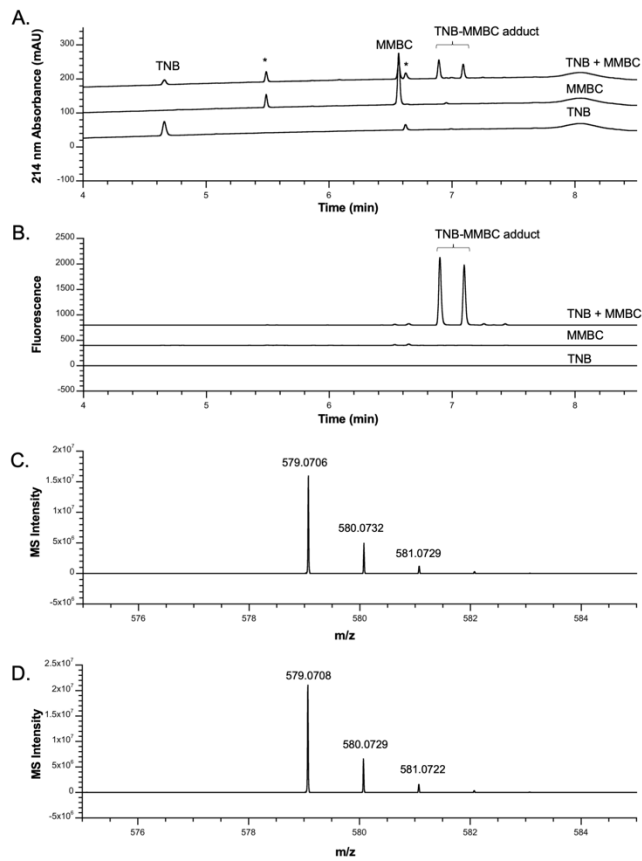
Figure 3.4. Reversed phase chromatogram of starting reagents (TNB, MMBC) and the TNB-MMBC adduct with A) 214 nm UV detection and B) 375 nm / 510 nm fluorescence detection. Asterisked peaks denote impurities associated with the TNB or MMBC starting materials. Mass spectra of the C) earlier-eluting and D) later-eluting TNB-MMBC adduct peaks.

3.3.2. Fluorescent Ellman retains versatility while improving limits of quantitation relative to Traditional Ellman

Figure 3.5 shows the fluorescent emission over time (during step II in Figure **3.1**) when applying the F.Ellman method to a set of cysteine standards. The F.Ellman method gives a dose-dependent fluorescent signal in response to a thiol substrate, and

fluorescence readings begin to plateau 30 minutes after the introduction of MMBC as

the reaction is completed at this point. By choosing the 30 minute timepoint as the

endpoint reading, a linear calibration curve relating cysteine concentration to

fluorescence was constructed (**Figure 3.6**). The slope of this calibration curve together

with the variation in blank measurement (i.e. noise) yield a limit of quantitation (LOQ) of

0.4 μM cysteine, a 4-fold improvement compared to the LOQ (1.6 μM of cysteine) for

Traditional Ellman method in our hands (**Table 3.1**).
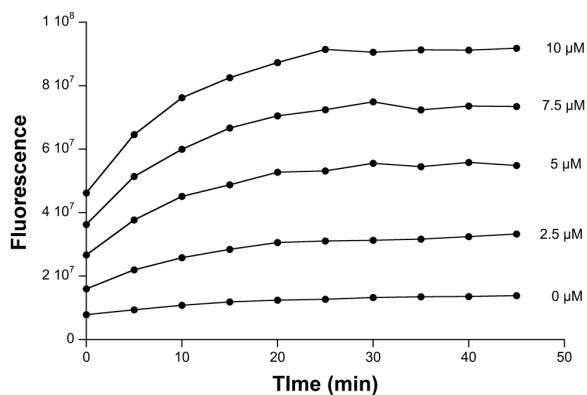
**Figure 3.5.** Fluorescence over time (MMBC reagent was introduced at time 0) of

cysteine standards using the F.Ellman assay. Similar curves are obtained for protein

samples.

Table 3.1. Limits of detection and quantitation for F. Ellman's vs. Traditional Ellman's

	Fluorescent Ellman's	Traditional Ellman's
LOD (µM SH)	0.14	0.55
LOQ (µM SH)	0.42	1.67

As shown in **Figure 3.6**, comparable calibration curves can be generated with the F.Ellman method using other thiol substrates i.e. glutathione and N-acetylated cysteine. Fluorescence readings plateau 30 minutes after the introduction of MMBC for these other thiol substrates as well, which indicates that the thiol exchange reaction with DTNB (step II in **Figure 3.1**) is complete and that MMBC is reacting with TNB^{2-} in all cases. Given the similar sensitivity of F.Ellman to different thiol substrates and the proposed mechanism of F.Ellman, we expect that the F.Ellman LOQ of 0.4 µM can be generalized to all thiols, irrespective of the nature of substrate, assuming the assay is performed as described. Additionally, the F.Ellman assay performs similarly under both native as well as denaturing conditions (**Figure 3.6**). In samples that exhibit tertiary structure such as protein samples, F.Ellman can be used to selectively interrogate free thiols that are solvent-accessible in the natively-folded substrate or to interrogate total free thiols (buried + solvent-accessible).
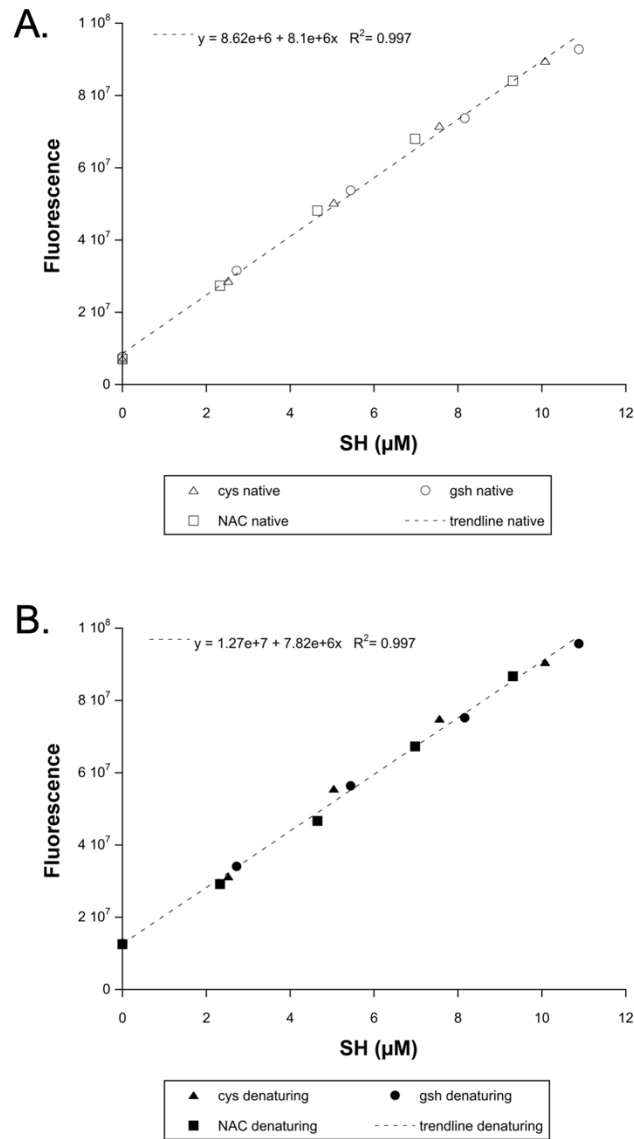
**Figure 3.6.** F.Ellman calibration curves using cysteine (cys), N-acetylated cysteine
(NAC), and glutathione (gsh) under both A) native and B) denaturing conditions.
Fluorescence readings were taken 30 minutes after introducing MMBC reagent.
Substrate-agnostic linear regressions (trendlines) in both plots were based on all plotted
data points. Substrate-specific linear regression parameters can be found in **Table
3.S2**.

3.3.3. Fluorescent Ellman can accurately and precisely quantify free thiols in complex proteins

The assay accuracy and precision of F.Ellman method was assessed using a panel of antibody-based proteins (under denaturing conditions) and their total (buried + solvent accessible) free thiols on a mole per mole basis are shown in **Figure 3.7**. The fluorescence readings for these protein samples also plateaued 30 minutes after introduction of the MMBC probe. Intermediate precision of F.Ellman was demonstrated using an abbreviated panel (7 out of 11 proteins) and the coefficients of variation were all < 8% (**Figure 3.7**). The full panel of proteins were interrogated using an orthogonal NcHM-tagged reverse-phase chromatography assay, and the total free thiol values were consistent with the F.Ellman results (**Figure 3.7**), suggesting comparable measurement accuracy of these two methods despite the significant difference in their detection modes.

Similar to the Traditional Ellman, the F.Ellman method is capable of determining free thiol content of chromatographically-challenging molecules (**Table 3.2**), which can include ADCs and IgG2 molecules. ADCs have conjugated hydrophobic drugs that often preclude reverse-phase separation due to significant non-specific interactions, while IgG2s contain disulfide bond isoforms that lead to multiple peaks on reverse-phase separation and complicate analysis. Both types of samples are amenable for analysis by F.Ellman but not by NcHM-tagged reverse-phase chromatography assay.
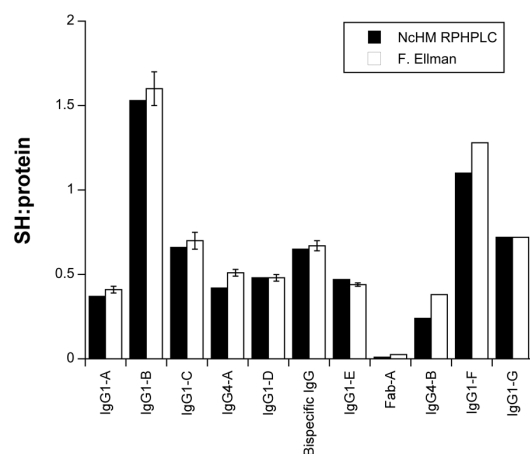
Figure 3.7. Bridging dataset between F. Ellman (denaturing) and the NcHM-tagging

RPLC assay, an orthogonal method for total free thiol quantitation of antibodies.

Intermediate precision for the F.Ellman was determined using the first seven molecules

(IgG1-A/B/C/D/E, IgG4-A, bispecific IgG) with the error bars representing one standard

deviation. F.Ellman coefficient of variation was < 8% for each molecule subjected to

intermediate precision.

Table 3.2. Free thiol values of chromatographically-challenging molecules using denaturing F.Ellman's. Chromatographically-challenging molecules can include antibody-drug conjugates (ADC) - which contain conjugated hydrophobic drugs that often preclude reverse-phase separation due to non-specific interactions - and IgG2 molecules – which contain disulfide bond isoforms that lead to multiple peaks on reverse-phase separation and complicate analysis.

Molecule	SH:Protein
ADC-A	0.39
ADC-B	0.29
IgG2-A	0.61

3.4. Discussion

While the F.Ellman method is a conceptually simple augmentation of the Traditional Ellman method, we were not certain it could be practicably implemented given the properties of TNB^{2-}. The electron withdrawing functional groups and electron delocalization - which give DTNB its uncharacteristically low bond dissociation energy[11] and make it so successful as a thiol exchanging agent – also render TNB^{2-} a poor nucleophile. Furthermore, the electron withdrawing functional groups and electron delocalization of TNB^{2-} could potentially quench the fluorescence of the conjugated TNB-fluorogenic probe through various mechanisms including photoinduced electron transfer, internal charge transfer, etc. [1, 13, 14] Therefore, it was not surprising that five of the seven probes tested failed to produce a suitable dose-dependent response to TNB^{2-}. However, our results showed that TNB^{2-} can be converted into a fluorescent

signal with the help of the fluorogenic probes ThioFluor 623 or MMBC (**Figure 3.S2**). To our knowledge, this is the first report demonstrating the transformation of TNB^{2-} into a fluorescent molecule.

ThioFluor 623 is a fluorogenic compound with a 2,4-dinitrobenzene sulfonamide (DNBS) functional group and its fluorescence is contingent upon the release of this DNBS group by a thiol substrate (**Figure 3.S1**). The deprotected ThioFluor 623 fluoresces modestly with a quantum yield of 0.01 in aqueous media.[3] While we did not pursue further development of ThioFluor 623 because MMBC appeared more sensitive, the fact that ThioFluor 623 produced a dose-dependent response to TNB^{2-} is intriguing and may warrant further exploration of the DNBS-containing class of fluorogenic probes; of particular interest may be DNBS-containing fluorogenic probes that selectively react with thiophenols and have significantly better quantum yields than ThioFluor 623.[4, 5, 15] MMBC is a fluorogenic compound with a maleimide functional group and its fluorescence is contingent upon nucleophilic attack by a thiol substrate on this maleimide (**Figure 3.1A**). Upon reacting with cysteine, MMBC fluoresces intensely with a quantum yield of 0.65.[2] It is not clear why MMBC was able to efficiently react and fluoresce with TNB^{2-} while other maleimide-based fluorogenic probes that we tested did not. We speculate that the energy landscape of the frontier molecular orbitals in the TNB-MMBC adduct preclude fluorescence quenching, although a mechanistic explanation for this phenomenon is beyond the scope of this study.

We determined the LOQs of F.Ellman and Traditional Ellman methods to be 0.4 µM and 1.6 µM SH, respectively, suggesting that the MMBC augmentation improved the limits of quantitation by ~4 fold (**Table 3.1**). This observed performance enhancement

can be explained by lower background signals in fluorescence measurement versus UV absorbance measurements, although the magnitude of enhancement appears modest when considering that fluorescence assays typically attain LOQs 3-4 orders of magnitude lower than UV absorbance assays. Further improvements to F.Ellman LOQ were likely limited by background DTNB hydrolysis, which introduces more noise to the fluorescence measurements. Nevertheless, the improved LOQ coupled with the fact that the F.Ellman method requires half the sample volume translate to needing ~ 8x less material in making a thiol determination with F.Ellman relative to Traditional Ellman.

It is important to note that our LOQ determination for Traditional Ellman method of 1.6 µM is higher than previously reported LOQs for Traditional Ellman method, which were in the range of 0.6 – 0.9 µM.[16, 17] An important difference in methodology, however, is that we incubated our samples with DTNB for 60 minutes (as opposed to 5 minutes in those previous studies). We deliberately chose a longer incubation time to allow free thiols on proteins to fully react with DTNB.[16] But as a result of the longer incubation time, there is also more opportunity for DTNB hydrolysis and background noise, hence the higher LOQ for Traditional Ellman method in our study. Wherever possible, we kept the methodology (i.e. reagents, consumables, instruments, etc) the same between the F.Ellman's and Traditional Ellman's methods, in order to fairly compare their method performance within the scope of this study. To our knowledge, the F.Ellman augmentation represents the biggest boost in sensitivity for the Traditional Ellman method since its inception over 60 years ago.

Notably, the F.Ellman method successfully preserves one of the key advantages of the Traditional Ellman's method over other fluorogenic free thiol assays: the

sensitivity of the F.Ellman method is agnostic to the nature of thiol substrate (**Figure 3.6**), assuming that DTNB and the thiol substrate are given sufficient time to react. Consequently, a single, universal calibration curve (with cysteine, for example) can be used in F.Ellman's to quantify thiols in a diverse set of samples, regardless of the nature of substrate(s) or the thiol microenvironment(s). This approach is not possible, for example, if we had used MMBC (without DTNB) to directly assay thiol substrates because MMBC exhibits different fluorescence efficiencies when conjugated to different substrates.[17] In this study, we successfully used a single cysteine calibration curve with F.Ellman's to accurately determine thiol content in 7 different IgG1s, a bispecific IgG, an IgG2, 2 IgG4s, 2 antibody-drug conjugates, a Fab fragment, and various small molecules.

There are some limitations to the F.Ellman method with MMBC. First, the solubility of MMBC is 20 µM in aqueous solutions and limits the upper substrate range of F.Ellman. Second, the F.Ellman method should always be performed with a calibration curve to control for background DTNB hydrolysis and to calibrate the fluorescence response, whereas a calibration curve is not necessary with the Traditional Ellman's if one relies on the extinction coefficient of TNB^{2-} (although this may not be advisable due to known matrix effects on TNB's extinction coefficient at 412nm[18]).

Finally, it is worth discussing an important consideration regarding buffer when performing F.Ellman (or Traditional Ellman) under denaturing conditions. Previous reports describe the use of high concentration guanidine hydrochloride in neutral pH phosphate buffers to create a denaturing environment.[10, 18, 19] However, phosphate under these conditions as a buffer system is a poor choice given the dramatic

dependence of phosphate's pKa on ionic strength.[20, 21] In **Figure 3.S3**, we compare the buffering capacity of a phosphate buffer and a MOPS buffer in the presence of 4 M guanidine hydrochloride. While the MOPS buffer, a Good's buffer, was able to reasonably buffer against both acid and base perturbations, the phosphate buffer in such a strong electrolyte environment had virtually no buffering capacity at neutral pH. High concentrations of urea, in contrast to guanidine hydrochloride, will not contribute significantly to a solution's ionic strength and therefore should be compatible with neutral pH phosphate buffers. Buffer considerations are easy to overlook and yet an incompatible buffer system will have significant ramifications for the accuracy and precision of the F.Ellman and Traditional Ellman assays.

3.5.   Conclusions

We have successfully demonstrated the feasibility of the F.Ellman augmentation. The concept was to transduce the UV absorbance signal of Traditional Ellman's into a fluorescent signal. We showed that the implementation of F.Ellman with MMBC yielded a dose response to free thiol concentration down to a quantitation limit that was 4-fold improved over Traditional Ellman's. We also applied the assay to accurately measure the free thiol content on several complex monoclonal antibodies. The augmentation with MMBC is a drop-in solution that improves the quantitation limits of Traditional Ellman's but otherwise behaves similarly to the latter. We anticipate that other research groups that have applied Traditional Ellman's to various scientific problems since its inception over 60 years ago will appreciate a boost in sensitivity while leveraging historical method development experience.
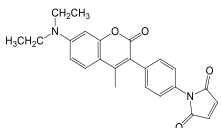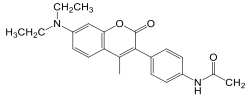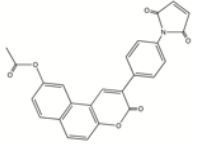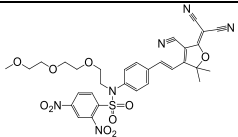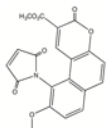
3.6. References

1.   Chen, X.; Zhou, Y.; Peng, X.; Yoon, J., Fluorescent and colorimetric probes for detection of thiols. *Chem Soc Rev* **2010,** *39* (6), 2120-35.

2.   Yang, J.; Langmuir, M. E., Synthesis and Properties of a Maleimide Fluorescent Thiol Reagent Derived from a Naphthopyranone. *J Heterocyclic Chem* **1991,** *28* (5), 1177-1180.

3.   Bouffard, J.; Kim, Y.; Swager, T. M.; Weissleder, R.; Hilderbrand, S. A., A highly selective fluorescent probe for thiol bioimaging. *Org Lett* **2008,** *10* (1), 37-40.

4.   Wang, Z.; Han, D. M.; Jia, W. P.; Zhou, Q. Z.; Deng, W. P., Reaction-based fluorescent probe for selective discrimination of thiophenols over aliphaticthiols and its application in water samples. *Anal Chem* **2012,** *84* (11), 4915-20.

5.   Jiang, W.; Fu, Q.; Fan, H.; Ho, J.; Wang, W., A highly selective fluorescent probe for thiophenols. *Angew Chem Int Ed Engl* **2007,** *46* (44), 8445-8.

6.   Maeda, H.; Matsuno, H.; Ushida, M.; Katayama, K.; Saeki, K.; Itoh, N., 2,4-Dinitrobenzenesulfonyl fluoresceins as fluorescent alternatives to Ellman's reagent in thiol-quantification enzyme assays. *Angew Chem Int Ed Engl* **2005,** *44* (19), 2922-5.

7.   Peng, H.; Chen, W.; Cheng, Y.; Hakuna, L.; Strongin, R.; Wang, B., Thiol reactive probes and chemosensors. *Sensors (Basel)* **2012,** *12* (11), 15907-46.

8.   Hoff, S.; Larsen, F. H.; Andersen, M. L.; Lund, M. N., Quantification of protein thiols using ThioGlo 1 fluorescent derivatives and HPLC separation. *Analyst* **2013,** *138* (7), 2096-103.

9.   Fu, Z. H.; Han, X.; Shao, Y.; Fang, J.; Zhang, Z. H.; Wang, Y. W.; Peng, Y., Fluorescein-Based Chromogenic and Ratiometric Fluorescence Probe for Highly Selective Detection of Cysteine and Its Application in Bioimaging. *Anal Chem* **2017,** *89* (3), 1937-1944.

10. Robotham, A. C.; Kelly, J. F., Detection and quantification of free sulfhydryls in monoclonal antibodies using maleimide labeling and mass spectrometry. *MAbs* **2019,** *11* (4), 757-766.

11. Oae, S., *Organic Sulfur Chemistry: Structure and Mechanism.* 1st ed.; CRC press: Boca Raton, FL, 1992.

12. Wei, B.; Jia, W.; Yang, Y.; Jazayri, M.; Fulchiron, D.; Jeong, J.; Cai, Q.; Li, C.; Briggs, J.; Ninonuevo, M.; Liu, H.; Liu, Z.; Zhang, Y. T., Development of a rapid reversed-phase liquid chromatographic method for total free thiol quantitation in protein therapeutics. *J Pharm Biomed Anal* **2020,** *189*, 113434.

13. Escudero, D., Revising Intramolecular Photoinduced Electron Transfer (PET) from First-Principles. *Acc Chem Res* **2016,** *49* (9), 1816-24.

14. Daly, B.; Ling, J.; de Silva, A. P., Current developments in fluorescent PET (photoinduced electron transfer) sensors and switches. *Chem Soc Rev* **2015,** *44* (13), 4203-11.

15. Lin, W.; Long, L.; Tan, W., A highly sensitive fluorescent probe for detection of benzenethiols in environmental samples and living cells. *Chem Commun (Camb)* **2010,** *46* (9), 1503-5.

16.   Wright, S. K.; Viola, R. E., Evaluation of methods for the quantitation of cysteines in proteins. *Anal Biochem* **1998,** *265* (1), 8-14.

17.   Riener, C. K.; Kada, G.; Gruber, H. J., Quick measurement of protein sulfhydryls with Ellman's reagent and with 4,4'-dithiodipyridine. *Anal Bioanal Chem* **2002,** *373* (4-5), 266-76.

18.   Riddles, P. W.; Blakeley, R. L.; Zerner, B., Reassessment of Ellman's reagent. *Methods Enzymol* **1983,** *91*, 49-60.

19.   Aitken, A.; Learmonth, M., Estimation of Disulfide Bonds Using Ellman's Reagent. In *The Protein Protocols Handbook. Springer Protocols Handbooks.*, Walker, J. M., Ed. Humana Press: Totowa, N. J. , 2009.

20.   Scatchard, G., Concentrated Solutions of Strong Electrolytes. *Chem Rev* **1936,** *19* (3), 309-327.

21.   Pitzer, K. S., Thermodynamics of electrolytes. I. Theoretical basis and general equations. *J Phys Chem* **1973,** *77* (2), 268-277.

3.7. Supplemental Information

Table 3.S1. List of fluorescent / fluorogenic probes tested

Name	Vendor	Excitation / Emission	Structure	Comments
Measure-iT Thiol Assay Kit	Life Technologies	494 / 517 nm	Disulfide, exact structure unknown	No dose-dependent response to TNB
CPM	Life Technologies	384 / 470 nm		No dose-dependent response to TNB
DCIA	Life Technologies	384 / 470 nm		No dose-dependent response to TNB
ThioGlo-3	Covalent Associates	378 / 446 nm		No dose-dependent response to TNB

Alexa Fluor 660 C$_2$ maleimide	Life Technologies	668 / 697 nm	Fluorescent maleimide, exact structure unknown	Fluorescent, not fluorogenic. High noise.
ThioFluor 623	Cayman Chemical	563 / 623 nm		Less sensitive than MMBC
MMBC (a.k.a. ThioGlo-1)	Combi-Blocks	379 / 513 nm		Most sensitive

*Traditional Ellman's method.* Cysteine standards (ranging from 0 to 40 µM) and protein samples (targeting a free thiol concentration of 20 µM) were prepared in either native conditions (111 mM MOPS, 1 mM EDTA, pH 7.25) or denaturing conditions (native conditions + 4 M guanidine hydrochloride). Sample protein concentrations were measured using a Nanodrop - blanking the spectrophotometer with a matched matrix - and the corresponding protein's extinction coefficient. Samples and standards were then incubated with 0.58 mM DTNB in the dark at r.t. for 60 minutes. One hundred microliters of each sample and standard were transferred in triplicates to a Corning 96-well half volume clear-bottom plate. Absorbance readings at 412 nm were taken on a Spectramax i3 plate reader. The thiol concentrations in each protein sample was determined by referencing its absorbance readings against the calibration curve (linear) derived using the cysteine standards. The free thiol content, on a mole per mole basis, could be calculated by dividing the sample thiol concentrations by the sample protein

concentrations determined via Nanodrop. During this procedure, multi-channel pipetting was used wherever possible.
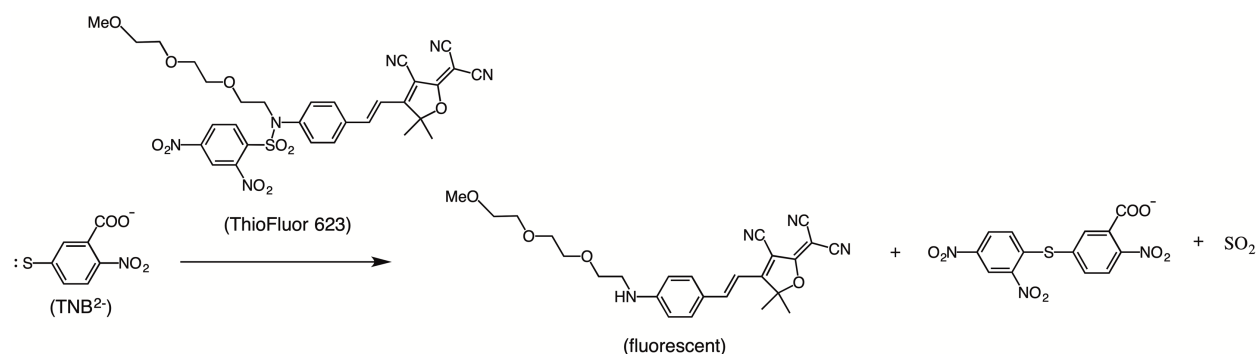
Figure 3.S1. Reaction schematic of TNB^{2-} and ThioFluor 623 to yield a deprotected fluorescent ThioFluor 623, following the pathway shown in **Figure 3.1** (IIB).
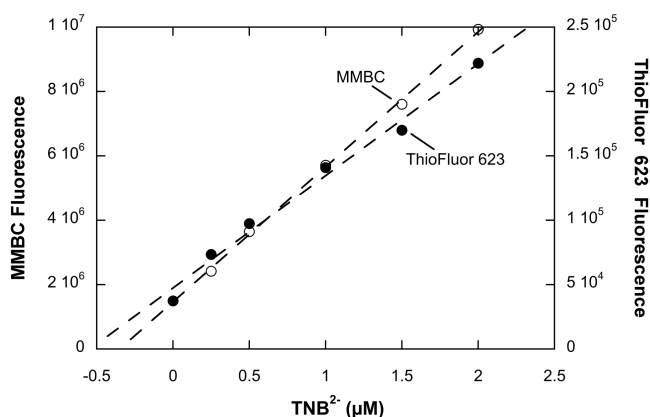

Figure 3.S2. Sensitivity of MMBC (open circles, left y-axis) versus ThioFluor 623 (closed circles, right y-axis) upon reacting with TNB^{2-} for 30 minutes. Note the magnitude of the resulting MMBC fluorescence is approximately 40x greater than the resulting ThioFluor 623 fluorescence.

Table 3.S2. Parameters and R^2 values from linear regression fits (y = mx + b) of calibration curves in **Figure 3.6**.

	native			denaturing		
	m	b	R^2	m	b	R^2
cys	8.25 e6	7.92 e6	>0.99	7.87 e6	1.35 e7	>0.99
NAC	8.37 e6	8.00 e6	>0.99	8.01 e6	1.12 e7	>0.99
gsh	7.80 e6	9.51 e6	>0.99	7.63 e6	1.33 e7	>0.99
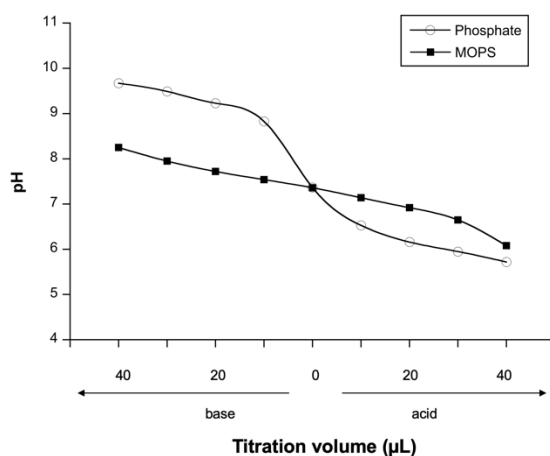
Figure 3.S3. Acid / base titrations comparing buffering capacities of phosphate versus MOPS buffer in the presence of 4M guanidine hydrochloride (phosphate buffer: 100 mM phosphate, 4M guanidine hydrochloride, 1 mM EDTA, pH 7.4; MOPS buffer: 100 mM MOPS, 4M guanidine hydrochloride, 1 mM EDTA, pH 7.4). Acid titration was performed with 1 N HCl and base titration was performed with 1 N NaOH.

Chapter 4.   **Interrogating the Co-purification of a Recombinant IgG1 Antibody and a Host-Cell Protein Containing an Unpaired Free Thiol**

4.1. Introduction

The biotechnology industry relies on recombinantly engineered host cells (e.g. CHO mammalian cells) to produce active and properly processed biotherapeutics since total synthesis of these proteins is not yet economically feasible. One inextricable consequence to producing biotherapeutics in host cells is the preponderance of proteins (secreted and intracellular) in the culture harvest that are endogenous to the host cell.[1, 2] Robust removal of these host cell proteins (HCP) after cell culture is critical for ensuring the product quality of biotherapeutics. HCPs in the purified drug product may contain epitopes recognized as non-human and may trigger safety signals or immune responses in human patients. [3-5] Certain HCPs in purified and formulated drug product can also catalyze the degradation of polysorbate 20 and polysorbate 80 (formulation excipients), which can lead to particle formation as well as adversely impacting the physical stability of the product i.e. aggregation, potentially limiting product shelf-life. [6-9]

HCPs in FDA-approved biologics generally do not exceed 100 parts per million (ppm). [10] For therapeutic IgGs, the typical purification process, which is comprised of a Protein A affinity step followed by one or more polishing chromatography steps, [11, 12] efficiently removes HCP down to those levels for most IgG products, and yet high level HCPs are occasionally observed in some IgG products. Some of the HCP copurification can be attributable to nonspecific interactions with chromatography resin backbones. [13, 14] However, it is becoming increasingly evident – from null HCCF (harvest cell culture fluid) and spiked null HCCF experiments,[15] from iterative flow through repurification studies,[16] and from high throughput batch purification studies with diverse panels of IgG products [17] – that IgG-HCP interactions are primarily responsible for HCP in the final

drug product. This is further corroborated by published instances of a single, predominant HCP (i.e. PLBL2, [18, 19] catalase subunit, [20] cathepsin D [21]) contributing to the majority of the HCP levels in a given product.

The cases of a single, predominant HCP for a given IgG product provide rare opportunities to further characterize the nature of IgG-HCP interactions. Previous studies with PLBL2, for example, showed that their interactions were more pronounced with IgG4 than IgG1 isotype, that binding could be quantified using surface plasmon resonance, and that avidity was potentially involved with the IgG-PLBL2 interactions. [19] Studies with cathepsin D also showed that binding could be quantified using surface plasmon resonance, but the investigators of this study took the characterization even further by identifying via mutation studies that a LYY motif in the CDR of their IgGs was responsible for cathepsin D binding. [22] Detailed characterization of additional cases of IgG-HCP interaction may yield further insights that are broadly useful for diagnosing or even anticipating future HCP challenges. Alternatively, a highly specific IgG-HCP interaction may be indicative of an isolated HCP copurification event.

Over 1000 ppm of HCP was found in the material used in pre-clinical toxicological studies of mAb1, a Genentech therapeutic IgG1 (lambda light chain). This finding led to the need to clear HCP levels down to acceptable levels. It was evident from SDS-PAGE that the high HCP levels in mAb1 were attributable to one predominant foreign protein, and subsequent mass spectrometry analysis of the excised SDS-PAGE bands suggested this HCP to be a glutathione S-transferase alpha (GSTα) based on homologous mouse and rat GSTα sequences. Further mechanistic studies were not

performed at the time because the full CHO genomic sequence was not available, but since then the full genomic sequence of CHO-K1 has been published. [23]

In the present study, we further granularized the GSTα found in mAb1 tox material to be GSTα3 by leveraging the full genomic CHO-K1 sequence. We recombinantly expressed CHO GSTα3 and interrogated the nature of the GSTα3 and mAb1 interaction, while paying close attention for any potential relationship between lambda light chain IgG1 antibodies and GSTα3 copurification. We demonstrate the usefulness of performing both mAb and HCP pulldowns to study IgG-HCP interactions and of photo-crosslinking experiments, which implicated mAb1 CDRs in the interaction with GSTα3. To our knowledge, this is the first report utilizing photo-crosslinking to trap and localize IgG-HCP interactions. We also discuss the benefits and challenges with working with an HCP with an unpaired free thiol functional group.

4.2. Materials and Methods

4.2.1. Materials

mAb1 (lambda light chain) and mAb2 (kappa light chain, negative control) are recombinant IgG1s manufactured at Genentech (South San Francisco, CA). pST239 was an in-house Genentech plasmid and 58F3 was an in-house Genentech *E. coli* strain (South San Francisco, CA). The codon-optimized DNA sequence for GSTα3 (**Figure 4.S1**) was ordered as an insert in the pUC57 plasmid (GenScript, Piscataway, NJ). DH5α and Top10 *E. coli* cells were purchased from (Invitrogen, Carlsbad, CA). Asp-N enzyme and trypsin enzyme were acquired from Roche (Basel, EU) and

Promega (Madison, WI) respectively. Glutathione, DTT, lysozyme, and iodoacetamide

(IAM) was purchased from Sigma (St. Louis, MO). Iodoacetic acid (IAA), iodoacetyl-

peg2-biotin, Slide-A-Lyzer (3mL, 10 kDa MWCO), GST interaction pulldown kit, sulfo-

KMUS (N-κ-maleimidoundecanoyl-oxysulfosuccinimide ester), sulfo-SBED (sulfo-N-

hydroxysuccinimidyl-2-(6-[biotinamido]-2-(p-azido benzamido)-hexanoamido) ethyl-1,3'-

dithioproprionate), and sulfo-SDAD (sulfosuccinimidyl 2-((4,4'-azipentanamido)ethyl)-

1,3'-dithiopropionate) were purchased from ThermoFisher Scientific (Waltham, MA).

GST Gravitrap columns, G-25 spin trap units, and NAP-5 columns were acquired from

GE Healthcare (Chicago, IL).

4.2.2. Glutathione agarose enrichment of GST in mAb1 tox material

In order to facilitate identification of the particular GST in mAb1 tox material, the GST

was first enriched using glutathione agarose beads. 17.5 mg of mAb1 tox material was

pH adjusted with 1 M Tris, pH 9.3 to a final pH of 8.0 and then subjected to the GST

interaction pulldown kit, following the manufacturer's instructions. Enriched proteins

were eluted from the agarose beads using 250 μL of 10 mM glutathione in 25 mM Tris,

150 mM NaCl, pH 8.0.

4.2.3. Asp-N peptide mapping followed by LC-MS/MS

Eluted sample from glutathione agarose enrichment was concentrated using an Amicon

0.5 mL centrifuge unit (10 kDa MWCO, EMD Millipore, Burlington, MA) to approximately

35 μL. The concentrated sample was diluted 1:1 with denaturing buffer (6.5 M guanidine

hydrochloride, 360 mM Tris, 3 mM EDTA, pH 8.6) and incubated at 37 °C for 1 hour in

the presence of 20 mM DTT. Liberated cysteines were alkylated with a subsequent incubation with 50 mM IAA for 15 minutes in the dark at r.t. The IAA alkylation reaction was quenched with an additional 10 mM DTT. To prepare the samples for peptide map digestion, the samples were buffer exchanged into Asp-N digestion buffer (25 mM Tris, 1 mM CaCl2, pH 8.3) using GE G-25 spintrap columns.

Asp-N digestion was performed by adding 120 ng of Asp-N enzyme (1:125, enzyme:substrate) to the buffer-exchanged sample and incubating at 37 °C for 4 hours. Asp-N digests were separated on a Waters H-Class UHPLC (Milford, MA) equipped with a Zorbax 300-SB C8 column (2.1x100 mm, 1.7 μm particle diameter, 300 Å pore size, Agilent, Santa Clara, CA). The column was equilibrated at a column temperature of 60 °C and with 100% mobile phase A (0.1% TFA in water) and 0% mobile phase B (0.08% TFA in acetonitrile). Peptides were eluted at 0.3 mL/min using an initial hold of equilibration conditions for 2 minutes followed by a 15 minute linear gradient from 0 to 20 %B and a 40 minute linear gradient from 20 to 55%B. The LC eluent was directed to waste for the first 3 minutes of the method, after which the LC eluent was directed to an Orbitrap Elite hybrid mass spectrometer (Thermo Electron, West Palm Beach, FL) equipped with an IonMax ESI source. IonMax source conditions typical for 0.3 mL/min flow rate were used. Full MS1 scans were acquired (Orbitrap detection, 60,000 resolution) followed by 3 data dependent tandem MS scans with CID fragmentation (LTQ Velos detection) and 3 data dependent tandem MS scans with ETD fragmentation (LTQ Velos detection) using Thermo XCalibur software. MASCOT (Matrix Science,

London, UK) and Byonic (Protein Metrics, San Carlos, CA) database searches were performed against the CHO proteome.

4.2.4. Expression of CHO GSTα3

Using standard molecular biology techniques and Qiagen kits, the codon-optimized DNA for GSTα3 was recombinantly engineered into a Genentech in-house plasmid (pST239) and then used to transform a Genentech in-house *E. coli* strain (58F3). [24] In brief, pUC57 plasmid containing the GSTα3 sequence and pST239 plasmid were amplified by transforming competent DH5α *E. coli* cells. The GSTα3 sequence was inserted into the pST239 plasmid via a two-way ligation utilizing XbaI and NotI restriction enzyme sites. The resulting pST239.GSTα3 plasmid was amplified by transforming competent Top10 *E. coli* cells, and then the amplified pST239.GSTα3 was used to transform competent 58F3 cells. The transformed 58F3 cells were grown in a phosphate-limiting media (C.R.A.P. media [25]) at 30 ºC for 24 hours.

4.2.5. Purification of CHO GSTα3

Cells were pelleted by centrifugation and lysed via freeze-thaw. Cell pellets were resuspended with PBS and treated with 1 mg/mL lysozyme on ice for 30 minutes. Following centrifugation, the supernatant was retained and filtered through a 0.45 um filter. Clarified supernatant was loaded onto GST GraviTrap columns which were pre-equilibrated with PBS. The columns were washed with 20 mL of PBS before eluting the GSTα3 with 10 mL of 50 mM glutathione, Tris, pH 8.0.

During our experiments, we observed that the excess free glutathione in the elution buffer would react with the unpaired free cysteine on GSTα3 to form mixed-disulfide. In order to reverse the glutathionylation and subsequently remove the excess free glutathione, the glutathionylated GSTα3 (which has no other native disulfide bonds) was reduced with 1 mM DTT and then buffer exchanged using Slide-a-lyzer dialysis cassettes into 100 mM sodium phosphate, 1 mM EDTA, pH 8.0.

4.2.6. Scaled down IgG affinity chromatography

In order to replicate the GSTα3 copurification observation, 3 mg/mL mAb samples were incubated with 7.9 μM of GSTα3 in 100 mM sodium phosphate, pH 8.0 for 30 minutes at r.t. Afterwards, the samples were subjected to scaled-down IgG affinity chromatography, which enabled study of the copurification phenomena while conserving reagents. Rainin electronic pipettes (Mettler-Toledo, Columbus, OH) equipped with Proplus affinity tips (40 μL MabSelect Sure resin, Phynexus, San Jose, CA) were programmed with equilibration, binding, washing, and elution steps as described in **Table 4.1**. Each step was performed in separate wells.

Table 4.1. Purification parameters used for scaled-down Protein A model

Step	Buffer	Flow (mL/min)	Volume (μL)	Repeat
Equilibrate	25 mM Tris, 150 mM NaCl, 5mM EDTA, pH 7.4 (Equil buffer)	0.14	600	1
Bind	Sample	0.09	397	4
Wash1	Equil buffer	0.14	350	1
Wash2	0.5 M TMAC in Equil buffer	0.14	390	1
Wash3	Equil buffer	0.14	350	1
Elute	100 mM acetic acid, pH 2.9	0.14	310	4

The extent of GSTα3 copurification was quantified by first reducing the elution pool with 10 mg/mL TCEP at 60 °C for 10 minutes. Reduced elution pools were then loaded onto a Waters H-Class UHPLC equipped with a BEH C4 column (2.1 x 150 mm, 1.7 μm particle diameter, 300 Å pore diameter, Waters, Milford, MA) that was pre-equilibrated at 70 °C with 38.5% solvent B (mobile phase A: 0.1% TFA in water; mobile phase B: 0.08% TFA in acetonitrile). After holding equilibration conditions for a brief 0.5 minutes, the proteins were eluted at 0.6 mL/min with a 1 minute linear gradient to 40% mobile phase B, followed by a 20 minute gradient to 60% mobile phase B before regenerating the column. The peak corresponding to GSTα3 on the 214 nm

chromatogram was integrated and compared against a standard curve of GSTα3

(ranging from 1 to 16 μg/mL) in order to determine the concentration of GSTα3. The

extent of GSTα3 copurification in terms of parts per million (ppm) was calculated by

dividing the GSTα3 concentration in the elution by the IgG concentration in the elution;

IgG concentration was determined by UV absorbance at 280 nm using a Nanodrop

2000 (ThermoFisher Scientific, Waltham, MA).

4.2.7. Intact LC-MS analysis of affinity elution pools

Select elution pools were examined with intact mass LC-MS to identify if any covalent

interactions such as disulfide bond formation were contributing to the copurification

mechanism. One μg was injected onto a Waters H-Class UHPLC system (Milford, MA)

equipped with a reversed-phase PLRP-S column (2.1 x 150 mm, 8 μm, 1000 Å, Agilent,

Santa Clara, CA), maintained at 70 °C and pre-equilibrated with 20% solvent B (mobile

phase A: 0.1% formic acid in water, mobile phase B: 0.1% formic acid in acetonitrile).

Proteins were eluted at a flowrate of 0.3 mL/min using a 1 minute linear gradient to 30%

solvent B, followed by a 7 minute gradient to 42 % solvent B. The column was

regenerated by washing for 1 minute with 95 % solvent B and by re-equilibrating for 5

minutes with 20 % solvent B. A switching valve was programmed to divert the LC eluent

to waste for the first 4 minutes of the method and afterwards divert to a Waters Xevo G2

QTOF mass spectrometer (Milford, MA) equipped with an ESI source for the remainder

of the method. Mass spectra from 500 to 4000 m/z were collected using MassLynx

software (Waters, Milford, MA). Mass deconvolutions were performed with Intact Mass software (Protein Metrics, San Carlos, CA).

4.2.8. GSTα3 alkylation with iodoacetamide

The unpaired free thiol on GSTα3 was alkylated with iodoacetamide to isolate the contribution of disulfide bond formation on the copurification mechanism. After treating with 1 mM DTT for 30 minutes at r.t. to ensure that the free thiol was liberated, 63 μM GSTα3 was subsequently alkylated by incubating with 10 mM iodoacetamide in 100 mM sodium phosphate, 1 mM EDTA, pH 8.0 for 15 minutes in the dark at r.t. The alkylation reaction was quenched with the addition of 5 mM DTT and the GSTα3-IAM was buffer exchanged using Slide-a-Lyzer cassettes into 100 mM sodium phosphate, 1 mM EDTA, pH 8.0. Copurification of GSTα3-IAM with mAb samples was interrogated using scaled-down IgG affinity chromatography as described in the above section.

4.2.9. Biotinylated GSTα3-streptavidin magnetic bead pulldowns

A GSTα3 that was biotinylated through its unpaired cysteine (GSTα3-peg2-biotin) was prepared by reacting 63 μM GSTα3 with 5 mM iodoacetyl-peg2-biotin for 25 minutes at r.t. in the dark. The biotinylation reaction was quenched with 5 mM DTT and the GSTα3-peg2-biotin was buffer exchanged using Slide-a-Lyzer cassettes into 100 mM sodium phosphate, 1 mM EDTA, pH 8.0. In order to bait the non-covalent interaction between GSTα3 and mAb1, 20 mg/mL of mAb samples and 0.8 μM GSTα3-peg2-biotin were incubated in 100 mM sodium phosphate, pH 8.0 for 1 hour at r.t. to allow non-

covalent mAb-GSTα3 complexes to form. Samples were then subjected to magnetic bead pulldowns as described below.

4.2.10. Trapping the non-covalent interaction between mAb1 and GSTα3 using photo-crosslinking

In our last set of experiments, we focused on trapping the non-covalent interaction between mAb1 and GSTα3 using photo-crosslinking experiments. We prepared two different GSTα3 conjugates, each containing a biotin affinity handle and one of two photo-crosslinking moieties: an aryl azide (GSTα3-SBED) and a diazirine (GSTα3-SDAD) photoactive functional group. GSTα3-SBED was prepared by reacting 200 μL of GSTα3-IAM with 3 μL of 8.5 mM sulfo-SBED for 30 minutes at r.t., followed by a buffer exchange into PBS using G-25 spin trap units (GE Healthcare). GSTα3-SDAD was prepared by reacting 200 μL of GSTα3-peg2-biotin with 2 μL of 8.5 mM sulfo-SDAD for 30 minutes at r.t., followed by a buffer exchange into PBS using G-25 spin trap units.

As a positive control, we prepared a mAb1 conjugated to glutathione, which is a natural substrate for GSTα3. In brief, 15 mg/mL mAb1 was conjugated with 0.3 mM sulfo-KMUS in PBS for 30 minutes at r.t. Afterwards, mAb1-KMUS samples were reacted with 0.5 mM glutathione for 30 minutes at r.t. followed by buffer exchange into PBS using Slide-A-Lyzer cassettes.

In order to perform the photo-crosslinking experiments, mAb1 and mAb2 were buffer exchanged out of their formulation buffers into PBS using G-25 spin trap units. Complex formation was encouraged by incubating 15.5 mg/mL of buffer exchanged

mAb1 or mAb2 with 0.8 μM of GSTα3 photo-crosslinking conjugate (i.e. GSTα3-SBED or GSTα3-SDAD) for 1 hour at r.t. For the positive control, 1.5 mg/mL of mAb1-KMUS-GSH was incubated with 0.8 μM of either GSTα3 photo-crosslinking conjugate. After incubation, one hundred sixty microliters of each sample were transferred to a 96 full-volume black microtiter plate (Corning, Corning, NY) and irradiated from the top with 365 nm light (ThermoFisher Scientific, 3UV lamp source, Waltham, MA) for 15 minutes at r.t. to induce covalent photo-crosslinking. Photo-crosslinked samples were then subjected to magnetic bead pulldowns as described below.

4.2.11.   Localization of non-covalent interaction site between mAb1 and GSTα3 using diazirine photo-crosslinking

Non-covalent interactions between mAb samples and GSTα3-SDAD were trapped via diazirine photo-crosslinking as described above. The photo-crosslinked samples were then subjected to streptavidin magnetic bead pulldowns as described below with the following modifications: a total of 2 mg of magnetic beads were used per samples and, instead of eluting with Laemelli buffer, the magnetic beads were reduced with 10 mM DTT in 50 μL of 50 mM ammonium bicarbonate, 8 M urea, pH 7.8 for 1 hour at 37 °C with constant mixing. Elutions were transferred to fresh Eppendorf tubes, alkylated with 30 mM IAM for 30 minutes at r.t., diluted 1:3 with 50 mM ammonium bicarbonate, pH 7.8, and overnight trypsin digested (1:50 enzyme:substrate ratio) at 37 °C. 50 μL of digested samples were loaded onto an Agilent 1290 UHPLC (Santa Clara, CA) equipped with an Acquity peptide CSH C18 reversed phase column (2.1 x 150 mm, 130

Å pore size, 1.7 μm, Waters, Milford, MA) equilibrated with 1% solvent B (mobile phase

A: 0.1% formic acid in water, mobile phase B: 0.1% formic acid in acetonitrile). The flow

rate was maintained at 0.2 mL/min with a column temperature set point of 77 °C. After a

2 minute hold at 1% solvent B, peptides were separated using a 5 minute linear gradient

from 1% to 13% solvent B, followed by a 35 minute gradient from 13% to 35% solvent

B, and finishing with a 8 minute gradient from 35% to 55% solvent B. The LC eluent was

coupled to a Thermo Orbitrap Fusion mass spectrometer (Thermo Electron, West Palm

Beach, FL) equipped with an IonMax NG ESI probe. IonMax NG source conditions

typical for 0.2 mL/min flow rate were used. Full MS1 scans were acquired (Orbitrap

detection, 60,000 resolution) followed by 3 data dependent tandem MS scans with CID

fragmentation (LTQ Velos detection). MS data was acquired using the Thermo XCalibur

software and analyzed using Byonic database search software (Protein Metrics, San

Carlos, CA).

4.2.12.   Biotin-streptavidin magnetic bead pulldowns

In brief, 1 mg of magnetic beads (Life Technologies, M-280 dynabeads, Waltham, MA)

pre-equilibrated with 20 mM sodium phosphate, 150 mM sodium chloride, 3 mM EDTA,

0.005% polysorbate 20, pH 7.4 were incubated with samples for 15 minutes at r.t. while

rotating. Beads were washed (5x) with 400 μL of 20 mM sodium phosphate, 150 mM

sodium chloride, 3 mM EDTA, 0.005% polysorbate 20, pH 7.4. After transferring the

magnetic beads to fresh Eppendorf tubes, all bound proteins were eluted by adding 25

μL of water and 25 μL of 2x Laemelli buffer and boiling at 90C for 10 minutes. Eluted

proteins were separated and visualized using SDS-PAGE (described below).

4.2.13.   SDS-PAGE analysis

Proteins were separated on a 4-12% BisTris gel in a XCell SureLock Mini-Cell

electrophoresis chamber (Life Technologies, Waltham, MA) according to manufacturer's

instructions using NuPAGE MES SDS running buffer. 10 μL of Precision Plus Protein™

unstained protein standard was included as the ladder. Bands were visualized by

staining with Coomassie Blue.

4.3.   Results

4.3.1. GSTα contaminant in mAb1 tox material is specifically GSTα3

The contaminant GSTα in the mAb1 tox material was enriched with glutathione-

beads and subjected to Asp-N peptide mapping, which yielded GSTα3 as the top hit

when searched against a translated CHO genome database. CHO GSTα3 was

confidently identified with over 96% sequence coverage (**Figure 4.1**). Interestingly, the

sequence of the identified CHO GSTα3 has no intramolecular disulfide bonds, but it has

one unpaired cysteine near the C-terminal end of the protein.

```
  1    AGKPVLHYFD GGGRMEPVRW LLAAAGVEFE EKFLKTRDDL ARLRNDGSLM

 51    FQQVPMVEID GMKLVQTRAI LNYIASKYNL YGKDMKERAL IDMYAEGIAD

101    LDEIVLHQPY IPQEEKEANL AKIKDKARNR YFPAYEKVLK GHGQDYLVGN

151    RLSRADVYLV ELLYHVEELD PSVLANFPLL KALRTRVSNL PTVKKFLQPG

201    SQRKPYEDEK CVESAMKIFS
```

**Figure 4.1**. Amino acid sequence of CHO GSTα3 identified in mAb1 tox vials. Sequence coverage by peptide mapping is indicated in blue (black indicates no sequence coverage). The unpaired cysteine is colored red. The N-terminal alanine was acetylated.

4.3.2. Quality of expressed recombinant GSTα3

Based on this CHO GSTα3 sequence, we expressed ~100 mg of recombinant GSTα3 in *E. coli*, which was subsequently purified using glutathione gravity columns. Analytical characterization verified the identity, integrity, and activity of the recombinant GSTα3 material. The observed deconvoluted mass of GSTα3 (25255 Da) by intact protein LC-MS agreed with the theoretical mass (25255 Da) (**Figure 4.S2**). The elution time during size-exclusion chromatography was consistent with a roughly 50 kDa species, which suggests that GSTα3 is properly folded and forms a noncovalent homodimer as expected, and the purity by SEC was > 97% (data not shown).[26] Furthermore, GSTα3 functioned as expected and could enzymatically catalyze CDNB in the presence of glutathione (**Figure 4.S3**).

4.3.3. Small scale Protein A chromatography reproduces GSTα3 carryover

Using the recombinant GSTα3, we sought to understand the copurification of GSTα3 with mAb1. We verified that GSTα3 copurifies with mAb1 using a scaled-down model of Protein A chromatography. After a brief incubation of GSTα3 and mAb1 at room temperature, samples were subjected to scaled-down Protein A purification. GSTα3 levels in the elution pool were determined using a reversed-phase chromatography assay; upon reducing elution pool samples, GSTα3 (due to its relative hydrophobicity) was easily resolved from antibody heavy and light chains on reversed-phase chromatography. More GSTα3 contamination was found in the elution pools when purifying mAb1 + GSTα3 compared with mAb2 + GSTα3 (**Figure 4.2**). However, the observed level of GSTα3 carryover with mAb2 (our negative control) in our scaled-down purification model was unexpected and initially puzzling because GSTα3 contamination was never observed in any mAb2 vials produced at-scale (a potential root cause for this observation is described in the discussion section).
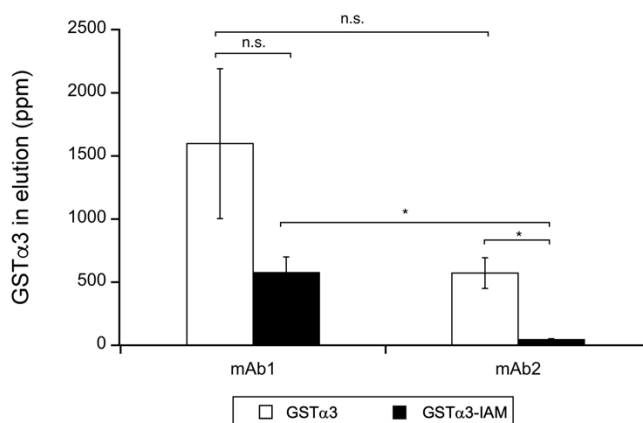

Figure 4.2. GSTα3 and GSTα3-IAM copurification with mAb1 and mAb2 using scaled-down model of Protein A affinity chromatography. Error bars represent one standard

deviation determined from n=3 experimental replicates. Welch's t-test was performed on select pairs of conditions (n.s. = not statistically significant; * = statistically significant with $p < 0.05$)

4.3.4. GSTα3 can form a mixed disulfide with mAb1 and mAb2

Further analytical characterization with intact LC-MS was performed on the scaled-down Protein A elution pools to determine if part of the copurification could be explained by covalent interactions involving GSTα3. Intact protein LC-MS of the mAb1+GSTα3 elution pools revealed a mass (47649 Da, **Figure 4.3**) consistent with GSTα3 disulfide bonded to mAb1 light chain (theoretical mass: 47649 Da; disulfide bond mediated by the mAb1 light chain cysteine that is typically involved in the heavy chain-light chain interchain disulfide bond). This finding was corroborated by identification of the particular mAb1 light chain peptide disulfide bonded to a GSTα3 peptide in non-reduced peptide mapping (data not shown). In order to determine what fraction of the GSTα3 copurification was attributable to disulfide bond formation involving GSTα3, we alkylated GSTα3's unpaired cysteine with IAM to yield GSTα3-IAM (**Figure 4.S4**) and repeated the scaled-down protein A purification experiments with GSTα3-IAM in place of GSTα3. **Figure 4.2** shows that alkylation of GSTα3's unpaired cysteine virtually eliminated GSTα3 copurification with mAb2. In contrast, alkylation of GSTα3's unpaired cysteine decreased GSTα3 copurification with mAb1, but the decrease was not statistically significant.
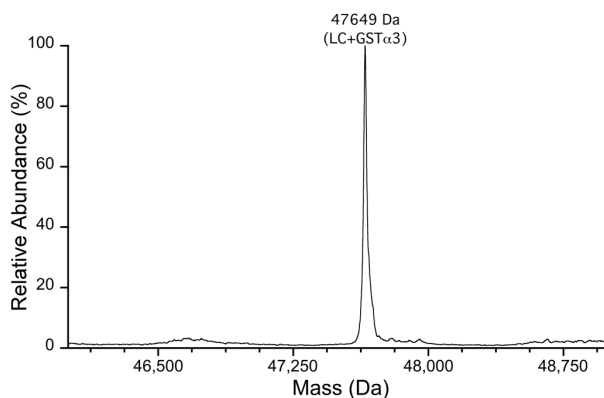
Figure 4.3. Deconvoluted mass of elutions from scaled-down Protein A purification of mAb1 spiked with GSTα3. The predominant mass is consistent with mAb1 light chain disulfide bonded to GSTα3.

4.3.5. GSTα3 associates non-covalently only with mAb1

In order to provide evidence of a putative non-covalent association between GSTα3 and mAb1, we baited the interaction with GSTα3 pulldowns. We first bioconjugated GSTα3's unpaired cysteine with a biotin-containing reagent to yield GSTα3-peg2-biotin (**Figure 4.S4**). Then, we incubated mAb1 and mAb2 samples with GSTα3-peg2-biotin followed by streptavidin magnetic bead pulldowns to affinity purify GSTα3 (in contrast to Protein A chromatography where mAb1 was affinity purified), and visualized the results using SDS-PAGE. The SDS-PAGE gel is shown in **Figure 4.4**. From left to right, after the protein ladder in the first lane, the next two lanes are a negative control and an experimental sample for mAb1, where mAb1 was incubated in the absence or presence of GSTα3-peg2-biotin, respectively, followed by streptavidin magnetic bead pulldowns. The two lanes after that are negative control and an

experimental sample for mAb2. We observed evidence of mAb1 capture (reflected as an IgG band intensity difference between experimental and negative control lanes) but no evidence of mAb2 capture during GSTα3 pulldowns. These results provided evidence for non-covalent capture of mAb1 (but not mAb2) during GSTα3 pulldowns. The GSTα3 pulldown results supported the scaled-down Protein A chromatography findings that mAb1 (but not mAb2) interacts non-covalently with GSTα3.
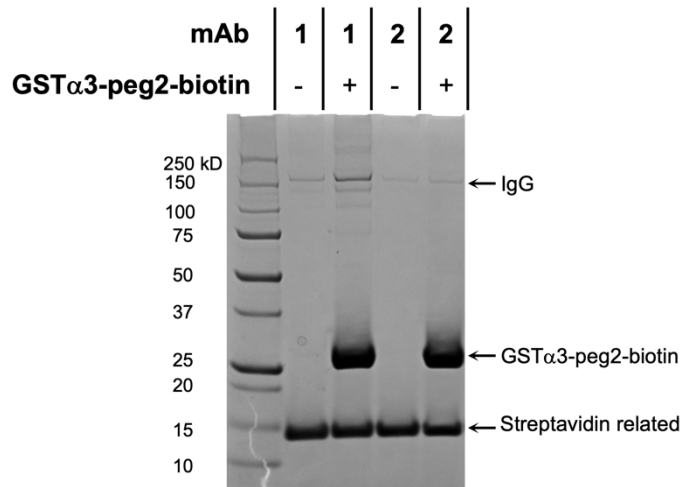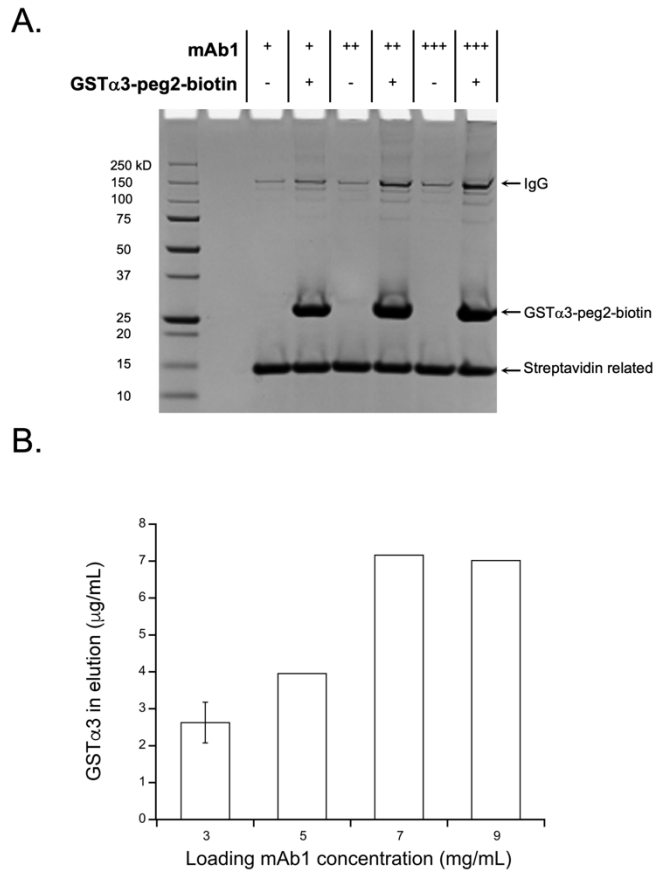
Figure 4.4. GSTα3-peg2-biotin streptavidin pulldowns to bait non-covalent IgG-HCP interactions. Pulldown elutions were separated using Coomassie-stained SDS-PAGE. Ladder (Precision Plus Protein™ unstained protein standard) is in the left-most lane.

Next, we designed an experiment to study non-covalent mAb1 capture during GSTα3 pulldowns as a function of starting mAb1 concentrations. The SDS-PAGE gel from this experiment is shown in **Figure 4.5A**. From left to right, after the protein ladder in the first lane, there is a series of paired lanes. Each pair is composed of a negative control and an experimental sample where mAb1 was incubated in the absence or presence of GSTα3-peg2-biotin followed by streptavidin magnetic bead pulldowns. Within the series, the starting concentration of mAb1 increases from left to right. The amounts of mAb1 capture when conducting GSTα3 pulldowns increased as a function of starting mAb1 concentrations (**Figure 4.5A**), which indicated that the non-covalent interactions are specific but also that mAb1 is the limiting reagent. This was further

corroborated by scaled down Protein A chromatography experiments which similarly showed that GSTα3-IAM carryover generally increased as a function of increasing starting mAb1 concentration (**Figure 4.5B**).

It was surprising that mAb1 was a limiting reagent when it was added in such molar excess (>160x) to GSTα3 during our GSTα3 pulldown experiments. We hypothesized that only a minor fraction of mAb1 – differentiated by a higher order structure difference or a post-translational modification, for example - was binding competent for GSTα3. To test the particular hypothesis that a post-translational modification was enabling mAb1 to bind to GSTα3, we subjected the mAb1 captured during GSTα3 pulldowns to intact LC/MS analysis and non-reduced lys-C peptide mapping. Unfortunately, we did not detect differences between the mAb1 captured during GSTα3 pulldowns and the starting mAb1 material by either of these techniques (data not shown). At this time, we cannot exclude the possibility that a higher order structure difference is responsible for a minor fraction of mAb1 binding to GSTα3.

Figure 4.5. Non-covalent interaction between GSTα3 and mAb1 is specific and increases as a function of starting mAb1 concentration. A) GSTα3-peg2-biotin streptavidin pulldowns with different levels of starting mAb1 concentrations. Pulldown elutions were separated using Coomassie-stained SDS-PAGE. Ladder (Precision Plus Protein™ unstained protein standard) is in the left-most lane. B) GSTα3-IAM carryover quantified using RPHPLC at different mAb1 loading concentrations using scaled-down protein A model. Error bar for 3 mg/mL mAb1 loading concentration represents one standard deviation based on n=3 experimental replicates. Other mAb1 loading concentrations were tested as a single replicate.

### 4.3.6. Photo-crosslinking experiments localize mAb1 interaction site

While analytical characterization of the mAb1 captured during GSTα3 pulldowns

did not identify the specific mAb1 fraction that was binding-competent for GSTα3 , we

were able to further localize the mAb1 interaction site using photo-crosslinking

experiments. In these experiments, GSTα3-IAM or GSTα3-peg2-biotin was further

derivatized with sulfo-SBED (aryl azide) or SDAD (diazirine) photo-crosslinkers,

respectively, to yield GSTα3-SBED or GSTα3-SDAD (**Figure 4.S4**); both GSTα3

conjugates included biotin as affinity handles. We irradiated these GSTα3 conjugates in

the presence of mAb1 or mAb2 to induce crosslinks between surface lysines of GSTα3

and mAb residues near the GSTα3-mAb interface, after which the photo-crosslinked

samples were subjected to streptavidin magnetic bead pulldowns and visualized using

SDS-PAGE. To demonstrate that our photo-crosslinking workflow was suitable for

detecting non-covalent interactions, a positive control mAb1 sample was prepared by

conjugating glutathione – a known substrate for GSTα3 – to mAb1 via a

heterobifunctional linker KMUS to yield mAb1-KMUS-GSH (**Figure 4.S4)**. **Figure 4.6**

shows the SDS-PAGE gel from our photo-crosslinking experiments. From left to right,

after the protein ladder, the next three lanes are GSTα3-SDAD irradiated in the

presence of mAb1, mAb2, or mAb1-KMUS-GSH, followed by streptavidin pulldowns.

The three lanes after that have same experimental conditions with the preceding three

lanes but with GSTα3-SBED instead. Finally, the last two lanes are control lanes that

include GSTα3-SDAD or GSTα3-SBED irradiated in the absence of any mAb sample,

followed by streptavidin pulldowns.
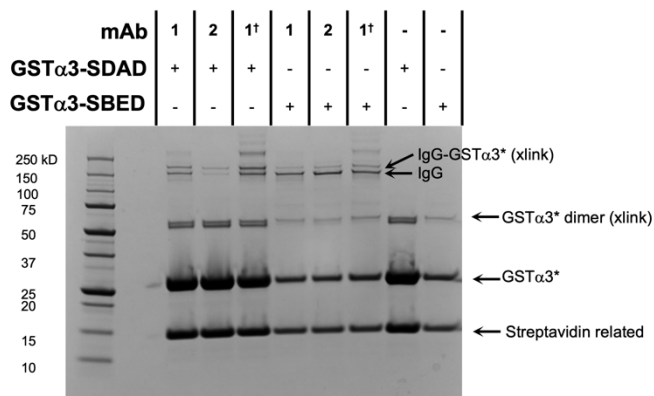
Figure 4.6. Photo-crosslinking at 365 nm followed by GSTα3-SDAD or GSTα3-SBED streptavidin pulldowns. Pulldown elutions were separated using Coomassie-stained SDS-PAGE. Ladder (Precision Plus Protein™ unstained protein standard) is in the left-most lane. GSTα3* refers to either GSTα3-SDAD or GSTα3-SBED. mAb1[†] denotes mAb1-KMUS-GSH, which was a mAb1 molecule conjugated to glutathione (GSH) via a sulfo-KMUS heterobifunctional linker and served as a positive control. "xlink" denotes photo-crosslinked species.

In our photo-crosslinking experiments, a SDS-PAGE band around 175 kDa would be consistent with an IgG photo-crosslinked to GSTα3. We observed a band around 175 kDa when GSTα3-SDAD was irradiated in the presence of mAb1 and mAb1-KMUS-GSH (positive control) but not mAb2 (negative control), suggesting that a specific complex between mAb1 and GSTα3 was being captured with diazirine photochemistry (**Figure 4.6**). In contrast, we observed a faint band around 175 kDa for all three mAb samples when the same experiment was performed with GSTα3-SBED, suggesting a lack of specificity with the aryl azide photochemistry (**Figure 4.6**).

Peptide mapping experiments were performed on streptavidin affinity enriched complexes of mAb1 photo-crosslinked to GSTα3-SDAD to identify the mAb1 interaction sites, since we observed evidence of specific complex formation. After reduction and IAM alkylation, we expected a mass modification of 216.0932 Da (**Figure 4.S5**) on mAb1 peptides that were successfully photo-crosslinked to GSTα3-SDAD. The observed masses and corroborating MS/MS spectra were consistent with two different mAb1 peptides with mass modifications of 216.0932 Da. Both peptides were part of mAb1's CDR loops, one in CDR-H3 (**Figure 4.7A**) and the other in CDR-L3 (**Figure 4.7B**). The MS/MS fragmentation patterns enabled further narrowing down of the photo-crosslinked site to the highlighted amino acids shown in **Figure 4.7**. Notably, similar peptide mapping experiments with mAb2 did not yield any peptides with mass modifications of 216.0932 Da.
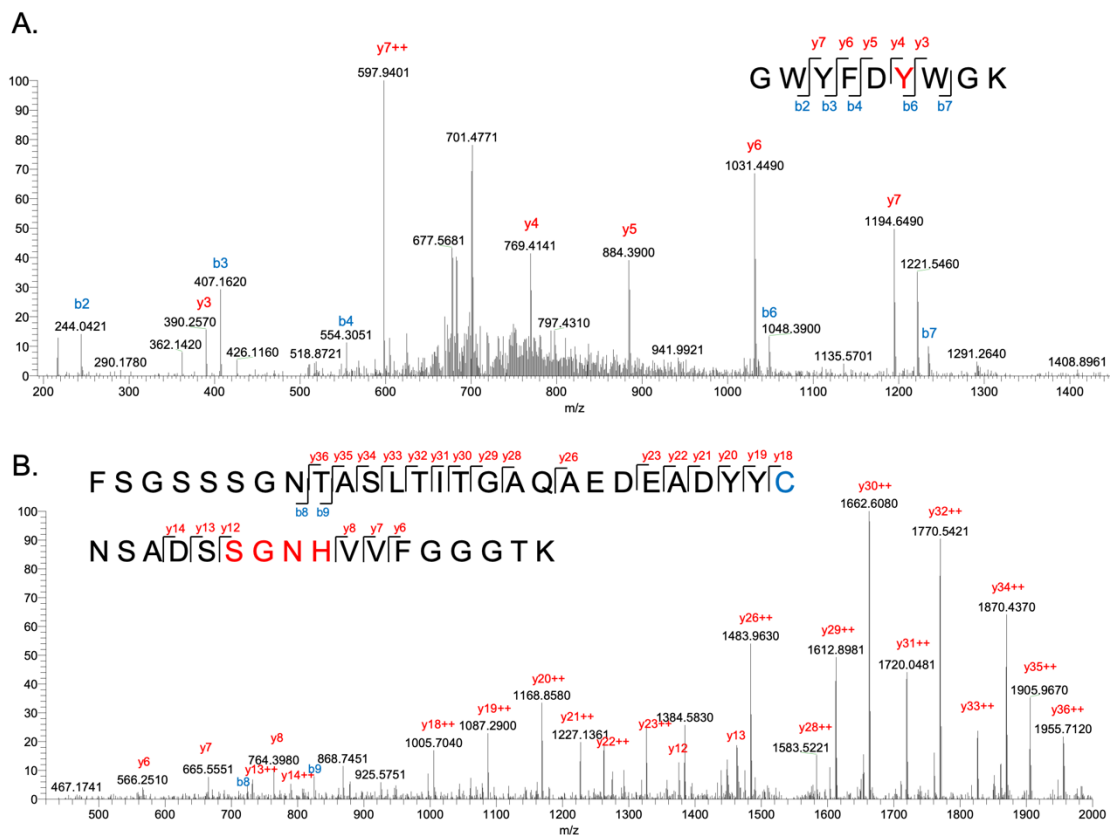
Figure 4.7. Two photo-crosslinked mAb1 tryptic peptides, resulting from 365nm irradiation in the presence of GSTα3-SDAD (diazirine conjugate), and evidenced by the expected mass modification of 216.0932 Da. A) MS/MS CID spectra of a CDR-H3 mAb1 tryptic peptide with the photo-crosslinking site localized to the tyrosine in red. B) MS/MS CID spectra of a CDR-L3 mAb1 tryptic peptide with the photo-crosslinking site localized to one of the four amino acids in red; the cysteine in blue was IAM alkylated. The photo-crosslinking site in the CDR-L3 mAb1 tryptic peptide could not be further localized due to the peptide fragmentation pattern.

4.4. Discussion

Carryover of host cell proteins during therapeutic IgG production is frequently cited in literature, and yet only a handful of IgG-HCP interactions have been characterized in detail. After identifying the primary sequence of the HCP (GSTα3) found in mAb1 tox material, we studied the interaction between GSTα3 and mAb1 and contribute to the limited body of knowledge regarding IgG-HCP interactions.

The GSTα3 and mAb1 interaction is rather unusual because it involves a strong binding event that can survive copious amounts of washing during magnetic bead pulldowns but only involves a minor fraction of mAb1. The latter point is supported by our mAb1 loading experiments (both using our scaled-down Protein A setup and magnetic bead pulldown setup), which indicate that mAb1 – despite being in tremendous excess - is the limiting reagent in the mAb1-GSTα3 interaction. It is also consistent with observations that GSTα3 binding to bulk mAb1 was not detected by isothermal calorimetry and bio-layer interferometry experiments (data not shown). In contrast, other studies examining specific HCPs (i.e. PLBL2,[19] cathepsin D[22]) have shown evidence of HCP binding to bulk IgG using techniques such as surface plasmon resonance; some research groups have proposed screening strategies to identify problematic HCPs based on their binding to bulk IgG. [27] Our studies suggest that IgG heterogeneity could be an important and often overlooked factor when considering IgG-HCP interactions.

While the identity of the minor fraction of mAb1 that is binding competent for GSTα3 remains elusive, we were able to determine via photo-crosslinking experiments

that mAb1's CDRs are likely involved in the interaction with GSTα3. **Figure 4.8** shows

the mAb1 residues that were covalently modified with a fragment of the diazirine photo-

crosslinker, which was originally conjugated to GSTα3, meaning that these sites are in

close proximity to the mAb1-GSTα3 binding interface. Interestingly, only amino acids in

the CDR loops of mAb1 were modified with the diazirine photo-crosslinker, and we can

infer from this data that the mAb1-GSTα3 interaction is likely mediated through mAb1's

CDRs. A specific interaction mediated by mAb1's CDRs suggests that GSTα3

copurification is likely not a liability for the broader class of lambda light chain

antibodies. Rather, it appears to be an isolated event that is a property of the unique

amino acid sequence found in mAb1's CDRs.
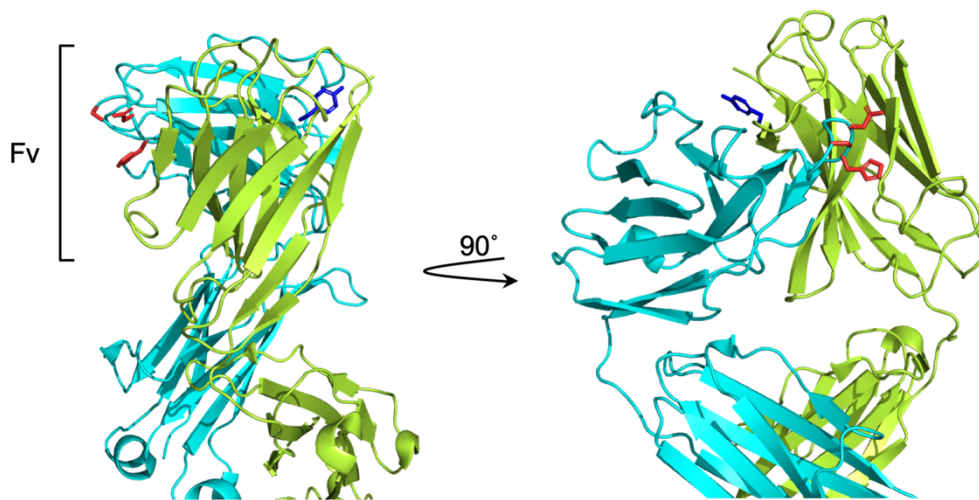
Figure 4.8. Crystal structure of mAb1 Fab region (PBD structure: 4OD2) showing the

identified photo-crosslinked sites (blue, CDR-H3; red, CDR-L3) after 365nm irradiation

in the presence of GSTα3-SDAD (diazirine conjugate). Visualization performed with

PyMol.

The gold standard for confirming that mAb1's CDRs mediate the interaction with GSTα3 would be to mutate out certain key residues on mAb1 and then test whether GSTα3 copurification becomes ameliorated. Prior groups performed such confirmatory experiments for a different IgG-HCP interaction system involving cathepsin D and identified a LYY motif on their IgGs responsible for the interaction. [22] Unfortunately, we were not able to pursue these confirmatory experiments for mAb1 and GSTα3.

Diazirine photo-crosslinking proved to be an effective means of covalently and specifically trapping the mAb1-GSTα3 interaction. We screened one other photo-crosslinking functional group, the aryl azide, which was not effective for trapping the mAb1-GSTα3 interaction. The results are somewhat confounded by the lower pulldown efficiency of GSTα3-SBED relative to GSTα3-SDAD, which may in part be explained by the unbiotinylated fraction in the former due to random lysine-conjugation. Nevertheless, there was no indication of a specific mAb1-GSTα3 photo-crosslinked complex with the aryl azide photochemistry. One plausible explanation is that the timescale of the aryl azide photo-crosslinking is too long. Prior mechanistic studies have suggested that ring expansion could lead to significantly longer-lived photoactivated aryl azide intermediates, [28, 29] which would promote promiscuous reactivity. On the other hand, photoactivated diazirines yield highly reactive carbenes, which are extremely short-lived (on the order of submicroseconds [30, 31]) and therefore promote privileged reactions between spatially adjacent species. Chemical crosslinkers react on even longer timescales than photo-crosslinkers, often on the order of seconds to minutes. While a

previous study interrogating the interaction between a mAb and cathepsin D host cell protein was able to glean insights using the chemical crosslinker BS3, [32] we suspect that chemical crosslinkers, similar to aryl azide photo-crosslinkers, suffer from promiscuous reactivity due to their long-lived reactions. To our knowledge, our study is the first report successfully utilizing diazirine photo-crosslinking to trap and localize IgG-HCP interactions.

It is worth mentioning the confounding role of GSTα3's unpaired free thiol on our studies. On the one hand, the unpaired free thiol on GSTα3 was a convenient bioconjugation handle for site-specific biotinylation, which ultimately enabled enrichment of non-covalent as well as photo-crosslinked mAb1-GSTα3 complexes. However, the unpaired free thiol on GSTα3 initially led to puzzling results in our scaled-down protein A purification experiments, where we observed some unexpected GSTα3 carryover with mAb2 (our negative control). Alkylation of GSTα3's free thiol with IAM completely inhibited GSTα3 copurification with mAb2 in our scaled-down purification model, suggesting that GSTα3's unpaired free thiol was likely contributing to artifactual carryover in our system, mediated by covalent disulfide bonding. The carryover mediated by GSTα3's unpaired free thiol may have been exacerbated in our scaled-down purification model because we used phosphate buffer at pH 8 as our loading condition, which poorly mimics the redox environment and pH of harvested HCCF. This serves as a cautionary tale that carefully controlled experiments are critical when investigating HCPs with reactive free thiols.

4.5.   Conclusions

We determined that GSTα3 was the identity of the predominant HCP found in

mAb1 tox material. GSTα3 was recombinantly expressed and used to probe its

interaction with mAb1 in a series of pulldown experiments involving either a scaled-

down Protein A purification system or GSTα3 magnetic bead pulldowns. These

experiments suggested that the mAb1-GSTα3 interaction was specific and strong, but

also indicated that only a minor fraction of the bulk mAb1 was involved in the

interaction. While the identity of the binding competent mAb1 remains elusive, diazirine

photo-crosslinking experiments successfully trapped the mAb1-GSTα3 complex and

implicated the mAb1 CDRs in the mAb1-GSTα3 binding interface. GSTα3 copurification

is not expected to be a liability for the broader class of lambda light chain IgG1

antibodies based on this data. This study adds to the limited catalogue of characterized

IgG-HCP interactions.

4.6.   References

1.   Champion, K. M.; Arnott, D.; Henzel, W. J.; Hermes, S.; Weikert, S.; Stults, J.;
      Vanderlaan, M.; Krummen, L., A two-dimensional protein map of Chinese
      hamster ovary cells. *Electrophoresis* **1999,** *20* (4-5), 994-1000.
2.   Tait, A. S.; Hogwood, C. E.; Smales, C. M.; Bracewell, D. G., Host cell protein
      dynamics in the supernatant of a mAb producing CHO cell line. *Biotechnol
      Bioeng* **2012,** *109* (4), 971-82.
3.   Fischer, S. K.; Cheu, M.; Peng, K.; Lowe, J.; Araujo, J.; Murray, E.;
      McClintock, D.; Matthews, J.; Siguenza, P.; Song, A., Specific Immune
      Response to Phospholipase B-Like 2 Protein, a Host Cell Impurity in
      Lebrikizumab Clinical Material. *AAPS J* **2017,** *19* (1), 254-263.
4.   Bailey-Kellogg, C.; Gutierrez, A. H.; Moise, L.; Terry, F.; Martin, W. D.; De
      Groot, A. S., CHOPPI: a web tool for the analysis of immunogenicity risk from
      host cell proteins in CHO-based protein production. *Biotechnol Bioeng* **2014,** *111*
      (11), 2170-82.

5. Wang, X.; Hunter, A. K.; Mozier, N. M., Host cell proteins in biologics development: Identification, quantitation and risk assessment. *Biotechnol Bioeng* **2009,** *103* (3), 446-58.

6. Zhang, S.; Xiao, H.; Molden, R.; Qiu, H.; Li, N., Rapid Polysorbate 80 Degradation by Liver Carboxylesterase in a Monoclonal Antibody Formulated Drug Substance at Early Stage Development. *J Pharm Sci* **2020,** *109* (11), 3300-3307.

7. Labrenz, S. R., Ester hydrolysis of polysorbate 80 in mAb drug product: evidence in support of the hypothesized risk after the observation of visible particulate in mAb formulations. *J Pharm Sci* **2014,** *103* (8), 2268-77.

8. Hall, T.; Sandefur, S. L.; Frye, C. C.; Tuley, T. L.; Huang, L., Polysorbates 20 and 80 Degradation by Group XV Lysosomal Phospholipase A2 Isomer X1 in Monoclonal Antibody Formulations. *J Pharm Sci* **2016,** *105* (5), 1633-1642.

9. MacDonald, M. L.; Hamaker, N.; Lee, K. H., Bioinformatic analysis of Chinese hamster ovary host cell protein lipases. *AIChE J* **2018,** *64* (12), 4247-4254.

10. Champion, K.; Madden, H.; Dougherty, J.; Shacter, E., Defining Your Product Profile and Maintaining Control Over It, Part 2. *Bioprocess Int* **2005**, 52-57.

11. Shukla, A. A.; Hubbard, B.; Tressel, T.; Guhan, S.; Low, D., Downstream processing of monoclonal antibodies--application of platform approaches. *J Chromatogr B Analyt Technol Biomed Life Sci* **2007,** *848* (1), 28-39.

12. Shukla, A. A.; Thommes, J., Recent advances in large-scale production of monoclonal antibodies and related proteins. *Trends Biotechnol* **2010,** *28* (5), 253-61.

13. Gagnon, P.; Nian, R.; Yang, Y.; Yang, Q.; Lim, C. L., Non-immunospecific association of immunoglobulin G with chromatin during elution from protein A inflates host contamination, aggregate content, and antibody loss. *J Chromatogr A* **2015,** *1408*, 151-60.

14. Tarrant, R. D.; Velez-Suberbie, M. L.; Tait, A. S.; Smales, C. M.; Bracewell, D. G., Host cell protein adsorption characteristics during protein A chromatography. *Biotechnol Prog* **2012,** *28* (4), 1037-44.

15. Shukla, A. A.; Hinckley, P., Host cell protein clearance during protein A chromatography: development of an improved column wash step. *Biotechnol Prog* **2008,** *24* (5), 1115-21.

16. Nogal, B.; Chhiba, K.; Emery, J. C., Select host cell proteins coelute with monoclonal antibodies in protein A chromatography. *Biotechnol Prog* **2012,** *28* (2), 454-8.

17. Sisodiya, V. N.; Lequieu, J.; Rodriguez, M.; McDonald, P.; Lazzareschi, K. P., Studying host cell protein interactions with monoclonal antibodies using high throughput protein A chromatography. *Biotechnol J* **2012,** *7* (10), 1233-41.

18. Vanderlaan, M.; Sandoval, W.; Liu, P.; Nishihara, J.; Tsui, G.; Lin, M.; Gunawan, F.; Parker, S.; Wong, R. M.; Low, J.; Wang, X.; Yang, J.; Veeravalli, K.; McKay, P.; Yu, C.; O'Connell, L.; Tran, B.; Vij, R.; Fong, C.; Francissen, K.; Zhu-Shimoni, J.; Quarmby, V.; Krawitz, D., Hamster phospholipase B-like 2 (PLBL2): A host-cell protein impurity in therapeutic

monoclonal antibodies derived from chinese hamster ovary cells. *BioProcess International* **2015,** *13*.

19. Tran, B.; Grosskopf, V.; Wang, X.; Yang, J.; Walker, D., Jr.; Yu, C.; McDonald, P., Investigating interactions between phospholipase B-Like 2 and antibodies during Protein A chromatography. *J Chromatogr A* **2016,** *1438*, 31-8.

20. Ahluwalia, D.; Dhillon, H.; Slaney, T.; Song, H.; Boux, H.; Mehta, S.; Zhang, L.; Valdez, A.; Krishnamurthy, G., Identification of a host cell protein impurity in therapeutic protein, P1. *J Pharm Biomed Anal* **2017,** *141*, 32-38.

21. Bee, J. S.; Tie, L.; Johnson, D.; Dimitrova, M. N.; Jusino, K. C.; Afdahl, C. D., Trace levels of the CHO host cell protease cathepsin D caused particle formation in a monoclonal antibody product. *Biotechnol Prog* **2015,** *31* (5), 1360-9.

22. Bee, J. S.; Machiesky, L. M.; Peng, L.; Jusino, K. C.; Dickson, M.; Gill, J.; Johnson, D.; Lin, H. Y.; Miller, K.; Heidbrink Thompson, J.; Remmele, R. L., Jr., Identification of an IgG CDR sequence contributing to co-purification of the host cell protease cathepsin D. *Biotechnol Prog* **2017,** *33* (1), 140-145.

23. Xu, X.; Nagarajan, H.; Lewis, N. E.; Pan, S.; Cai, Z.; Liu, X.; Chen, W.; Xie, M.; Wang, W.; Hammond, S.; Andersen, M. R.; Neff, N.; Passarelli, B.; Koh, W.; Fan, H. C.; Wang, J.; Gui, Y.; Lee, K. H.; Betenbaugh, M. J.; Quake, S. R.; Famili, I.; Palsson, B. O.; Wang, J., The genomic sequence of the Chinese hamster ovary (CHO)-K1 cell line. *Nat Biotechnol* **2011,** *29* (8), 735-41.

24. Szeto, W.; Jiang, W.; Tice, D. A.; Rubinfeld, B.; Hollingshead, P. G.; Fong, S. E.; Dugger, D. L.; Pham, T.; Yansura, D. G.; Wong, T. A.; Grimaldi, J. C.; Corpuz, R. T.; Singh, J. S.; Frantz, G. D.; Devaux, B.; Crowley, C. W.; Schwall, R. H.; Eberhard, D. A.; Rastelli, L.; Polakis, P.; Pennica, D., Overexpression of the retinoic acid-responsive gene Stra6 in human cancers and its synergistic induction by Wnt-1 and retinoic acid. *Cancer Res* **2001,** *61* (10), 4197-205.

25. Simmons, L. C.; Reilly, D.; Klimowski, L.; Raju, T. S.; Meng, G.; Sims, P.; Hong, K.; Shields, R. L.; Damico, L. A.; Rancatore, P.; Yansura, D. G., Expression of full-length immunoglobulins in Escherichia coli: rapid and efficient production of aglycosylated antibodies. *J Immunol Methods* **2002,** *263* (1-2), 133-47.

26. Dirr, H.; Reinemer, P.; Huber, R., X-ray crystal structures of cytosolic glutathione S-transferases. Implications for protein architecture, substrate recognition and catalytic function. *Eur J Biochem* **1994,** *220* (3), 645-61.

27. Aboulaich, N.; Chung, W. K.; Thompson, J. H.; Larkin, C.; Robbins, D.; Zhu, M., A novel approach to monitor clearance of host cell proteins associated with monoclonal antibodies. *Biotechnol Prog* **2014,** *30* (5), 1114-24.

28. Borden, W. T.; Gritsan, N. P.; Hadad, C. M.; Karney, W. L.; Kemnitz, C. R.; Platz, M. S., The interplay of theory and experiment in the study of phenylnitrene. *Acc Chem Res* **2000,** *33* (11), 765-71.

29. Preston, G. W.; Wilson, A. J., Photo-induced covalent cross-linking for the analysis of biomolecular interactions. *Chem Soc Rev* **2013,** *42* (8), 3289-301.

30.   Jumper, C. C.; Bomgarden, R.; Rogers, J.; Etienne, C.; Schriemer, D. C., High-resolution mapping of carbene-based protein footprints. *Anal Chem* **2012,** *84* (10), 4411-8.

31.   Jumper, C. C.; Schriemer, D. C., Mass spectrometry of laser-initiated carbene reactions for protein topographic analysis. *Anal Chem* **2011,** *83* (8), 2913-20.

32.   Ranjan, S.; Chung, W. K.; Hofele, R.; Heidbrink Thompson, J.; Bee, J.; Zhang, L.; Robbins, D.; Cramer, S. M., Investigation of cathepsin D-mAb interactions using a combined experimental and computational tool set. *Biotechnol Bioeng* **2019,** *116* (7), 1684-1697.

4.7.   Supplemental Information

```
1      GCAGGTAAACCTGTACTACATTACTTCGAT  GGTGGTGGTCGTATGGAACCGGTCCGTTGG

61     CTGCTGGCGGCTGCGGGTGTTGAATTTGAA  GAAAAATTTCTGAAAACCCGTGATGACCTG

121    GCACGTCTGCGCAACGATGGCAGCCTGATG  TTCCAGCAAGTGCCGATGGTTGAAATTGAC

181    GGTATGAAACTGGTGCAGACGCGTGCGATT  CTGAACTATATCGCCAGCAAATACAACCTG

241    TACGGCAAAGATATGAAAGAACGCGCGCTG  ATCGACATGTATGCAGAAGGTATTGCTGAT

301    CTGGACGAAATCGTTCTGCATCAGCCGTAC  ATTCCGCAAGAAGAAAAAGAAGCGAACCTG

361    GCCAAAATCAAAGATAAAGCACGTAATCGC  TATTTTCCGGCTTACGAAAAAGTCCTGAAA

421    GGTCATGGCCAGGATTACCTGGTTGGCAAT  CGTCTGAGTCGCGCGGACGTCTATCTGGTG

481    GAACTGCTGTACCACGTGGAAGAACTGGAC  CCGAGCGTGCTGGCGAACTTTCCGCTGCTG

541    AAAGCCCTGCGTACCCGCGTTAGCAATCTG  CCGACGGTCAAAAAATTCCTGCAACCGGGT

601    TCTCAGCGTAAACCGTATGAAGACGAAAAA  TGCGTTGAATCGGCAATGAAAATCTTCTCC
```

Figure 4.S1. Codon-optimized DNA sequence for GSTα3.
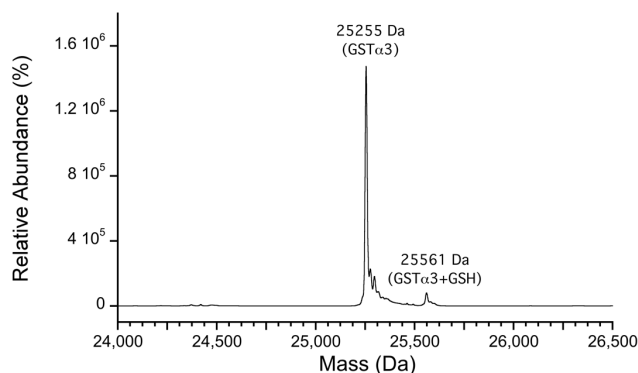
Figure 4.S2. Deconvoluted mass of purified recombinant GSTα3. A small fraction of glutathionylated GSTα3 (GSTα3+GSH) was also observed.
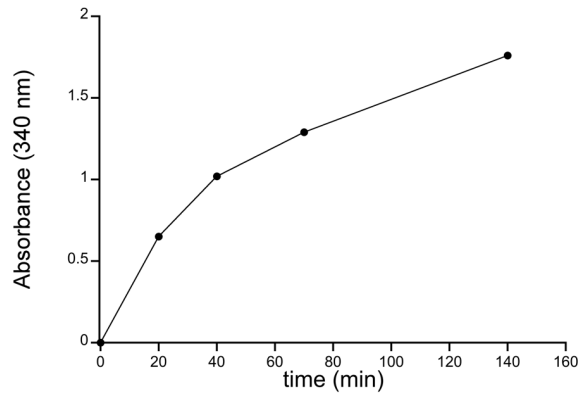
Figure 4.S3. GSTα3 activity assay with CDNB (1-chloro-2,4-dinitrobenzene) substrate. A solution of 1 mM CDNB, 1 mM glutathione, 0.1 M potassium phosphate, pH 6.5 was incubated with 2.5 nM GSTα3 in a cuvette. UV absorbance (340 nm) indicates successful enzymatic conversion of CDNB to glutathionylated dinitrobenzene.
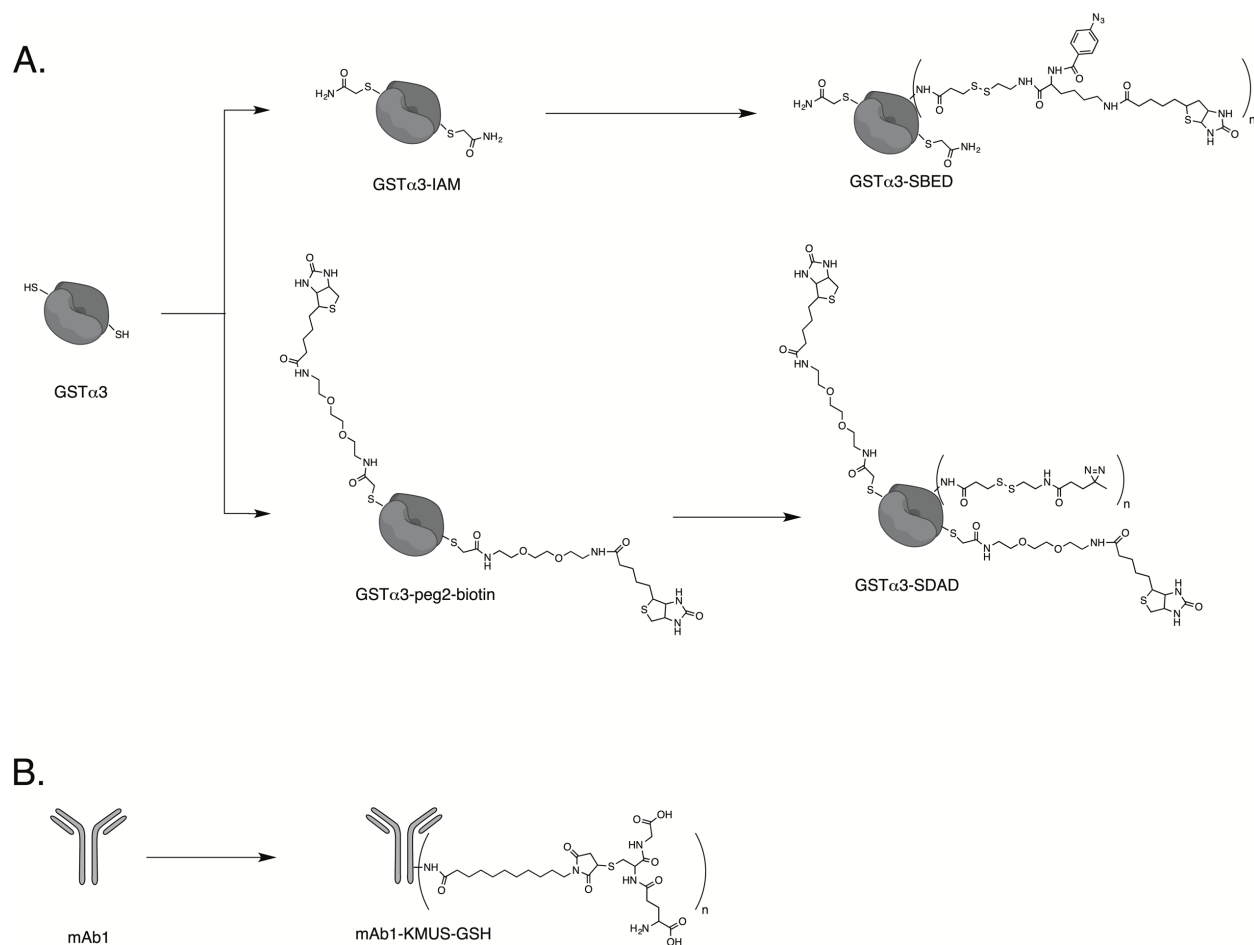
Figure 4.S4. Bioconjugates prepared for this study. A) GSTα3 conjugates were prepared by alkylating the free thiols with either IAM (iodoacetamide) or iodoacetyl-peg2-biotin. The GSTα3-IAM or GSTα3-peg2-biotin conjugates were further derivatized via surface lysines with either sulfo-SBED or SDAD photo-crosslinking reagents, respectively. B) mAb1 conjugation to glutathione (GSH) was mediated by the heterobifunctional linker sulfo-KMUS. Sulfo-KMUS was first conjugated to surface lysines of mAb1 and then GSH was conjugated to the maleimide of KMUS. The subscript n denotes the possibility of multiple conjugations due to random lysine conjugation.
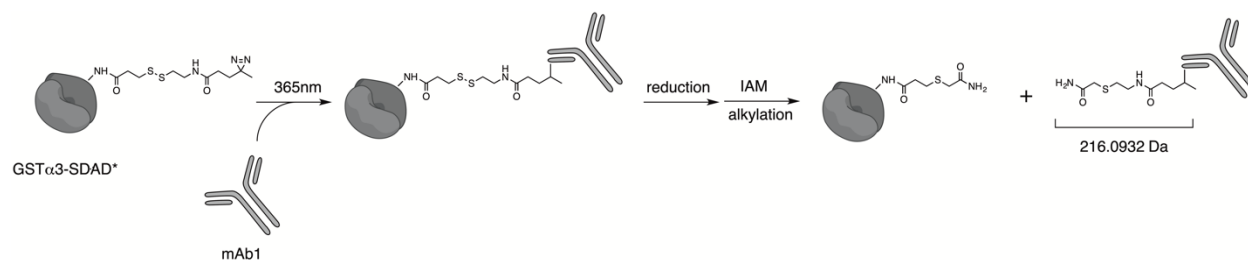
Figure 4.S5. Diazirine photo-crosslinking between GSTα3-SDAD and mAb1 followed by reduction and IAM alkylation lead to a label transfer. The mass modification of the resulting label transfer is 216.0932 Da. *: for simplicity, GSTα3-SDAD is depicted here with just one conjugated SDAD linker and without its peg2-biotin affinity handles. For a more complete structure of the GSTα3-SDAD conjugate, refer to **Figure 4.S4**.

Chapter 5. Summary and Future Directions

5.1. Summary

In Chapter 2, we examined the *in vivo* reoxidation kinetics of free thiols on IgG1 antibodies in a non-clinical animal model and gained a better understanding of what might happen to this post-translational modification after administration to patients. In Chapter 3, we augmented the classic optical method for free thiol detection, the Ellman's method, into the Fluorescent Ellman's method, which improved free thiol quantitation limits and made the assay more amenable for routinely monitoring free thiol levels on antibody therapeutics. In Chapter 4, we interrogated the interaction between an antibody therapeutic and a contaminating host cell protein that contained a free thiol, GSTα3. Through a combination of bioconjugation (mediated by the free thiol) and photo-crosslinking, we implicated the antibody CDR's involvement in this specific antibody-host cell protein interaction, cataloguing another example of how host-cell proteins can co-purify with antibody therapeutics to end up in the final product.

5.2. Future Directions

There is likely to be continued interest in free thiols in the context of therapeutic proteins, since free thiols are one of the more chemically reactive groups in biology. One natural extension to this body of work would be reconciling differences in free thiol reoxidation rates observed in *in vivo* non-clinical models and in *in vitro* redox systems. A stronger *in vitro-in vivo* correlation would reduce the burden for additional *in vivo* studies and enable the rapid prediction/screening of *in vivo* reoxidation behaviors of free thiols of new therapeutic antibodies as well as other novel biotherapeutics. If presented the

opportunity, it would also be valuable to validate our non-clinical *in vivo* free thiol reoxidation rates with observations from a clinical study.

At the same time, we anticipate there will continue to be an appetite for increasingly sensitive assays to monitor free thiols as a measure of product quality of therapeutic proteins. There may be opportunities to further enhance the sensitivity of the current iteration of Fluorescent Ellman's method with other novel fluorogenic probes.

Finally, host cell protein contamination will always be a challenging issue as long as biotherapeutics are manufactured in host cells. While we studied a particular host cell protein that happened to bear a free thiol (which is likely uncommon), the general strategy of incorporating an affinity handle into the host cell protein in conjunction with photo-crosslinkers to interrogate and localize host cell protein-biotherapeutic interactions sites may be useful for studying other host cell protein systems. The effort required for these studies are substantial so this approach should be reserved for the most stubborn and problematic host cell proteins.